Title
Chemical Methods for Imaging Glycans during Development

Author
Dehnert, Karen Worthington

Publication Date
2011

Peer reviewed|Thesis/dissertation

Chemical Methods for Imaging Glycans during Development

by

Karen Worthington Dehnert

A dissertation submitted in partial satisfaction of the
requirements for the degree

Doctor of Philosophy

in

Chemistry

in the

Graduate Division

of the

University of California, Berkeley

Committee in charge:

Professor Carolyn R. Bertozzi, Chair
Professor Christopher J. Chang
Professor Sharon L. Amacher

Spring 2011

Chemical Methods for Imaging Glycans during Development

by Karen Worthington Dehnert

Abstract

Chemical Methods for Imaging Glycans during Development

by

Karen Worthington Dehnert

Doctor of Philosophy in Chemistry

University of California, Berkeley

Professor Carolyn R. Bertozzi, Chair

Glycans are carbohydrate structures that cover the surfaces of all cells and mediate cell-cell interactions essential for the functioning of multicellular organisms. Glycans play roles in cell adhesion, signaling, and differentiation processes, particularly during embryonic development. A better understanding of these processes at the molecular level would benefit from the ability to visualize glycans in living organisms.

As post-translational modifications of proteins and head groups of lipids, glycans are not directly encoded in the genome. As a result, they cannot be labeled and imaged using the standard genetic techniques used to tag proteins with fluorescent probes. To enable imaging of glycans in living systems, we have developed a chemical reporter strategy in which glycans are tagged with a small reporter group that is not naturally found in biological systems. This can be achieved by supplying endogenous biosynthetic pathways with azide-labeled monosaccharides that become incorporated into cell-surface glycans. In a second step, the chemical reporter can be visualized by covalent ligation to a fluorescent probe.

This dissertation describes the development of chemical methods for imaging glycans during zebrafish embryogenesis. Zebrafish are popular vertebrate model organisms with transparent embryos that develop externally, characteristics that render them ideal for optical imaging. In Chapter 1 of this dissertation, I present an overview of the structures and functions of eukaryotic glycans and methods for imaging them in living systems. In Chapter 2, I discuss a method for visualizing mucin-type O-glycans during early embryogenesis by microinjecting zebrafish embryos at the one-cell stage with azide-functionalized precursor molecules. This method enabled imaging of glycans as early as 7 hours post-fertilization, during the gastrulation stage of development, and revealed dramatic trafficking of glycans to the cleavage furrow of dividing cells. In Chapters 3 and 4, I describe the extension of this metabolic labeling strategy toward fucosylated and sialylated glycans, respectively. Finally, in Chapter 5, I present a non-metabolic method for chemical labeling of sialylated glycans. This method enabled the simultaneous visualization of two distinct classes of glycans in live embryos.

This dissertation is dedicated to my family.

Chemical Methods for Imaging Glycans during Development

Table of Contents

List of Figures

List of Tables

Acknowledgements

I am truly grateful to all of the people who have shaped my graduate education at Berkeley. First and foremost, I thank Professor Carolyn Bertozzi, the best advisor I could have hoped for. Carolyn has been an exceptional teacher and mentor over the past five years. She has created a wonderful research environment, and I have appreciated all the opportunities she has provided. I admire Carolyn's great insight, creativity, and focus on big ideas. The emphasis she has placed on effective writing and presentation skills has also had a big impact on me, and I know that I will carry the skills I have learned from Carolyn through the rest of my career. Above all, I thank Carolyn for her unwavering support throughout my graduate education.

I also thank Professor Sharon Amacher, who has been a wonderful collaborator and mentor. I will always appreciate how warmly Sharon has welcomed me into her lab. Over the past few years, she has been incredibly encouraging and supportive, always making time to meet when I need help. I have learned about a whole new area of science from Sharon, and I have really enjoyed spending time in her lab.

This dissertation research is the result of several wonderful collaborations, and I thank the great scientists and friends who have been part of it. Scott Laughlin introduced me to imaging and taught me how to best design experiments with the big picture in mind. He has provided a great deal of guidance throughout these projects. Jeremy Baskin was always an entertaining labmate, and I appreciate and admire his enthusiasm for trying out new ideas. More recently, Brendan Beahm has been a great addition to the project and a pleasure to work with. I also thank Eric Trautman, a bright undergraduate student, for the efforts he contributed to our work.

In the Amacher Lab, I am especially grateful to Thinh Huynh, who was a dedicated collaborator on this work. Emilie Delaune, Thomas Gallagher, Adrienne Maxwell, Jasmine McCammon, Nathan Shih, and Katherine Brown have all been generous with their time and expertise, answering my questions and helping me learn new techniques. I also thank Jen St. Hilaire, Deborah Weinman, and Keely McDaniel for their help and zebrafish care.

This research has benefitted from the contributions of many other scientists. Emilie Delaune, Anjali Ganguli, John Jewett, Isaac Miller, David Rabuka, Ellen Sletten, Lauren Wagner, and Wei Wang have generously provided reagents for these projects. I thank Holly Aaron at the Berkeley Molecular Imaging Center for her assistance with confocal fluorescence microscopy.

The Bertozzi Group has been a wonderful place to work over the past five years because of all the people here. I thank Asia Avelino, Olga Martinez, Karen Carkhuff, and Sia Kruschke for the help they have provided on a daily basis. Cheryl McVaugh and Tanya Leavy got me started in the lab when I rotated and first joined. Mike Boyce, Mark Breidenbach, Zev Gartner, and Phung Gip and have all helped me with biology techniques. Mike Schelle, Zev Gartner, and Kimberly Beatty were great labmates in 802 during the first half of graduate school. Over the past two years, I have truly enjoyed spending my days with Jason Hudak, Brian Belardi, and Lauren Wagner. I will really miss our conversations, their great sense of humor, and their friendship. I have also appreciated the support of my classmates, particularly Ellen Sletten, Kanna Palaniappan,

and Kim Sogi, who have been by my side during all of graduate school. Thanks especially to Ellen, a great friend and the person I always go to first with all my questions. Anderson Lo, Brian Carlson, and Scott Laughlin have also been great friends, and I have appreciated their support over the years. Thanks to everyone, those listed above and all the others, who have been part of many good times during graduate school.

Finally, I thank my family for their love and encouragement. This dissertation is dedicated to them.

Chapter 1

Imaging Glycans in Living Systems

Chapter 1. Imaging Glycans in Living Systems

Introduction

All cell surfaces are adorned with glycans, which act as essential mediators of the myriad interactions that take place between cells and their environments. These carbohydrate structures may be appended post-translationally to proteins or modify lipids, and their great diversity and privileged position at the cell surface has enabled their participation in a wide variety of biological processes, including host-pathogen interactions, inflammation, and cancer metastasis (*1*, *2*). In embryonic development, the proper spatial and temporal expression of cell-surface glycans is essential for cell-cell adhesion and signaling events (*3*).

Molecular imaging has greatly advanced our understanding of dynamic biological processes, including embryonic development, at the molecular level. However, standard imaging tools such as genetically-encoded fluorescent fusion proteins cannot be used to image glycans because glycan biosynthesis is not encoded directly in the genome. Rather, glycans are assembled by hundreds of glycosyltransferase enzymes that act at different points in the secretory pathway, without a template to direct them. Glycosyltransferases link individual monosaccharide building blocks together at different positions and with different linkage configurations (α or β) to create a great variety of potential isomers. The resulting structures are difficult to isolate or identify by mass spectrometry, for example, and have made the study of glycans especially challenging.

In this chapter, I first describe several major classes of eurkaryotic glycans and their roles in biological processes including embryonic development. I then present methods for labeling and imaging glycans in living systems, with a particular focus on chemical reporters and bioorthogonal ligation techniques.

Cell-Surface Glycans in Eukaryotes

The structural diversity of glycans is derived from the attachment sites and configurations of their constituent monosaccharides. In vertebrates, there are nine common monosaccharide building blocks that are incorporated into glycans (Figure 1.1). These monosaccharides (and their abbreviations) are: D-glucose (Glc), *N*-acetyl-D-glucosamine (GlcNAc), D-glucuronic acid (GlcA), D-galactose (Gal), *N*-acetyl-D-galactosamine (GalNAc), D-mannose (Man), D-xylose (Xyl), L-fucose (Fuc), and sialic acid (Sia), primarily *N*-acetylneuraminic acid (Neu5Ac).

The major classes of glycans (Figure 1.2) are based on the type of attachment between the carbohydrate structure and the underlying protein. N-linked glycans contain a core pentasaccharide structure that is attached to the nitrogen of an asparagine residue in the protein backbone (Figure 1.3, panel A). Mucin-type O-linked glycans are attached via a core GalNAc residue to the oxygen of a serine or threonine (Figure 1.3, panel B). Finally, glycosaminoglycans are primarily attached to serine residues through a conserved core tetrasaccharide structure that begins with a xylose residue (Figure 1.3, panel C). Other types of O-glycosylation, which will not be discussed further here,

include O-fucosylation, O-mannosylation and O-glucosylation, which are far less common than the classes described above, and O-GlcNAcylation, a dynamic and reversible modification of cytosolic and nuclear proteins.

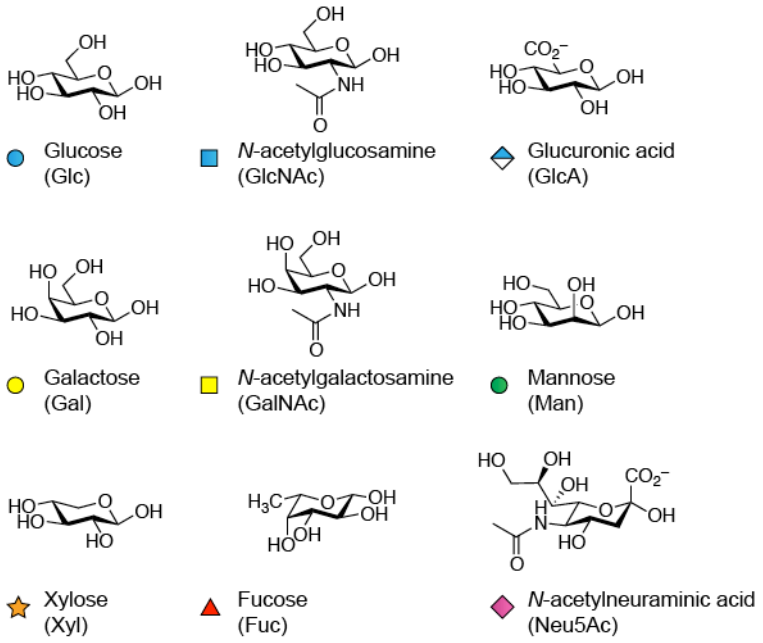

Figure 1.1. Nine common monosaccharide building blocks found in vertebrates. Adapted from Varki *et al.*, *Essentials of Glycobiology, 2nd ed.* (*4*).

Beyond the core attachment of the carbohydrate structure to the underlying protein, these classes of glycans display great diversity. N-glycans and mucin-type O-glycans are frequently decorated by terminal sugars such as fucose and sialic acids (discussed in more detail in Chapters 3 and 4, respectively). Glycosaminoglycans contain long, linear polymers of disaccharide units that undergo extensive remodeling reactions, including epimerization, acetylation, and sulfation, that endow them with specific reactivity.

N-glycans

N-linked glycosylation is an abundant modification of cytosolic, membrane, and secreted proteins. It is initiated by a single enzyme, oligosaccharyltransferase, that transfers a large, pre-assembled oligosaccharide "core", $Glc_3Man_9GlcNAc_2$, onto a nascent protein in the endoplasmic reticulum (ER). The site of this modification is an asparagine residue within the consensus sequence Asn-Xaa-Ser/Thr, where Xaa is any amino acid other than proline (*5*). This consensus sequence is useful for predicting sites of N-linked glycosylation, although only an estimated two-thirds are occupied by a carbohydrate (*6*, *7*). As N-glycans proceed through the ER and Golgi compartments, the original oligosaccharide structures are trimmed down by glycosidase enzymes (*8*). In the Golgi, glycosyltransferases then add diverse monosaccharides such as GlcNAc, Gal, Fuc, and Sia to yield more complex, branched structures (Figure 1.3, panel A) (*9*).

N-glycans play a central role in protein folding through interaction with chaperone proteins in the ER (*10*, *11*). N-glycans also affect protein oligomerization and stability (*12*). At the cell surface, N-glycans have roles in cell-cell interactions and signaling (*13*). Importantly, N-glycans are often modified by extending sugars such as fucose and sialic acids, which form specific epitopes, described in more detail in Chapters 3 and 4, that play important roles in development.

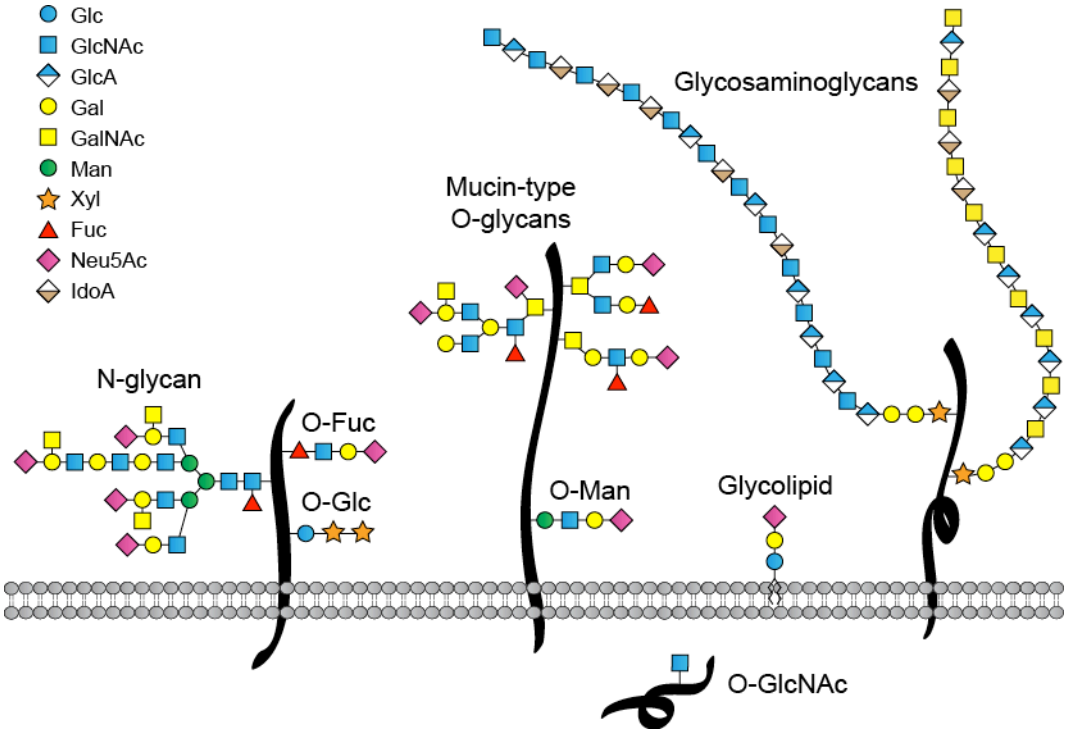

Figure 1.2. Types of glycosylation in eukaryotes. The major classes of cell-surface glycans include N-glycans, mucin-type O-glycans, and glycosaminoglycans. In glycosaminoglycans, GlcA can be epimerized to L-iduronic acid (IdoA). Glycans can also be attached to lipids, as glycolipids. O-fucosylation, O-glucosylation, and O-mannosylation are relatively rare forms of glycosylation. The O-GlcNAc modification is found on cytosolic and nuclear proteins.

Mucin-type O-glycans

Mucin-type O-glycans are a structurally diverse class of glycans characterized by a core GalNAc residue linked in an α configuration to a serine or threonine residue of a protein backbone (*14*, *15*). This core α-GalNAc residue can serve as an attachment point, at its 3- and 6-hydroxyl groups, for further elaboration, resulting in complex, branched structures. A single polypeptide can have many mucin-type O-glycans, which are often clustered together in "mucin domains" that are rich in serine, threonine, and proline residues (*16*) (Figure 1.3, panel B). The conformation of the attachment of α-GalNAc to the protein scaffold forces the polypeptide backbone into an extended conformation (*17*). Therefore, many mucin-type O-glycans are thought to extend far above the cell surface.

There, they contribute to both the physical properties of the cell surface as well as to specific molecular recognition events.

For example, mucin-type O-glycans are highly hydrated and can serve as a protective barrier for cells, particularly those in the digestive and reproductive tracts (*17*). Mucins also play important roles in cell-cell adhesion (*18*), signaling (*19*), sperm-egg fertilization (*20*), and host-pathogen interactions (*21*). Some truncated and aberrantly-sialylated mucins serve as hallmarks of cancer, such as the Tn, sialyl Tn, and sialyl T antigens (*22*). Mucins and the polypeptide GalNAc transferases (ppGalNAcTs) that initiate their biosynthesis are differentially regulated during development (*3*, *23*).

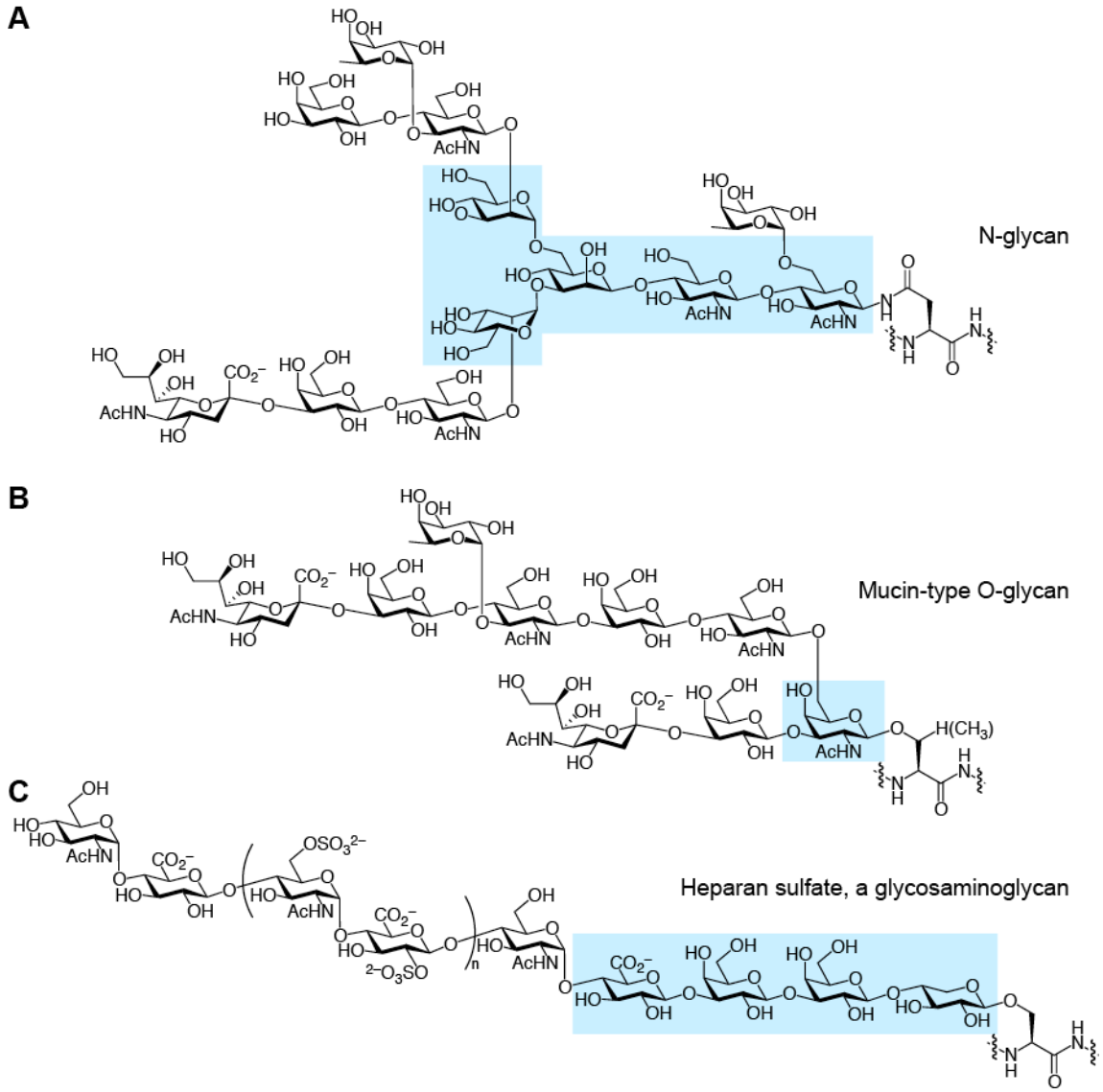

Figure 1.3. Examples of the three major classes of glycoproteins at the cell surface. (A) An N-glycan, with the conserved $Man_3GlcNAc_2$ structure highlighted in blue. (B) A mucin-type O-glycan, with the core GalNAc in blue. (C) A heparan sulfate glycosaminoglycan, with the core GlcA-Gal-Gal-Xyl structure in blue. The repeating disaccharide units (n=40–100), one example of which is shown, can be modified by deacetylation, sulfation, and epimerization.

Glycosaminoglycans

Like mucins, glycosaminoglycans (GAGs) are a class of cell-surface and secreted glycans that play important roles in a variety of biological processes, including embryonic development. When GAGs are linked to proteins called proteoglycans, their biosynthesis is initiated by the addition of Xyl to a serine or threonine residue and further elaboration by two Gal residues and GlcA, resulting in the final linkage tetrasaccharide GlcA-Gal-Gal-Xyl-Ser/Thr. This tetrasaccharide is further extended with tens to thousands of disaccharide units that make up the bulk of the proteoglycan and define the type of GAG. For example, heparan sulfate consists of polymers of GlcNAc-α1,4-GlcA-β1,4 units (Figure 1.3, panel C), and chondroitin sulfate contains GalNAc-β1,4-GlcA-β1,3 units. At specific positions along these long polymers, the disaccharide units are further modified by epimerization, deacetylation, and sulfation reactions (*24*). These processes produce highly charged GAGs with an impressive degree of diversity.

GAGs are a primary constituent of the extracellular matrix (ECM), where they were originally thought to play mostly structural roles (*25*). Cell-surface proteoglycans have since been discovered to participate in many signaling events (*26*-*28*). Heparan-sulfate proteoglycans are essential for Fibroblast growth factor receptor function (*29*) and cooperate with integrins to control cell adhesion (*30*). Proteoglycans are also involved in many signaling pathways, such as Hedgehog and Wnt, that are essential for embryonic development (*31*, *32*).

Methods for Imaging Glycans

Due to the fact that development is an inherently dynamic process, the study of glycans during development would benefit from molecular imaging tools that would enable visualization of glycans in real time. However, because glycans are not directly encoded in the genome, they cannot be imaging using typical genetic techniques for imaging proteins, such as fusion to fluorescent proteins. Glycans are also not recognized by small molecule probes of the types used for imaging metal ions (*33*) and reactive oxygen species (*34*) inside cells.

In nature, glycans are recognized by carbohydrate-binding proteins known as lectins, and there are also several antibodies that recognize glycan epitopes. Alternatively, glycans can be labeled, typically via endogenous metabolic pathways, with small chemical reporter groups that can be visualized through a subsequent reaction with a fluorescent probe.

Glycan-binding lectins and antibodies

Lectins are glycan-binding proteins that are found naturally in most organisms (*35*). Lectins have evolved to recognize specific glycan epitopes, typically monosaccharides or small oligosaccharides, which has made them useful for profiling cell-surface glycans using flow cytometry or fluorescence microscopy. However, lectins are large, multimeric proteins (~25–300 kDa) with poor tissue penetrance, which limits their use in vivo. Additionally, they exhibit relatively low binding affinity for their

epitopes and require multivalency for binding (*36*). Nevertheless, lectins are powerful tools for imaging glycans in fixed samples, and they have been used to visualize mucin-type O-glycans in whole-mount *Drosophila* embryos (*37*) and fucosylated glycans in sectioned zebrafish brain (*38*).

Antibodies are also large proteins (~150 kDa) with limited tissue penetrance, but they typically have high specificity and affinity for their glycan epitopes. Many antibodies have been used to image glycans in fixed cells and tissue sections, including, for example, heparan sulfate and chondroitin sulfate GAGs in sectioned zebrafish embryos (*39*). Mouse and human stem cells are frequently identified using antibodies against the classic stage-specific embryonic antigens (SSEAs), three of which are glycan epitopes found on proteins and lipids (Figure 1.4, panel A) (*40*, *41*). However, only one glycan-binding antibody, MECA-79, has been used to image glycans in a living animal (*42*). In this work, an endothelial glycan that acts as a ligand for the leukocyte adhesion molecule L-selectin was imaged in the lymph nodes of live mice (Figure 1.4, panel B). The inherent bioavailability and specificity limitations posed by large glycan-binding proteins such as lectins and antibodies have prompted the development of a chemical reporter strategy that can be used for dynamic, in vivo imaging.

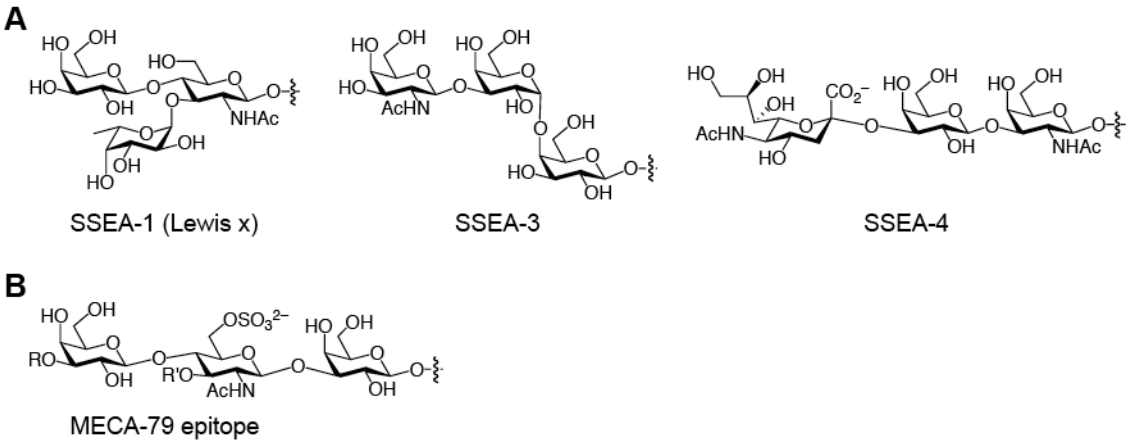

Figure 1.4. Several glycan epitopes that can be imaged using antibodies. (A) Stage-specific embryonic antigens (SSEAs) that can be imaged in cultured cells. SSEA-1 is also known as Lewis x. (B) The glycan epitope of MECA-79, which has been used to image the carbohydrate ligands of L-selectin in the lymph nodes of live mice. In the L-selectin ligand, R and R' are NeuAc and Fuc, respectively.

The chemical reporter strategy for imaging glycans

The chemical reporter strategy is used to introduce small, unnatural chemical groups into cell-surface glycans. These unnatural groups, if sufficiently different from natural functionality on the cell surface, can serve as specific labels, termed chemical reporters, of the glycans to which they are attached (*43*). In a second step, the chemical reporter is reacted with an appropriately-functionalized imaging probe for visualization.

Importantly, this reaction must proceed under physiological conditions and not interfere with the biological system, characteristics that render it bioorthogonal (*44*).

The most common method for introducing chemical reporter groups into glycans is via metabolic labeling. This strategy, pioneered by Mahal *et al.* with ketone-labeled sialic acid precursors (*45*), takes advantage of the tolerance of endogenous biosynthetic pathways for small chemical modifications. In this approach, cells are typically treated with a cell-permeable, per-*O*-acetylated version of a precursor monosaccharide that has been chemically modified with a reporter group such as a ketone, azide, or alkyne (Figure 1.5). If the modification is small enough, the unnatural sugar analog will be accepted by the necessary biosynthetic enzymes and become installed on nascent glycans. This metabolic incorporation strategy is the most versatile technique for labeling glycans because the chemical reporter group can be selected by the researcher.

Sialic acids in particular can also be labeled using a non-metabolic, chemical method (Figure 1.5, panel B). It has long been known that an aldehyde can be introduced at the C7 position of sialic acid by mild periodate treatment, which does not oxidize other monosaccharides at low concentrations. Paulson and coworkers recently utilized this unique reactivity to introduce aldehydes into sialylated glycans on the surface of cells (*46*).

Once labeled with chemical reporter groups, glycans can be imaged via bioorthogonal ligations to appropriately-functionalized probe molecules. Several bioorthogonal reactions have been developed to proceed rapidly under physiological conditions and create covalent ligation products that can be purified or imaged.

The earliest chemical reporters took advantage of the facile condensation reactions of aldehydes and ketones with hydrazide and aminooxy probes (Figure 1.6). These reactions take place in aqueous solution, and although they proceed most rapidly at acidic pH, they can be accelerated at pH 7 by an aniline catalyst (*46*, *47*). One drawback of this reaction, however, is that the hydrazone and oxime ligation products are susceptible to hydrolysis in aqueous solution (*48*).

The development of several recent bioorthogonal reactions has expanded the possibilities for imaging glycans using the chemical reporter strategy. Among the most exciting chemical reporter groups is the azide, N_3. The azide is small, kinetically stable, and completely absent from biological systems. Azides react specifically with triarylphosphine reagents, terminal alkynes in the presence of copper(I) catalyst, and cycloctyne reagents to form covalent ligation products. The azide has been incorporated into many different biomolecules in living systems, including proteins (*49*, *50*), nucleic acids (*51*, *52*), lipids (*53*), and glycans. Among glycans, the azide has been metabolically incorporated into sialic acids (*54*), mucin-type O-glycans (*55*), and fucosylated glycans (*56*), and has been used to image all three of these classes of glycans in living zebrafish (*57-59*).

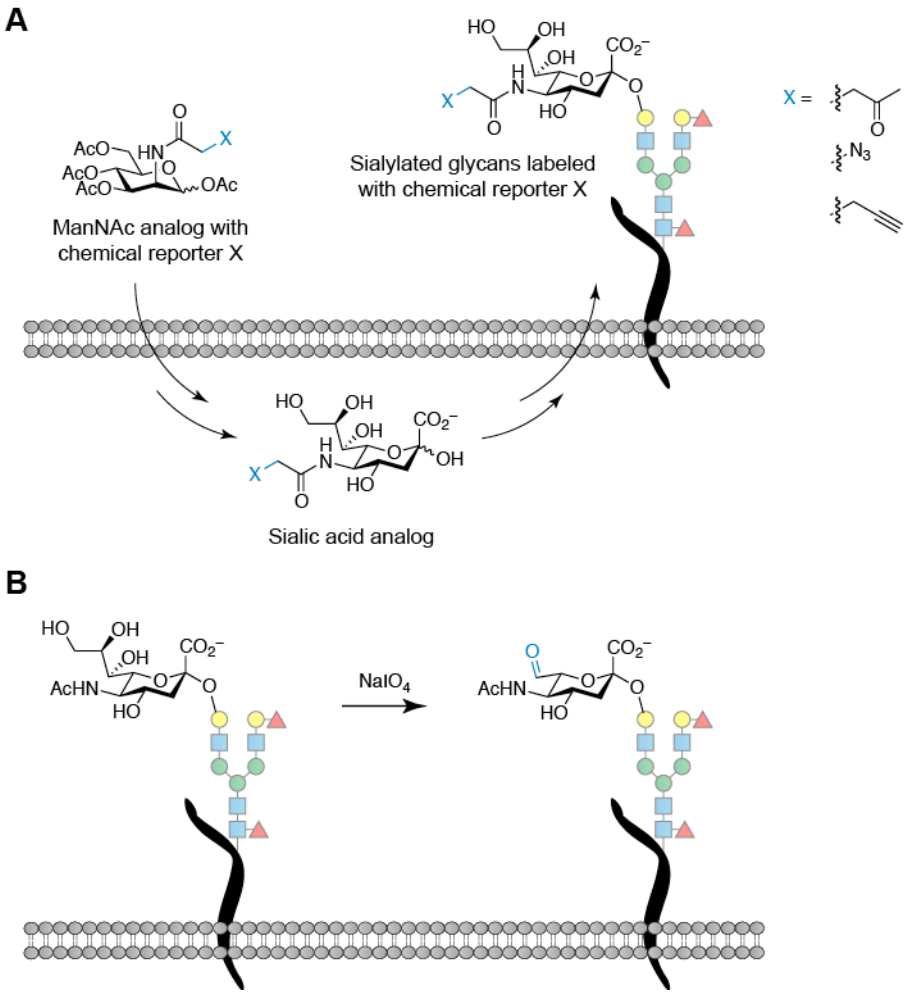

Figure 1.5. Methods for introducing chemical reporter groups into glycans. (A) A chemical reporter group is introduced into sialic acids via metabolic incorporation. Cells are treated with a ManNAc analog bearing the chemical reporter group X. This analog traverses the sialic acid salvage pathway and is incorporated into cell-surface glycans. (B) Sodium periodate specifically oxidizes sialic acids at the cell surface, endowing them with an aldehyde chemical reporter.

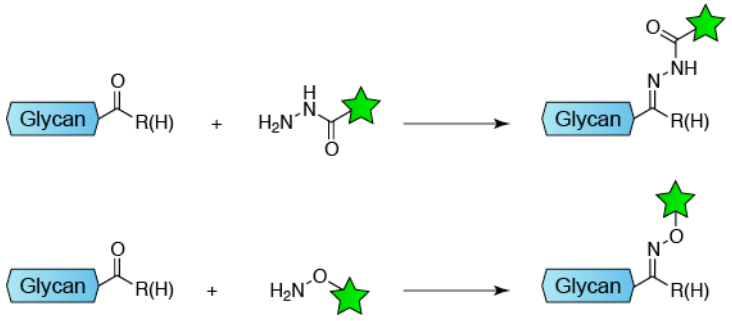

Figure 1.6. Condensation of aldehydes and ketones with hydrazide and aminooxy reagents.

The first bioorthogonal reaction developed for azides, termed the Staudinger ligation, exploits the mechanism of the Staudinger reduction to trap a reactive intermediate and form a covalent amide bond between the azide-bearing glycan and a triarylphosphine reagent (Figure 1.7, panel A) (*54*). This reaction suffers from relatively slow reaction kinetics (with a bimolecular rate constant of $k = 2 \times 10^{-3}$ $M^{-1}s^{-1}$), and the triarylphosphine reagents are susceptible to oxidation in air (*60*). Nevertheless, Staudinger reagents exhibit good bioavailability within living animals and have been the most successful reagents developed to date for labeling azidosugars in live mice (*61*, *62*).

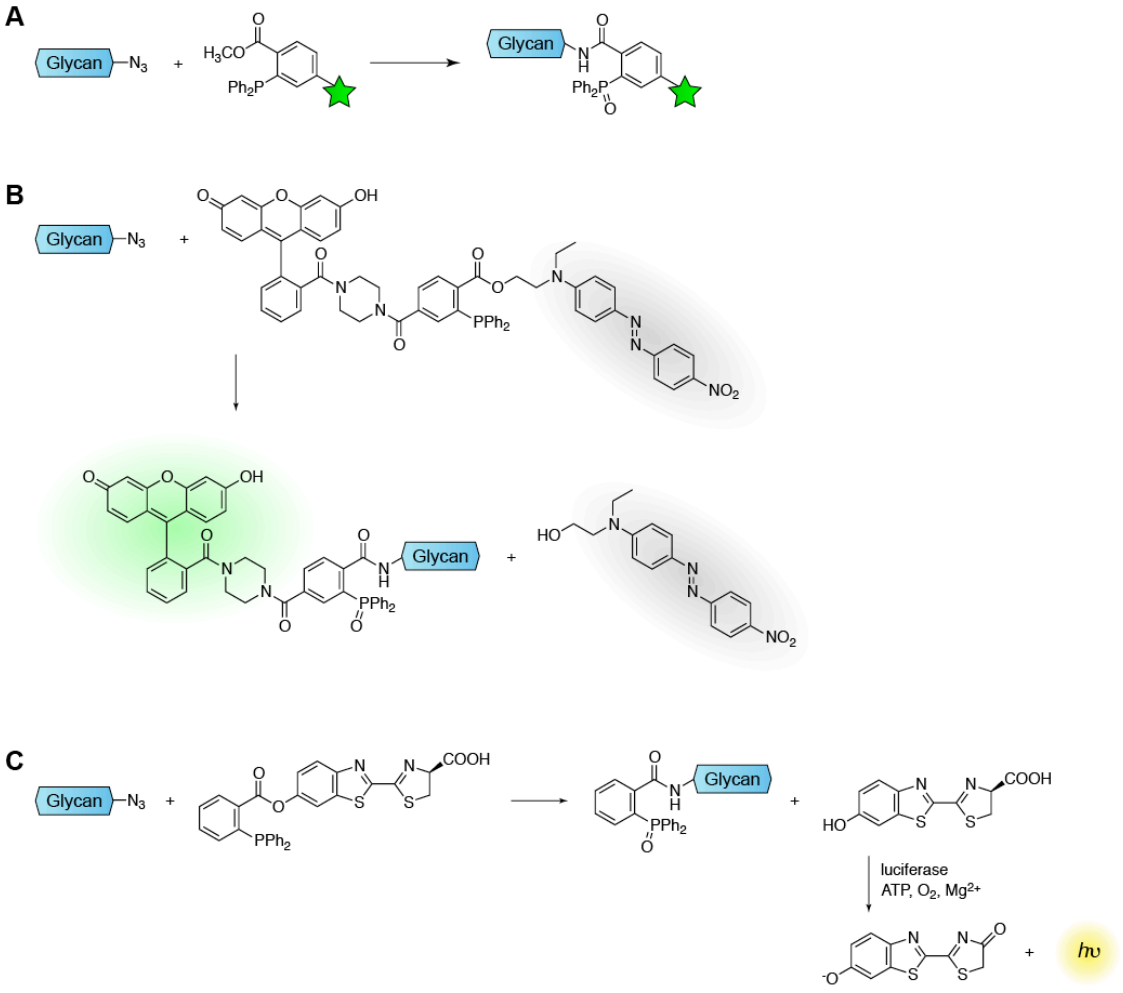

Figure 1.7. The Staudinger ligation between azides and triarylphosphine reagents. (A) Overview of the Staudinger ligation. (B) A FRET-based fluorogenic probe. Upon reaction with azide, the quencher molecule is released and the probe becomes fluorescent. (C) A luciferin-modified triarylphosphine reagent for bioluminescence imaging. Upon reaction with azide, a molecule of luciferin is released and turned over by luciferase to produce a photon of light.

Furthermore, the unique mechanism of the Staudinger ligation, in which an ester bond is cleaved during the course of the reaction, has provided opportunities for

specialized imaging probes. By attaching a quencher group at the ester position, Hangauer *et al.* developed a FRET-based fluorogenic triarylphosphine probe that became fluorescent only upon reaction with azides and used it to image glycans on live cells (Figure 1.7, panel B) (*63*). To create a probe for bioluminescence imaging, Cohen *et al.* attached luciferin at the ester position so that upon reaction with azides, free luciferin was released and utilized by endogenous luciferase to produce a photon of light (Figure 1.7, panel C) (*64*).

Another unique means of reactivity for the azide is as a 1,3-dipole in the [3+2] Huisgen cycloaddition reaction with alkynes (*65*). Normally, this reaction requires high temperatures that would be incompatible with biological systems (*66*). However, recent work has demonstrated that this reaction can be activated by copper(I) catalysis or ring strain.

The copper(I)-catalyzed "click" reaction developed independently by Sharpless and Meldal produces triazole products between azides and terminal alkynes reagents (Figure 1.8, panel A) (*67*, *68*). This reaction is very fast and proceeds in water under physiological conditions. However, the Cu(I) catalyst is toxic to cells, which has limited its use in living systems, although the development of ligands that reduce the toxicity of the Cu(I) metal may extend its utility (*69*, *70*). Because, like an azide, a terminal alkyne is a small chemical group that is absent from biological systems, it too has been used as a chemical reporter. In this case, alkyne-labeled glycans are reacted in a second step with an azido probe, frequently 3-azidocoumarin, which becomes fluorescent once it reacts with an alkyne (Figure 1.8, panel B) (*71*, *72*). Alkynyl substrates have been used to image sialylated and fucosylated glycans (*73*, *74*), as well as proteins (*72*), nucleic acids (*52*), and lipids (*75*, *76*).

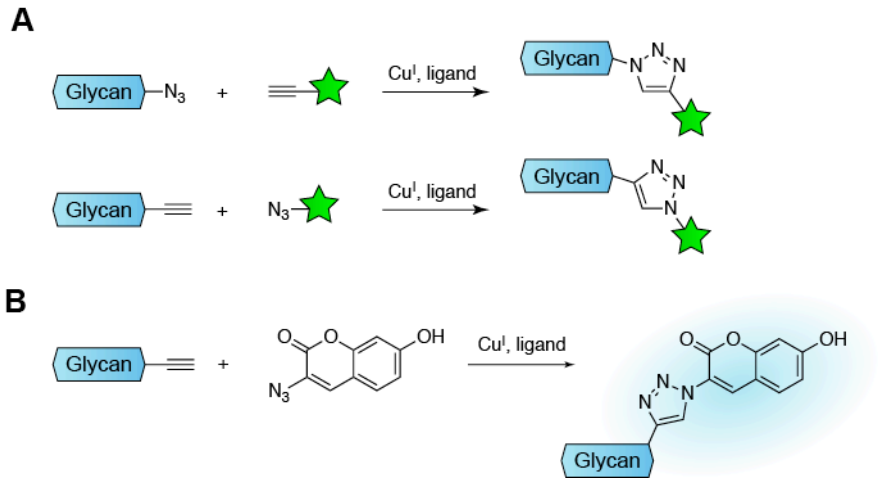

Figure 1.8. Copper-catalyzed click reaction between azides and terminal alkynes. (A) Overview of the cycloaddition reaction to produce a triazole-containing product. Either the azide or the alkyne can be incorporated into glycans, then reacted with the appropriate reaction partner in the presence of copper(I) and ligand. (B) A fluorogenic azido-coumarin reagent that becomes fluorescent upon reaction with terminal alkynes.

As an alternative to copper(I) catalysis, the azide-alkyne cycloaddition reaction can be activated by ring strain (Figure 1.9, panel A). When the alkyne is placed in an eight-membered ring, the angles around the triple bond are constrained from the ideal 180° to approximately 160° (*77*), which contributes to ring strain of ~18 kcal/mol (*78*). With such a highly destabilized ground state, the cycloaddition reaction with azide to produce the triazole product proceeds under metal-free and physiological conditions (*79*). The rate of this reaction with a simple cyclooctyne reagent, such as OCT (Figure 1.9, panel B), is similar to that of the Staudinger ligation, with a bimolecular rate constant k = 2.4 x 10^{-3} $M^{-1}s^{-1}$. The kinetics of this reaction have been enhanced by installation of electron-withdrawing fluorine atoms, as in the difluorinated cyclooctyne (DIFO) reagent (Figure 1.9, panel B), which reacts rapidly enough with azides (k = 7.6 x 10^{-2} $M^{-1}s^{-1}$) to enable imaging of glycan trafficking on the minute timescale (*80*). The ring strain of cyclooctyne reagents can be increased by the addition of aryl groups, as demonstrated by 4-dibenzocyclooctynol (DIBO) (*81*) and biarylazacycloctynone (BARAC) (*82*) reagents (Figure 1.9, panel B), the latter of which exhibits the fastest bimolecular rate constant reported to date (k = 0.96 $M^{-1}s^{-1}$) and has been used to image sialylated glycans on the surface of living cells at concentrations as low as 100 nM. Apparently, the all-carbon core of some of these reagents may lead to sequestration by serum proteins, resulting in reduced bioavailability in living animals. A more hydrophilic cyclooctyne, 6,7-dimethoxyazacyclooct-4-yne (DIMAC) (Figure 1.9, panel B) (*83*), shows superior labeling in live mice (*62*). Further research in this area continues to yield new reagents with improved solubility properties and reaction rates that could facilitate live animal imaging.

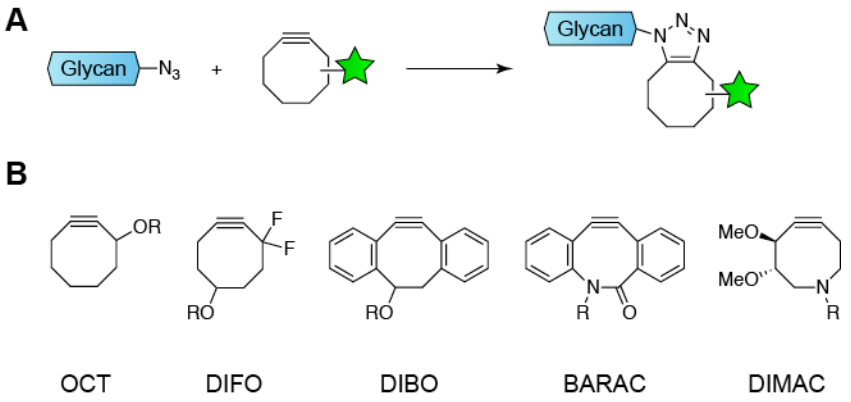

Figure 1.9. Copper-free click reaction between azides and cyclooctyne reagents. (A) Overview of the cyclization reaction, in the absence of copper, to produce a triazole product. (B) Several cyclooctyne reagents developed to date.

These various bioorthogonal ligation reactions provide several options for imaging of glycans. Further improvements to reaction rates and biocompatibility will expand this toolkit further. Importantly, the existence of several different reactions that are orthogonal to one other raises possibilities for imaging several classes of

biomolecules at once. This strategy has been applied to labeling mucin-type O-glycans and sialylated glycans simultaneously in living cells (*84*) and zebrafish (*59*).

Conclusion

The unique challenges glycans pose for imaging, in large part because of their complex structures and biosynthesis, has led to the development of new methods for their labeling and visualization. In particular, the chemical reporter method has enabled imaging of several classes of glycans and has also been extended to other classes of biomolecules. Further improvements in these technologies should help to expand the capabilities for imaging glycans in live cells and multicellular organisms.

In this dissertation, I describe chemical methods for metabolic labeling and visualization of several classes of glycans in live zebrafish. Chapter 2 describes visualization of mucin-type O-glycans as early as 7 hours post-fertilization (hpf) via microinjection of azide-functionalized GalNAc precursors. This strategy was extended in Chapter 3 by utilizing downstream metabolic precursors to label and image fucosylated glycans, which could not be labeled using the fucose salvage pathway. In Chapter 4, sialylated glycans labeled with azide-functionalized precursors that enabled dynamic imaging over the first five days of development. Finally, in Chapter 5, a non-metabolic labeling strategy using perioxide oxidation of sialic acids enabled their imaging via the aldehyde-aminooxy condensation reaction. Because this reaction is orthogonal to the azide-alkyne cycloaddition, this technique provided a means to image mucin-type O-glycans and sialylated glycans simultaneously.

References

1. Varki, A. (1993) Biological roles of oligosaccharides: all of the theories are correct, *Glycobiology 3*, 97-130.

2. Varki, A. (2008) Sialic acids in human health and disease, *Trends Mol. Med. 14*, 351-360.

3. Haltiwanger, R. S., and Lowe, J. B. (2004) Role of glycosylation in development, *Annu. Rev. Biochem. 73*, 491-537.

4. Varki, A., Cummings, R. D., Esko, J. D., Freeze, H. H., Stanley, P., Bertozzi, C. R., Hart, G. W., and Etzler, M. E. (2009) Essentials of Glycobiology, Cold Spring Harbor Laboratory Press, Cold Spring Harbor, N.Y.

5. Imperiali, B., and Hendrickson, T. L. (1995) Asparagine-linked glycosylation: Specificity and function of oligosaccharyl transferase, *Bioorg. Med. Chem. 3*, 1565-1578.

6. Apweiler, R., Hermjakob, H., and Sharon, N. (1999) On the frequency of protein glycosylation, as deduced from analysis of the SWISS-PROT database, *Biochim. Biophys. Acta 1473*, 4-8.

7. Petrescu, A.-J., Milac, A.-L., Petrescu, S. M., Dwek, R. A., and Wormald, M. R. (2004) Statistical analysis of the protein environment of N-glycosylation sites: implications for occupancy, structure, and folding, *Glycobiology 14*, 103-114.

8. Herscovics, A. (1999) Importance of glycosidases in mammalian glycoprotein biosynthesis, *Biochim. Biophys. Acta 1473*, 96-107.

9. Roth, J. (2002) Protein N-glycosylation along the secretory pathway: Relationship to organelle topography and function, protein quality control, and cell interactions, *Chem. Rev. 102*, 285-304.

10. Molinari, M. (2007) N-glycan structure dictates extension of protein folding or onset of disposal, *Nat. Chem. Biol. 3*, 313-320.

11. Helenius, A., and Aebi, M. (2004) Roles of N-linked glycans in the endoplasmic reticulum, *Annu. Rev. Biochem. 73*, 1019-1049.

12. Mitra, N., Sinha, S., Ramya, T. N. C., and Surolia, A. (2006) N-linked oligosaccharides as outfitters for glycoprotein folding, form and function, *Trends Biochem. Sci. 31*, 156-163.

13. Crocker, P. R. (2002) Siglecs: sialic-acid-binding immunoglobulin-like lectins in cell-cell interactions and signalling, *Curr. Opin. Struct. Biol. 12*, 609-615.

14. Strous, G. J., and Dekker, J. (1992) Mucin-type glycoproteins, *Crit. Rev. Biochem. Mol. Biol 27*, 57-92.

15. Hang, H. C., and Bertozzi, C. R. (2005) The chemistry and biology of mucin-type O-linked glycosylation, *Bioorg. Med. Chem. 13*, 5021-5034.

16. Perez-Vilar, J., and Hill, R. L. (1999) The structure and assembly of secreted mucins, *J. Biol. Chem. 274*, 31751-31754.

17. Bansil, R., Stanley, E., and LaMont, J. T. (1995) Mucin biophysics, *Annu. Rev. Physiol. 57*, 635-657.

18. Fukuda, M. (2002) Roles of mucin-type O-glycans in cell adhesion, *Biochim. Biophys. Acta 1573*, 394-405.

19. Carraway, K. L., Ramsauer, V. P., Haq, B., and Carothers Carraway, C. A. (2003) Cell signaling through membrane mucins, *BioEssays 25*, 66-71.

20. Wassarman, P. M. (2008) Zona pellucida glycoproteins, *J. Biol. Chem. 283*, 24285-24289.

21. Dharmani, P., Srivastava, V., Kissoon-Singh, V., and Chadee, K. (2009) Role of intestinal mucins in innate host defense mechanisms against pathogens, *J. Innate Immun. 1*, 123-135.

22. Brockhausen, I. (1999) Pathways of O-glycan biosynthesis in cancer cells, *Biochim. Biophys. Acta 1473*, 67-95.

23. Kingsley, P. D., Hagen, K. G. T., Maltby, K. M., Zara, J., and Tabak, L. A. (2000) Diverse spatial expression patterns of UDP-GalNAc:polypeptide N-acetylgalactosaminyl-transferase family member mRNAs during mouse development, *Glycobiology 10*, 1317-1323.

24. Esko, J. D., and Selleck, S. B. (2002) Order out of chaos: Assembly of ligand binding sites in heparan sulfate, *Annu. Rev. Biochem. 71*, 435-471.

25. Schaefer, L., and Schaefer, R. M. (2010) Proteoglycans: from structural compounds to signaling molecules, *Cell Tissue Res. 339*, 237-246.

26. Elfenbein, A., and Simons, M. (2010) Auxiliary and autonomous proteoglycan signaling networks, *Methods Enzymol. 480*, 3-31.

27. Couchman, J. R. (2010) Transmembrane signaling proteoglycans, *Annu. Rev. Cell Dev. Biol. 26*, 89-114.

28. Tumova, S., Woods, A., and Couchman, J. R. (2000) Heparan sulfate proteoglycans on the cell surface: versatile coordinators of cellular functions, *Int. J. Biochem. Cell Biol. 32*, 269-288.

29. Spivak-Kroizman, T., Lemmon, M. A., Dikic, I., Ladbury, J. E., Pinchasi, D., Huang, J., Jaye, M., Crumley, G., Schlessinger, J., and Lax, I. (1994) Heparin-induced oligomerization of FGF molecules is responsible for FGF receptor dimerization, activation, and cell proliferation, *Cell 79*, 1015-1024.

30. Morgan, M. R., Humphries, M. J., and Bass, M. D. (2007) Synergistic control of cell adhesion by integrins and syndecans, *Nat. Rev. Mol. Cell Biol. 8*, 957-969.

31. Lin, X. (2004) Functions of heparan sulfate proteoglycans in cell signaling during development, *Development 131*, 6009-6021.

32. Hacker, U., Nybakken, K., and Perrimon, N. (2005) Heparan sulphate proteoglycans: the sweet side of development, *Nat. Rev. Mol. Cell Biol. 6*, 530-541.

33. Domaille, D. W., Que, E. L., and Chang, C. J. (2008) Synthetic fluorescent sensors for studying the cell biology of metals, *Nat. Chem. Biol. 4*, 168-175.

34. Chang, M. C. Y., Pralle, A., Isacoff, E. Y., and Chang, C. J. (2004) A selective, cell-permeable optical probe for hydrogen peroxide in living cells, *J. Am. Chem. Soc. 126*, 15392-15393.

35. Lis, H., and Sharon, N. (1998) Lectins: carbohydrate-specific proteins that mediate cellular recognition, *Chem. Rev. 98*, 637-674.

36. Lee, Y. C., and Lee, R. T. (1995) Carbohydrate-protein interactions: basis of glycobiology, *Acc. Chem. Res. 28*, 321-327.

37. Tian, E., and Hagen, K. G. T. (2007) O-linked glycan expression during *Drosophila* development, *Glycobiology 17*, 820-827.

38. Ohata, S., Kinoshita, S., Aoki, R., Tanaka, H., Wada, H., Tsuruoka-Kinoshita, S., Tsuboi, T., Watabe, S., and Okamoto, H. (2009) Neuroepithelial cells require fucosylated glycans to guide the migration of vagus motor neuron progenitors in the developing zebrafish hindbrain, *Development 136*, 1653-1663.

39. Dolez, M., Nicolas, J.-F., and Hirsinger, E. (2011) Laminins, via heparan sulfate proteoglycans, participate in zebrafish myotome morphogenesis by modulating the pattern of Bmp responsiveness, *Development 138*, 97-106.

40. Muramatsu, T., and Muramatsu, H. (2004) Carbohydrate antigens expressed on stem cells and early embryonic cells, *Glycoconjugate J. 21*, 41-45.

41. Lanctot, P. M., Gage, F. H., and Varki, A. P. (2007) The glycans of stem cells, *Curr. Opin. Chem. Biol. 11*, 373-380.

42. Licha, K., Debus, N., Emig-Vollmer, S., Hofmann, B., Hasbach, M., Stibenz, D., Sydow, S., Schirner, M., Ebert, B., Petzelt, D., Bührer, C., Semmler, W., and Tauber,

R. (2005) Optical molecular imaging of lymph nodes using a targeted vascular contrast agent, *J. Biomed. Opt. 10*, 041205.

43. Laughlin, S. T., and Bertozzi, C. R. (2009) Imaging the glycome, *Proc. Natl. Acad. Sci. U.S.A. 106*, 12-17.

44. Sletten, E. M., and Bertozzi, C. R. (2009) Bioorthogonal chemistry: Fishing for selectivity in a sea of functionality, *Angew. Chem. Int. Ed. 48*, 6974-6998.

45. Mahal, L. K., Yarema, K. J., and Bertozzi, C. R. (1997) Engineering chemical reactivity on cell surfaces through oligosaccharide biosynthesis, *Science 276*, 1125-1128.

46. Zeng, Y., Ramya, T. N. C., Dirksen, A., Dawson, P. E., and Paulson, J. C. (2009) High-efficiency labeling of sialylated glycoproteins on living cells, *Nat. Methods 6*, 207-209.

47. Dirksen, A., Hackeng, T. M., and Dawson, P. E. (2006) Nucleophilic catalysis of oxime ligation, *Angew. Chem. Int. Ed. 45*, 7581-7584.

48. Kalia, J., and Raines, R. T. (2008) Hydrolytic stability of hydrazones and oximes, *Angew. Chem. Int. Ed. 47*, 7523-7526.

49. Kiick, K. L., Saxon, E., Tirrell, D. A., and Bertozzi, C. R. (2002) Incorporation of azides into recombinant proteins for chemoselective modification by the Staudinger ligation, *Proc. Natl. Acad. Sci. U.S.A. 99*, 19-24.

50. Chin, J. W., Cropp, T. A., Anderson, J. C., Mukherji, M., Zhang, Z., and Schultz, P. G. (2003) An expanded eukaryotic genetic code, *Science 301*, 964-967.

51. Sylvers, L. A., and Wower, J. (1993) Nucleic acid-incorporated azidonucleotides: Probes for studying the interaction of RNA or DNA with proteins and other nucleic acids, *Bioconjugate Chem. 4*, 411-418.

52. Salic, A., and Mitchison, T. J. (2008) A chemical method for fast and sensitive detection of DNA synthesis in vivo, *Proc. Natl. Acad. Sci. U.S.A. 105*, 2415-2420.

53. Hang, H. C., Geutjes, E.-J., Grotenbreg, G., Pollington, A. M., Bijlmakers, M. J., and Ploegh, H. L. (2007) Chemical probes for the rapid detection of fatty-acylated proteins in mammalian cells, *J. Am. Chem. Soc. 129*, 2744-2745.

54. Saxon, E., and Bertozzi, C. R. (2000) Cell surface engineering by a modified Staudinger reaction, *Science 287*, 2007-2010.

55. Hang, H. C., Yu, C., Kato, D. L., and Bertozzi, C. R. (2003) A metabolic labeling approach toward proteomic analysis of mucin-type O-linked glycosylation, *Proc. Natl. Acad. Sci. U.S.A. 100*, 14846-14851.

56. Rabuka, D., Hubbard, S. C., Laughlin, S. T., Argade, S. P., and Bertozzi, C. R. (2006) A chemical reporter strategy to probe glycoprotein fucosylation, *J. Am. Chem. Soc. 128*, 12078-12079.

57. Laughlin, S. T., Agard, N. J., Baskin, J. M., Carrico, I. S., Chang, P. V., Ganguli, A. S., Hangauer, M. J., Lo, A., Prescher, J. A., and Bertozzi, C. R. (2006) Metabolic labeling of glycans with azido sugars for visualization and glycoproteomics, *Methods Enzymol. 415*, 230-250.

58. Baskin, J. M., Dehnert, K. W., Laughlin, S. T., Amacher, S. L., and Bertozzi, C. R. (2010) Visualizing enveloping layer glycans during zebrafish early embryogenesis, *Proc. Natl. Acad. Sci. U.S.A. 107*, 10360-10365.

59. Dehnert, K. W., Beahm, B. J., Huynh, T. T., Baskin, J. M., Laughlin, S. T., Wang, W., Wu, P., Amacher, S. L., and Bertozzi, C. R. (2011) Metabolic labeling of fucosylated glycans in developing zebrafish, *ACS Chem. Biol.* in press.

60. Lin, F. L., Hoyt, H. M., van Halbeek, H., Bergman, R. G., and Bertozzi, C. R. (2005) Mechanistic investigation of the Staudinger ligation, *J. Am. Chem. Soc. 127*, 2686-2695.

61. Prescher, J. A., Dube, D. H., and Bertozzi, C. R. (2004) Chemical remodelling of cell surfaces in living animals, *Nature 430*, 873-877.

62. Chang, P. V., Prescher, J. A., Sletten, E. M., Baskin, J. M., Miller, I. A., Agard, N. J., Lo, A., and Bertozzi, C. R. (2010) Copper-free click chemistry in living animals, *Proc. Natl. Acad. Sci. U.S.A. 107*, 1821-1826.

63. Hangauer, M. J., and Bertozzi, C. R. (2008) A FRET-based fluorogenic phosphine for live-cell imaging with the Staudinger ligation, *Agnew. Chem. Int. Ed. 47*, 2394-2397.

64. Cohen, A. S., Dubikovskaya, E. A., Rush, J. S., and Bertozzi, C. R. (2010) Real-time bioluminescence imaging of glycans on live cells, *J. Am. Chem. Soc. 132*, 8563-8565.

65. Huisgen, R. (1963) 1,3-Dipolar cycloadditions. Past and future, *Angew. Chem. Int. Ed. 2*, 565-598.

66. Hartzel, L. W., and Benson, F. R. (1954) Synthesis of 4-alkyl-v-triazoles from acetylenic compounds and hydrogen azide, *J. Am. Chem. Soc. 76*, 667-670.

67. Rostovtsev, V. V., Green, L. G., Fokin, V. V., and Sharpless, K. B. (2002) A stepwise huisgen cycloaddition process: Copper(I)-catalyzed regioselective "ligation" of azides and terminal alkynes, *Angew. Chem. Int. Ed. 41*, 2596-2599.

68. Tornøe, C. W., Christensen, C., and Meldal, M. (2002) Peptidotriazoles on solid phase: [1,2,3]-triazoles by regiospecific copper(I)-catalyzed 1,3-dipolar cycloadditions of terminal alkynes to azides, *J. Org. Chem. 67*, 3057-3064.

69. Soriano del Amo, D., Wang, W., Jiang, H., Besanceney, C., Yan, A. C., Levy, M., Liu, Y., Marlow, F. L., and Wu, P. (2010) Biocompatible copper(I) catalysts for in vivo imaging of glycans, *J. Am. Chem. Soc. 132*, 16893-16899.

70. Hong, V., Steinmetz, N. F., Manchester, M., and Finn, M. G. (2010) Labeling live cells by copper-catalyzed alkyne−azide click chemistry, *Bioconjugate Chem. 21*, 1912-1916.

71. Sivakumar, K., Xie, F., Cash, B. M., Long, S., Barnhill, H. N., and Wang, Q. (2004) A fluorogenic 1,3-dipolar cycloaddition reaction of 3-azidocoumarins and acetylenes, *Org. Lett. 6*, 4603-4606.

72. Beatty, K. E., Liu, J. C., Xie, F., Dieterich, D. C., Schuman, E. M., Wang, Q., and Tirrell, D. A. (2006) Fluorescence visualization of newly synthesized proteins in mammalian cells, *Angew. Chem. Int. Ed. 45*, 7364-7367.

73. Hsu, T.-L., Hanson, S. R., Kishikawa, K., Wang, S.-K., Sawa, M., and Wong, C.-H. (2007) Alkynyl sugar analogs for the labeling and visualization of glycoconjugates in cells, *Proc. Natl. Acad. Sci. U.S.A 104*, 2614-2619.

74. Sawa, M., Hsu, T.-L., Itoh, T., Sugiyama, M., Hanson, S. R., Vogt, P. K., and Wong, C.-H. (2006) Glycoproteomic probes for fluorescent imaging of fucosylated glycans in vivo, *Proc. Natl. Acad. Sci. U.S.A. 103*, 12371-12376.

75. Neef, A. B., and Schultz, C. (2009) Selective fluorescence labeling of lipids in living cells, *Angew. Chem. Int. Ed. 48*, 1498-1500.

76. Jao, C. Y., Roth, M., Welti, R., and Salic, A. (2009) Metabolic labeling and direct imaging of choline phospholipids in vivo, *Proc. Natl. Acad. Sci. U.S.A. 106*, 15332-15337.

77. Meier, H., Petersen, H., and Kolshorn, H. (1980) Die ringspannung von cycloalkinen und ihre spektroskopischen auswirkungen, *Chem. Ber. 113*, 2398-2409.

78. Turner, R. B., Jarrett, A. D., Goebel, P., and Mallon, B. J. (1973) Heats of hydrogenation. IX. Cyclic acetylenes and some miscellaneous olefins, *J. Am. Chem. Soc. 95*, 790-792.

79. Agard, N. J., Prescher, J. A., and Bertozzi, C. R. (2004) A strain-promoted [3 + 2] azide-alkyne cycloaddition for covalent modification of biomolecules in living systems, *J. Am. Chem. Soc. 126*, 15046-15047.

80. Baskin, J. M., Prescher, J. A., Laughlin, S. T., Agard, N. J., Chang, P. V., Miller, I. A., Lo, A., Codelli, J. A., and Bertozzi, C. R. (2007) Copper-free click chemistry for dynamic in vivo imaging, *Proc. Natl. Acad. Sci. U.S.A. 104*, 16793-16797.

81. Ning, X., Guo, J., Wolfert, M. A., and Boons, G. (2008) Visualizing metabolically labeled glycoconjugates of living cells by copper-free and fast Huisgen cycloadditions, *Angew. Chem. Int. Ed. 47*, 2253-2255.

82. Jewett, J. C., Sletten, E. M., and Bertozzi, C. R. (2010) Rapid Cu-free click chemistry with readily synthesized biarylazacyclooctynones, *J. Am. Chem. Soc. 132*, 3688-3690.

83. Sletten, E. M., and Bertozzi, C. R. (2008) A hydrophilic azacyclooctyne for Cu-free click chemistry, *Org. Lett. 10*, 3097-3099.

84. Chang, P. V., Prescher, J. A., Hangauer, M. J., and Bertozzi, C. R. (2007) Imaging cell surface glycans with bioorthogonal chemical reporters, *J. Am. Chem. Soc. 129*, 8400-8401.

Chapter 2

Visualization of Mucin-type O-Glycans during Early Embryogenesis

Chapter 2: Visualization of Mucin-type O-Glycans during Early Embryogenesis[1]

Introduction

Embryogenesis is a highly dynamic process characterized by rapid cell division, differentiation, cell migration, and morphogenesis (*1*). Developmental biologists have sought noninvasive imaging techniques to capture in detail these physiological changes (*2*-*4*). Molecular imaging tools such as fluorescent protein fusions and antibody conjugates, which can be used to track specific biomolecules in vivo, have enhanced our understanding of embryogenesis at a molecular level (*5*). The zebrafish, a popular vertebrate model of embryogenesis, has provided deep insight into the cellular and molecular details of development by virtue of its transparent embryos and external development (*6*). The zebrafish was thus an ideal model organism to apply chemical tools for imaging glycans, which are key regulators of developmental processes but are difficult to visualize (*7*).

All cells are decorated with glycans, which are oligosaccharide structures found as post-translational modifications of integral membrane proteins and as head groups of membrane-resident lipids (*8*). In development, glycans have numerous functions, which derive from both their bulk properties as well as their specific molecular structures (*9*). However, genetic redundancy amongst biosynthetic genes has frustrated efforts to study certain classes of glycans, notably mucin-type O-glycans (*9*). Critically, glycans cannot be visualized easily using the standard tools of molecular imaging due to the non-genetically encoded nature of their biosynthesis and the dearth of available glycan-binding antibodies (*7*, *10*).

We have developed a two-step chemical strategy for labeling glycans with imaging agents in vivo. This approach entails (a) metabolic labeling with synthetic azidosugars that hijack glycan biosynthesis, followed by (b) covalent chemical tagging of the azide-labeled glycans with a compound bearing both an azide-reactive group and an imaging probe (*11*). In previous work, we showed that a membrane-permeable azidosugar, peracetylated *N*-azidoacetylgalactosamine (Ac_4GalNAz), can be used to metabolically label mucin-type O-glycans in developing zebrafish (*12*). In a second step, the metabolically labeled zebrafish larvae were incubated in solutions containing a fluorophore conjugate of a difluorinated cyclooctyne (DIFO) reagent, enabling visualization of glycans in vivo using copper-free click chemistry (*12*, *13*).

Those studies revealed dramatic differences in cell-surface expression, intracellular trafficking patterns, and tissue distributions of glycans at different stages of zebrafish larval development. However, we were unable to detect labeled glycans in zebrafish embryos earlier than 24 hours post-fertilization (hpf). Because many important developmental events including cell migration, tissue morphogenesis, and cell differentiation occur in the first 24 hours of zebrafish embryogenesis, and glycan biosynthesis is known to occur before 24 hpf (*14*, *15*), we sought to develop new methods to image glycans in early embryos.

[1] Jeremy Baskin and Scott Laughlin contributed to the work presented in this chapter.

Here we report that microinjection of azidosugars enables imaging of cell-surface glycans in the enveloping layer of zebrafish embryos as early as 7 hpf, a few hours after expression of zygotic genes is known to occur (*16*). Additionally, we employed a complementary, non-metabolic method to target a second class of glycans, those bearing sialic acid. This technological advance enabled the simultaneous imaging of both classes of glycans in vivo. Time-lapse and multicolor imaging experiments highlighted differences between O-glycans and sialylated glycans in the cells of the enveloping layer during the gastrulation and segmentation periods. Our studies also revealed a dramatic and rapid reorganization of cell-surface glycans during mitosis.

Results and Discussion

Microinjection of the nucleotide sugar UDP-GalNAz enables visualization of glycans during gastrulation

En route to incorporation into mucin-type O-glycans, Ac_4GalNAz must first traverse the biosynthetic steps of the *N*-acetylgalactosamine (GalNAc) salvage pathway, resulting in its conversion to the nucleotide sugar uridine diphosphatidyl *N*-azidoacetylgalactosamine (UDP-GalNAz) (Figure 2.1). UDP-GalNAz, the azido variant of the natural nucleotide sugar UDP-GalNAc, serves as a substrate for the polypeptide GalNAc transferases (ppGalNAcTs), which transfer GalNAz to Ser and Thr residues of nascent glycoproteins (*17*). To achieve metabolic labeling earlier in embryogenesis, we sought to bypass the GalNAc salvage pathway by using the downstream intermediate UDP-GalNAz as a labeling substrate. However, because this compound is not cell-permeable, we elected to microinject it directly into the yolk sac of the embryo. At the one-cell stage, cell-impermeable reagents that are microinjected into the yolk gain access to all cells in the developing organism (*18*).

Following microinjection with 25 pmol of synthetic UDP-GalNAz (*17*) or the control sugar UDP-GalNAc, the embryos were allowed to develop for several hours and then bathed in a solution of an Alexa Fluor 488 conjugate of DIFO, termed DIFO-488 (*13*), to detect azide-labeled glycans (Figure 2.2). We performed the copper-free click reaction at various timepoints, and we were able to detect, by confocal microscopy, labeling of cell-surface glycans in vivo as early as the 65% epiboly stage of gastrulation (~7 hpf), but not before (Figure 2.3). A larger dose of UDP-GalNAz, 125 pmol, also yielded robust labeling of cell-surface glycans with DIFO-488, but this dose caused developmental defects by 24 hpf (Figure 2.4). Thus, we elected to inject 25 pmol of azidosugar in subsequent experiments.

These results validated that microinjection of a nucleotide sugar precursor could enable imaging of glycans at much earlier stages of development than was achievable by bathing with Ac_4GalNAz. Given that the transcription of zygotic genes starts at 3 hpf (*16*), four hours before our technique yields detectable signal, this microinjection approach enables detection of the early events of glycan biosynthesis. We considered that it might be possible, however, that treatment with a bacterial protease to remove the chorion, which is a standard step in our protocol, might remove some cell-surface glycoproteins and thereby delay the onset of detectable signal using our reagents. To

examine this possibility, we performed an analogous imaging experiment in which chorions were removed manually, with forceps, instead. We observed the same results, with earliest detectable labeling at the 65% epiboly stage (Figure 2.5).

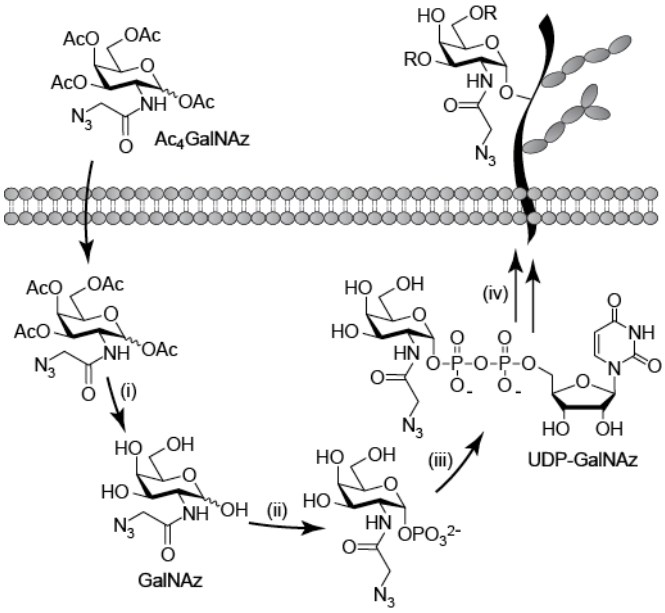

Figure 2.1. Metabolic labeling of mucin-type O-glycans with azidosugars via the GalNAc salvage pathway. The enzymatic transformations shown are catalyzed by (i) nonspecific esterases, (ii) GalNAc-1-phosphate kinase, (iii) UDP-GalNAc pyrophosphorylase, and (iv) ppGalNAcTs and other glycosyltransferases.

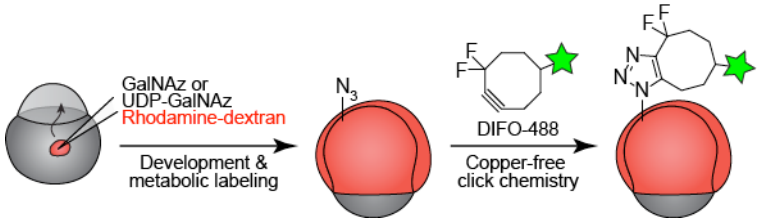

Figure 2.2. Two-step strategy for imaging glycans in vivo. Zebrafish embryos at the 1–8-cell stage are microinjected with azidosugars along with the tracer dye rhodamine-dextran, and then the embryos are allowed to develop. In a second step, the metabolically-incorporated azidosugars are visualized by reaction with a difluorinated cyclooctyne (DIFO) probe via copper-free click chemistry.

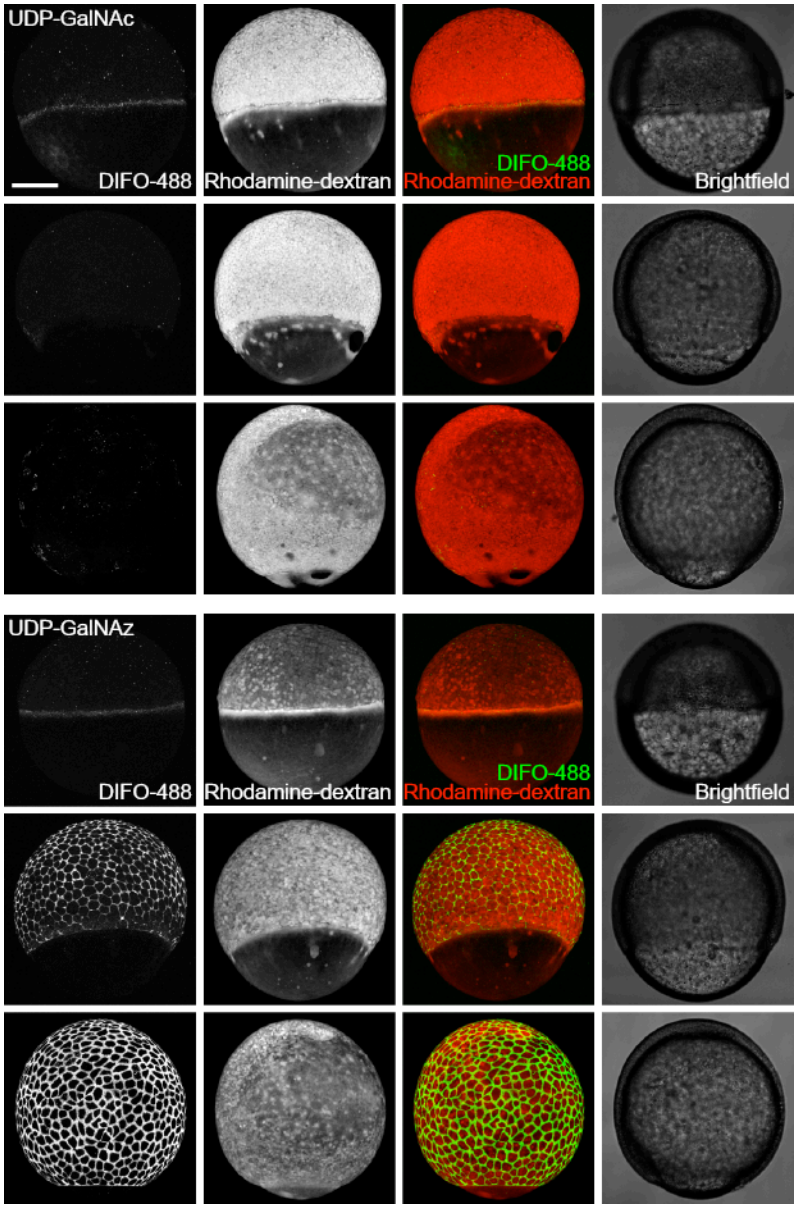

Figure 2.3. Microinjection of UDP-GalNAz provides labeling of mucin-type O-glycans during gastrulation. Zebrafish embryos were microinjected with 25 pmol of UDP-GalNAc (top panels) or UDP-GalNAz (bottom panels), along with the tracer dye rhodamine-dextran, and were allowed to develop, reacted with DIFO-488 (100 μM, 1 h), and imaged by confocal microscopy. Shown are maximum intensity z-projection images. Green, DIFO-488; red, rhodamine-dextran. Scale bar: 200 μm.

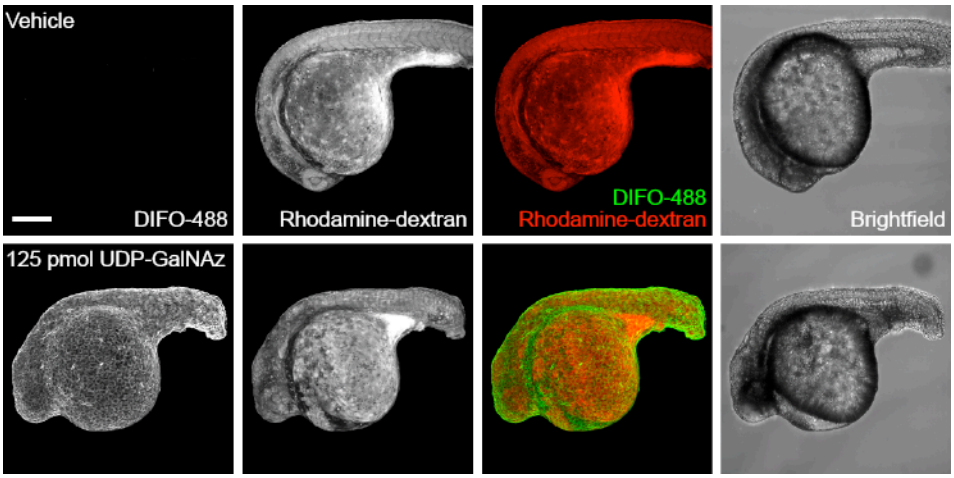

Figure 2.4. Microinjection of higher doses of UDP-GalNAz causes toxicity. Zebrafish embryos were microinjected with vehicle alone (top panel) or 125 pmol of UDP-GalNAz (bottom panel). The embryos were allowed to develop to 24 hpf, reacted with DIFO-488 (100 μM, 1 h), and imaged by confocal microscopy. Shown are maximum intensity z-projection fluorescence images and corresponding brightfield images. Green, DIFO-488; red, rhodamine-dextran. Scale bar: 200 μm.

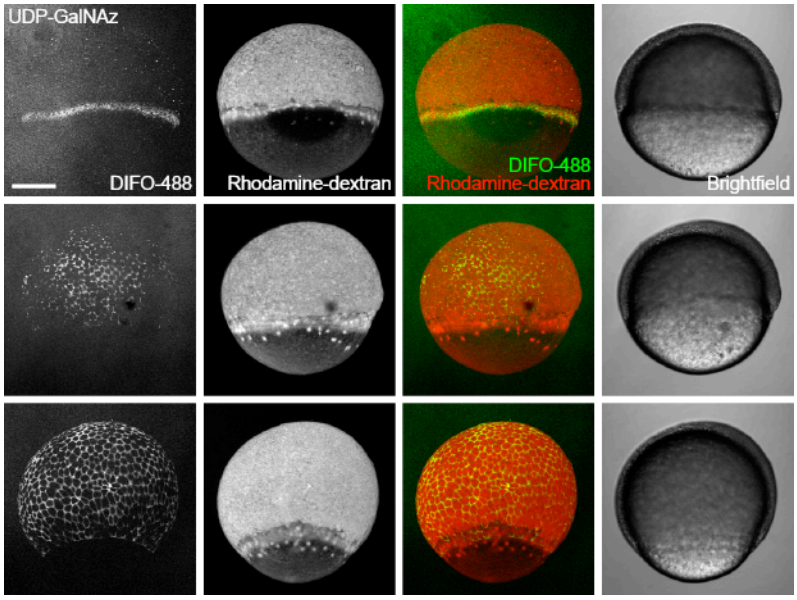

Figure 2.5. Manual dechorionation with forceps does not afford labeling before 65% epiboly. Zebrafish embryos were microinjected with 25 pmol of UDP-GalNAz and the tracer dye rhodamine-dextran, manually dechorionated using forceps at 3 hpf, and allowed to develop to 50% epiboly (5.5 hpf, 1st row), 65% epiboly (7 hpf, 2nd row), or 80% epiboly (8.5 hpf, 3rd row). Embryos were then reacted with DIFO-488 (100 μM, 1 h) and imaged by confocal microscopy. Shown are maximum intensity z-projection fluorescence images and corresponding brightfield images. Green, DIFO-488; red, rhodamine-dextran. Scale bar: 200 μm.

Microinjection of GalNAz also affords metabolic labeling during gastrulation

Our initial choice of UDP-GalNAz to achieve metabolic labeling at early developmental stages centered on its ability to bypass biosynthetic steps in the GalNAc salvage pathway. To determine whether the GalNAc salvage pathway was responsible for the delay in metabolic labeling that we observed with our bathing protocol, we microinjected the free sugar, GalNAz. Reaction with DIFO-488 at various timepoints revealed labeling starting at 65% epiboly, the same result as seen with UDP-GalNAz (Figure 2.6). Thus, the GalNAc salvage pathway does not appear to be the bottleneck in our labeling technique.

This observation – that microinjecting embryos with GalNAz yields signal significantly before bathing them in Ac_4GalNAz does – may be explained by two different possibilities. First, microinjection could result in a higher intracellular concentration of azidosugar at earlier timepoints than bathing. Alternatively, the conversion of Ac_4GalNAz to GalNAz by promiscuous cytosolic esterases may be a bottleneck step in the labeling method. To test this second possibility, we microinjected embryos with Ac_4GalNAz and reacted them with DIFO-488 at 12 hpf. These Ac_4GalNAz-injected embryos exhibited DIFO-derived fluorescence that was comparable in intensity to that from similarly labeled embryos injected instead with free GalNAz (Figure 2.7). These results indicate that cytosolic esterases are able to efficiently convert Ac_4GalNAz to GalNAz during the first 12 hours of embryogenesis.

At these early stages of development, we noticed that the cells labeled with DIFO-488 during gastrulation appeared to be members of the enveloping layer, the embryo's outermost layer of cells (Figure 2.8). To analyze the labeling of all the cells in the organism, we turned to flow cytometry. GalNAz-injected embryos were reacted with DIFO-488 at 10 hpf to label azide-containing glycans on the enveloping layer. The embryos were subsequently dissociated, and the resulting cell suspension was labeled with an Alexa Fluor 647 conjugate of DIFO (DIFO-647) (Figure 2.9, panel A). We found that most of the dissociated cells displayed DIFO-647-derived signal, indicating that most cells of the embryo were metabolically labeled with GalNAz (Figure 2.9, panel B). By contrast, approximately 0.5% of the cells were labeled with DIFO-488, indicating that they were accessible to this reagent while part of the intact embryo. Interestingly, the enveloping layer cells labeled by DIFO-488 when the embryo was intact also displayed the highest DIFO-647 signal, suggesting that these cells may possess higher levels of mucin glycoproteins than other cells in the embryo.

We extended our labeling timecourse out to 96 hpf, when the zebrafish are at the larval stage, to evaluate the duration of time that a single bolus of GalNAz or UDP-GalNAz could still yield detectable azide-dependent signal with the DIFO reagents. In this experiment, zebrafish injected with the appropriate azidosugar were allowed to develop normally and reacted at a single timepoint between 12 and 96 hpf with DIFO-488 (Figure 2.10). We found that zebrafish injected with either GalNAz or UDP-GalNAz exhibited azide-dependent fluorescence throughout the four-day experiment. Further, when embryos were treated at 85 hpf with tris(2-carboxyethyl)phosphine (TCEP) to reduce any surface-exposed azides present at that time (12), then allowed to develop to 96 hpf and reacted with an Alexa Fluor 555 conjugate of DIFO (DIFO-555), they showed

robust labeling, indicating that new azide-containing glycans were presented at the cell surface during this later period (85-96 hpf) (Figure 2.11).

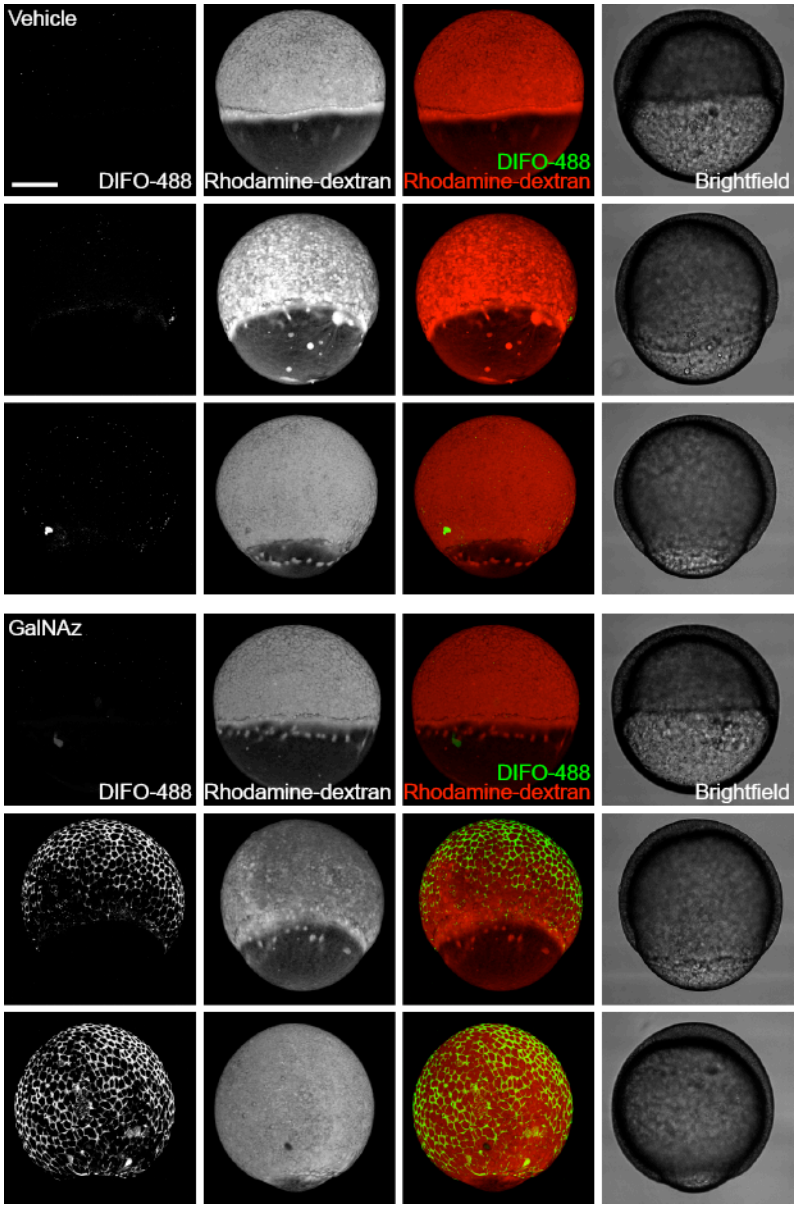

Figure 2.6. Microinjection of GalNAz also provides labeling of mucin-type O-glycans during gastrulation. Zebrafish embryos were microinjected with vehicle alone (top panels) or 25 pmol of GalNAz (bottom panels), along with the tracer dye rhodamine-dextran, and then were allowed to develop, reacted with DIFO-488 for 1 h, and imaged by confocal microscopy. Shown are maximum intensity z-projection images. Green, DIFO-488; red, rhodamine-dextran. Scale bar: 200 μm.

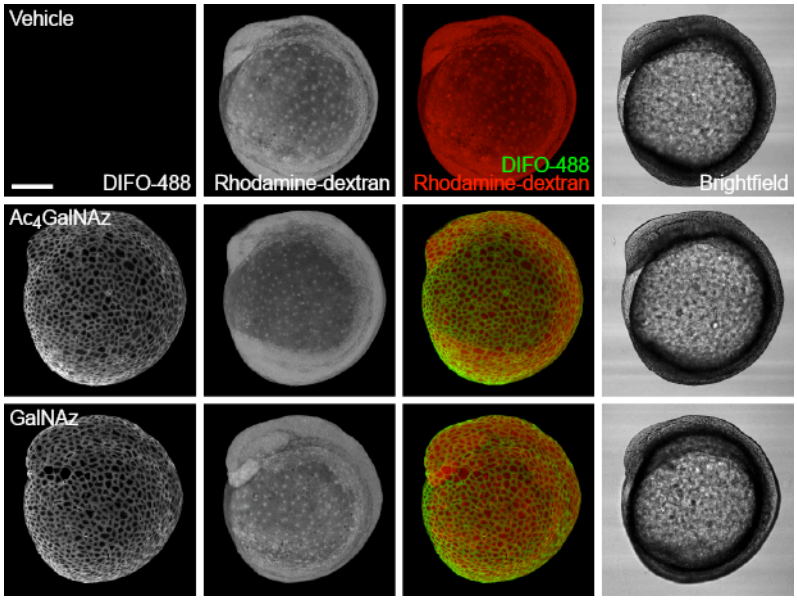

Figure 2.7. Microinjection of Ac_4GalNAz and GalNAz afford comparable labeling before 24 hpf. Zebrafish embryos were microinjected with 25 pmol of GalNAz, 25 pmol of Ac_4GalNAz, or vehicle alone, along with the tracer dye rhodamine-dextran, and allowed to develop. At 10 hpf, the embryos were reacted with DIFO-488 and imaged by confocal microscopy. Shown are maximum intensity z-projection fluorescence images and corresponding brightfield images. Green, DIFO-488; red, rhodamine-dextran. Scale bar: 200 μm.

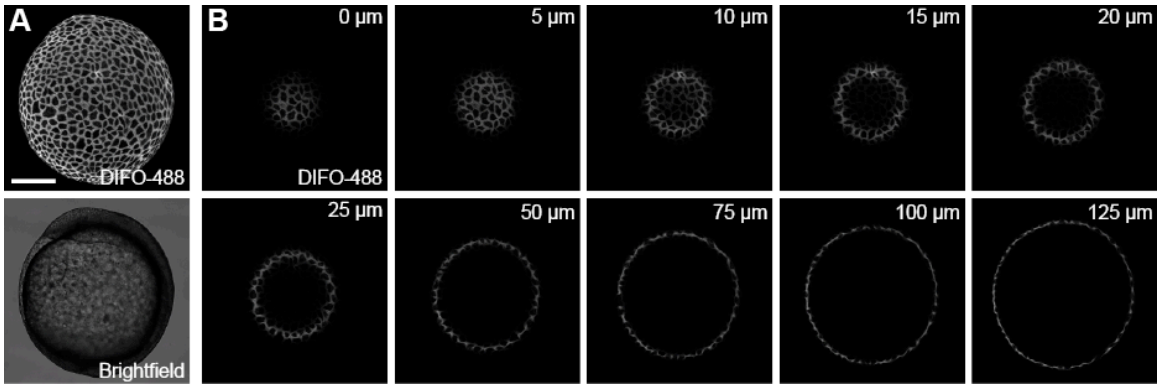

Figure 2.8. DIFO-488 labels cell-surface glycans in the enveloping layer of GalNAz-injected embryos. Zebrafish embryos were microinjected with 25 pmol of GalNAz, allowed to develop to 10 hpf, and then reacted with DIFO-488. (A) Maximum intensity z-projection fluorescence image and corresponding brightfield image. (B) Several individual z-planes from the z-projection shown in (A), demonstrating labeling of the surface cells. Distances indicated are in the z direction from the top of the embryo. Scale bar: 200 μm.

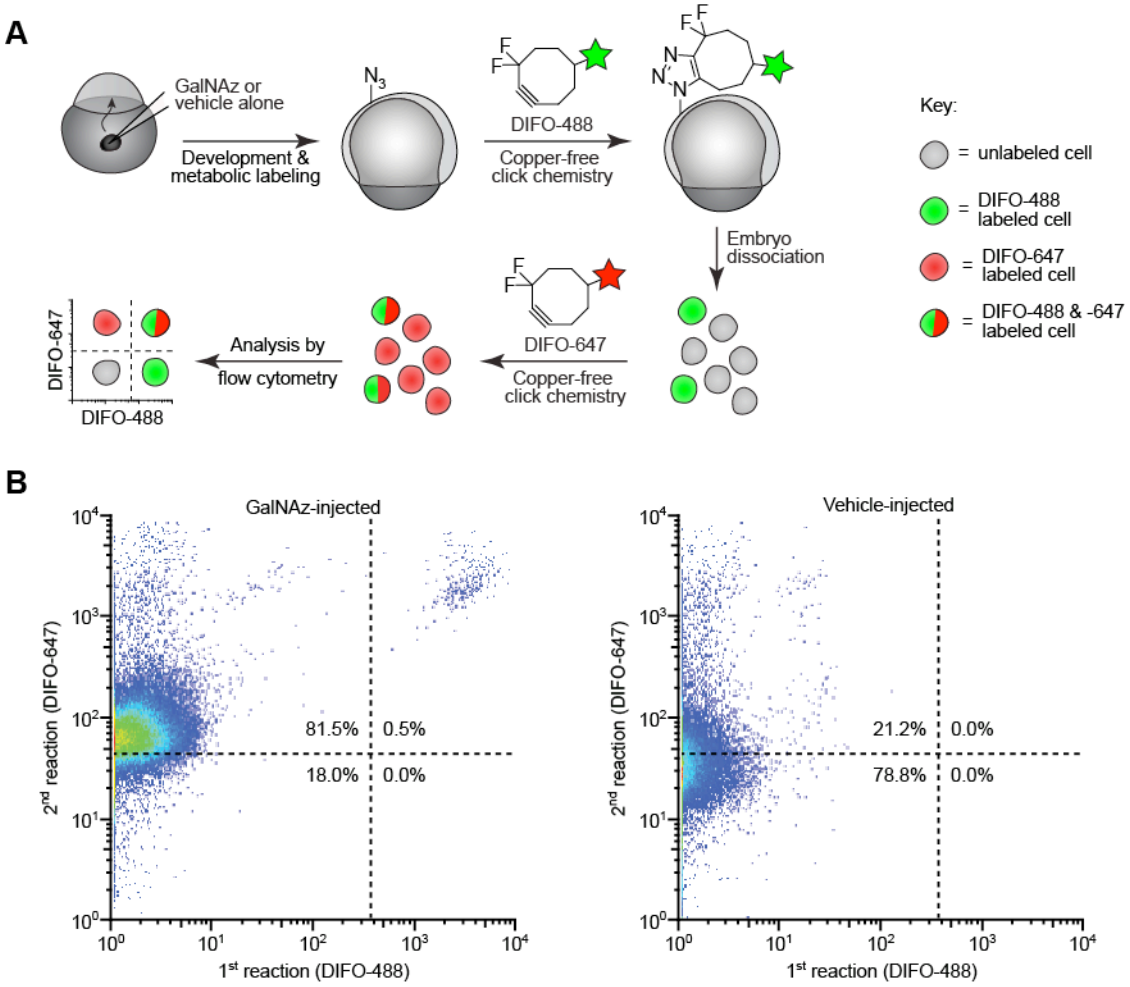

Figure 2.9. Distribution of GalNAz- and DIFO-488-labeled cells from 10 hpf embryos analyzed by flow cytometry. Zebrafish embryos were microinjected with 25 pmol of GalNAz, allowed to develop to 10 hpf, and then reacted with DIFO-488 (100 μM, 1 h). (A) Schematic of dual-labeling flow experiment. Following microinjection with GalNAz and reaction with DIFO-488, embryos were dissociated, and the resulting cell suspension was labeled with DIFO-647 (100 μM, 30 min) and then analyzed by flow cytometry. (B) Representative dot plots of cells from embryos injected with GalNAz (left) or vehicle alone (right). In GalNAz-injected embryos, most of the cells displayed DIFO-647-derived signal, indicating that most cells of the embryo were metabolically labeled with GalNAz. Approximately 0.5% of cells were also labeled with DIFO-488, indicating that these cells were accessible to this reagent while part of the intact embryo.

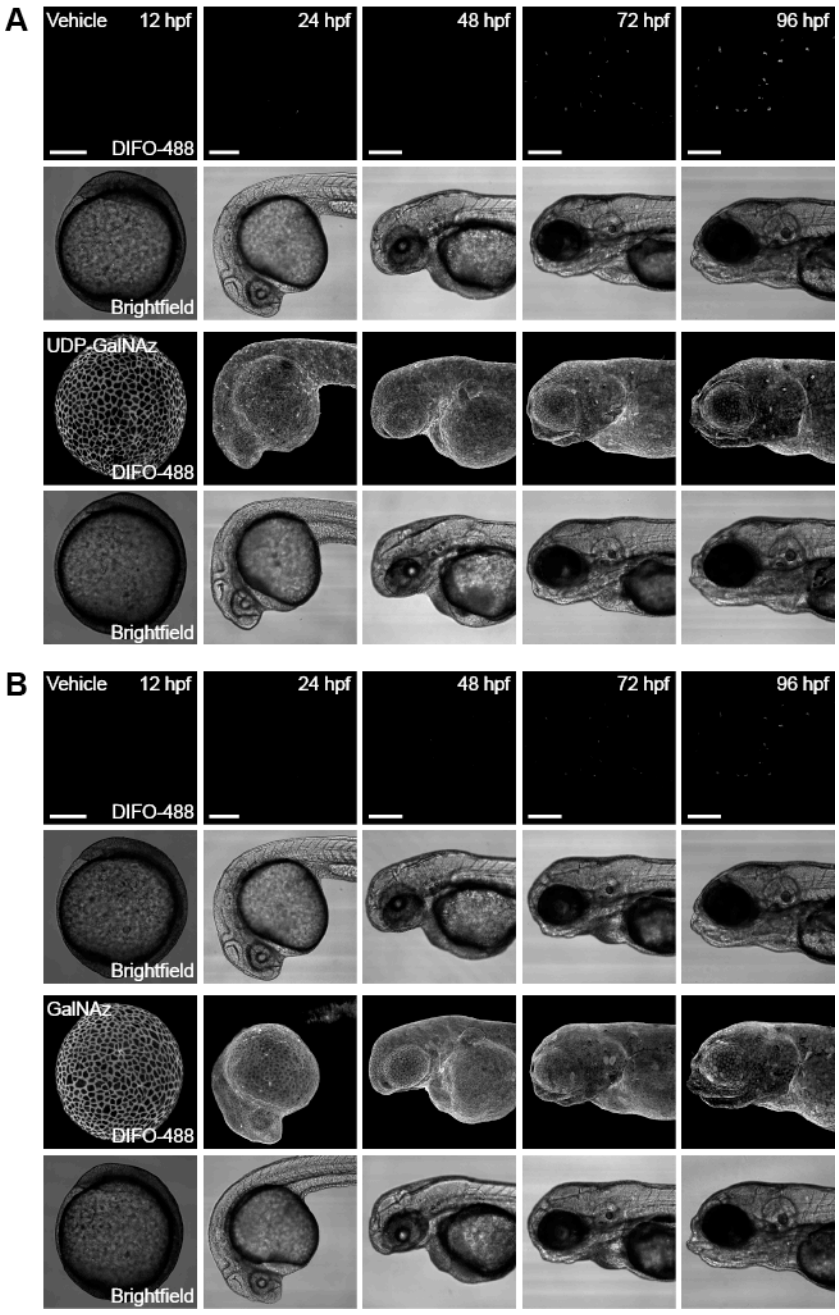

Figure 2.10. Labeling from a single bolus of GalNAz or UDP-GalNAz persists for 96 hpf. Zebrafish embryos were microinjected with 25 pmol of UDP-GalNAz (A, bottom panels), 25 pmol of GalNAz (B, bottom panels), or vehicle alone (A and B, top panels), and were allowed to develop normally. At each timepoint shown, embryos were reacted with DIFO-488 and imaged by confocal microscopy. Shown are maximum intensity z-projection fluorescence images and corresponding brightfield images. Scale bar: 200 μm.

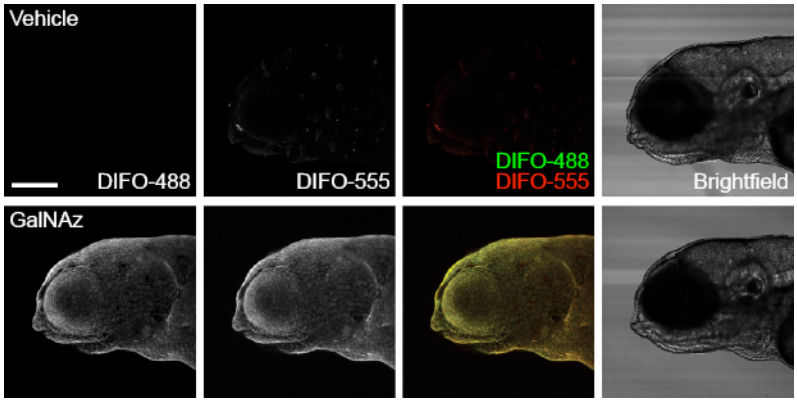

Figure 2.11. New azide-containing glycans are presented on the surface of cells out to 96 hpf. Zebrafish embryos were microinjected with vehicle alone (top) or 25 pmol of GalNAz (bottom) and allowed to develop to 84 hpf, at which point they were reacted with DIFO-488 for 1 h. Unreacted azides were immediately quenched by using tris(2-carboxyethyl)phosphine (TCEP) (50 mM, 10 min), and the embryos were allowed to develop further. At 96 hpf, the embryos were reacted with DIFO-555 for 1 h and then imaged by confocal microscopy. Shown are maximum intensity z-projection fluorescence images of surface epithelial cells and corresponding brightfield images. Green, DIFO-488; red, DIFO-555. Scale bar: 200 μm.

These results prompted us to continue our experiments with GalNAz, which is more readily synthesized in the laboratory and is not prone to hydrolysis *in vitro*. Importantly, we observed no toxicity or developmental abnormalities during the duration of these four-day experiments, suggesting that microinjection of 25 pmol of GalNAz or UDP-GalNAz followed by detection with copper-free click chemistry is not harmful to the organism.

Two-color, time-resolved labeling enables visualization of O-glycan trafficking

To image two temporally distinct populations of O-glycans, we adopted a two-color labeling strategy involving successive reactions with different DIFO-fluorophore conjugates. In these experiments, embryos were injected with GalNAz at the one-cell stage, allowed to develop to 90% epibody (9 hpf), and then reacted with DIFO-488. The embryos were rinsed and allowed to develop further for two or 12 hours, at which point they were reacted with DIFO-555. In this manner, “old” and “new” glycans within the same embryo could be distinguished using confocal microscopy.

In the experiment with a two-hour window for development and metabolic labeling between the two copper-free click reactions, we observed substantial differences in spatial distribution between the two populations of glycans (Figure 2.12, panel A). The newer glycans, shown in red, were spread evenly across the cell surface, including close to the edge of the cell. Older glycans, shown in green, had migrated away from this region and were likely undergoing internalization.

The two-color experiment with a 12-hour delay between copper-free click reactions demonstrated very little overlap between old and new glycan populations, indicating that substantial glycan biosynthesis and turnover had occurred during that time

period (Figure 2.12, panel B). Interestingly, the DIFO-555 signal from 21 hpf embryos is much more evenly distributed across the surface of the cells than the DIFO-555 signal from embryos reacted at 12 hpf. These results suggest that internalization of glycans may be faster at 12 hpf than at 21 hpf; alternatively, the data may reflect differences in enveloping layer cell morphologies at the two developmental timepoints.

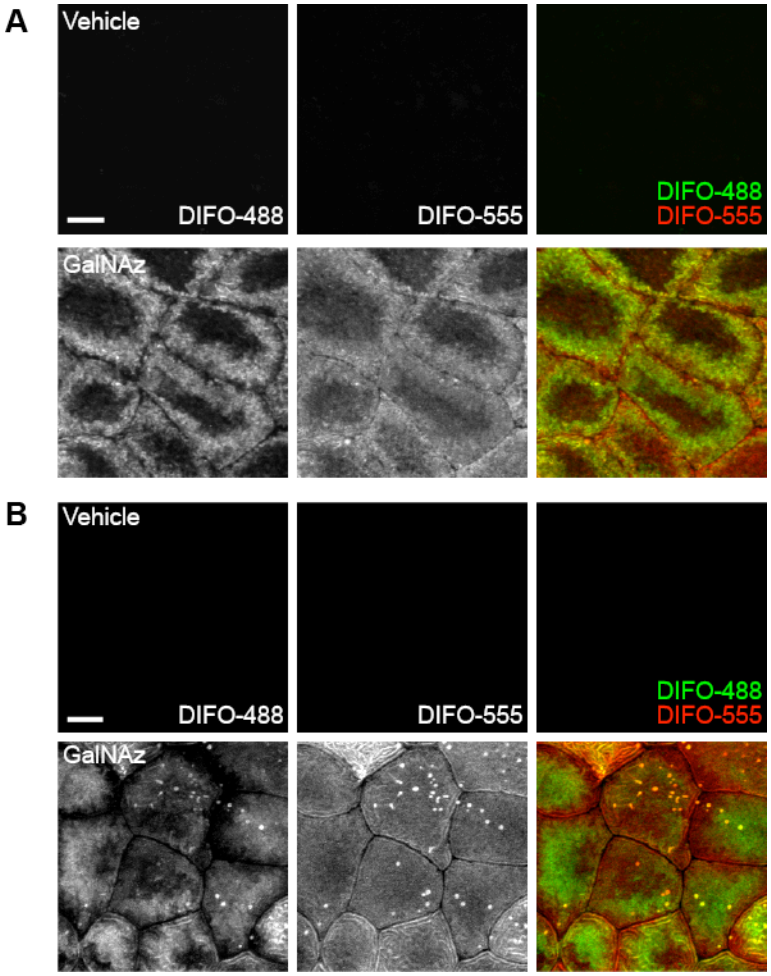

Figure 2.12. Two-color, time-resolved labeling enables visualization of O-glycan trafficking. Zebrafish embryos were microinjected with GalNAz, allowed to develop to 9 hpf, and reacted with DIFO-488. The embryos were then allowed to further develop for 2 h (A) or 12 h (B), at which point they were reacted with DIFO-555 and then imaged by confocal microscopy. Shown are maximum intensity z-projection images of superficial enveloping layer cells. Green, DIFO-488; red, DIFO-555. Scale bars: 10 μm.

Collectively, these two-color experiments using GalNAz injections and labeling with DIFO-fluorophore conjugates highlighted the dynamics of O-glycan biosynthesis in surface epithelial cells during the early stages of embryogenesis. At this point, we were interested in evaluating whether other sectors of the glycome also exhibited this behavior

and whether we might discern differences in the generation, trafficking, and degradation of distinct classes of glycans during embryogenesis.

Time-lapse monitoring of mitotic cells reveals dramatic glycan reorganization during cell division

During the course of our studies, we noticed an intense staining pattern derived from our reagents at what appeared to be the cleavage furrow of dividing cells (Figure 2.13). To evaluate whether these cells were indeed undergoing mitosis, we utilized a transgenic zebrafish ubiquitously expressing a GFP-fused histone protein (H2A-GFP), enabling visualization of cell nuclei by confocal microscopy (*19*). In these experiments, GalNAz was microinjected into embryos at the one-cell stage, and the zebrafish were allowed to develop until the end of epiboly (10 hpf), at which point they were reacted with DIFO-647.

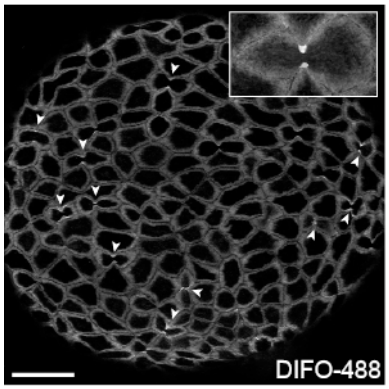

Figure 2.13. Dividing cells exhibit intense DIFO-derived signal at the cleavage furrow. Wild-type zebrafish embryos were microinjected with GalNAz, allowed to develop to 10 hpf, reacted with DIFO-488 for 1 h, and imaged by confocal microscopy. Arrowheads indicate intense staining at the cleavage furrow of dividing cells. Maximum intensity z-projection images are shown. Scale bar: 100 μm.

Time-lapse imaging of the labeled embryos revealed that during metaphase, the DIFO-derived signal was uniform around the cell membrane (Figure 2.14). However, moments after the beginning of anaphase, which is marked by the rapid separation of the sister chromatids, we observed an intensification of the fluorescent signal at the cleavage furrow. The DIFO-derived signal continued to concentrate as the two patches of membrane that constitute the furrow began to invaginate during cytokinesis, but surprisingly, we did not observe the two labeled glycan populations touch one another. Instead, the intense signal dissipated over time. We allowed the labeled embryos to continue to develop over subsequent days and observed no developmental abnormalities, suggesting that cell division was indeed proceeding normally.

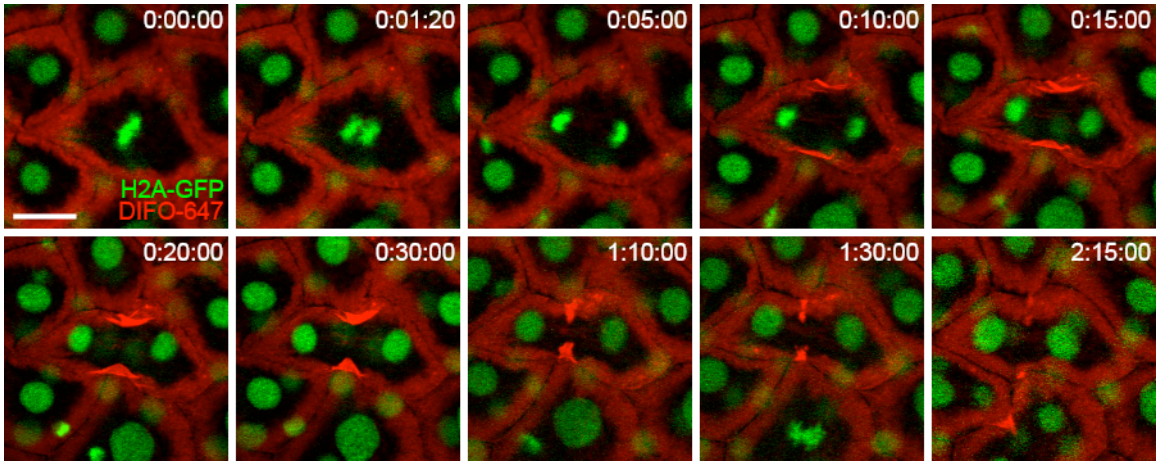

Figure 2.14. Time-lapse monitoring of mitotic cells reveals dramatic glycan reorganization during cell division. H2A-GFP transgenic zebrafish embryos were microinjected with GalNAz and allowed to develop to 10 hpf. The embryos were reacted with DIFO-647 for 1 h and imaged by confocal microscopy. Shown are single z-plane frames from a time-lapse movie. Indicated in the top right of each image is time (h:min:sec). Green, H2A-GFP; red, DIFO-647. Maximum intensity z-projection images are shown. Scale bar: 20 μm.

Labeling of cell-surface glycans differs substantially from a plasma membrane marker during mitosis

To visualize the plasma membrane during cell division, we co-injected H2A-GFP embryos at the one-cell stage with a mixture of GalNAz and the mRNA for membrane-mCherry (memCherry), a fusion of the membrane-localized domain of Lyn with the fluorescent protein mCherry (*20*, *21*). The embryos were allowed to develop to 10 hpf, at which point they were reacted with DIFO-647 and imaged (Figure 2.15, panel A). This experiment revealed two important pieces of information. First, the memCherry signal appeared between the two daughter cells within seconds of the formation of the cleavage furrow, suggesting that cytokinesis was indeed occurring normally. Second, we noticed no intensification of the memCherry signal at the cleavage furrow, in contrast to the DIFO signal.

These results suggest that the substantial recruitment of glycans to the cleavage furrow cannot be explained by a simple reorganization of the plasma membrane. Further, the lack of DIFO-derived signal between daughter cells (Figure 2.15, panel B) suggests that glycans within that region of plasma membrane had not migrated from other regions of plasma membrane during the mitotic event. Therefore, the glycans within this patch of membrane are likely biosynthesized *de novo*, consistent with previous studies of membrane addition during cytokinesis in different organisms (*22-24*). We attempted to label the putative newly-synthesized glycans in the new membrane between daughter cells by reacting GalNAz-injected embryos sequentially with DIFO-555 and, immediately afterward, DIFO-488. In all cases, we observed colocalization of the two labels (Figure 2.16). This result suggests either that the process of new membrane addition at the furrow and subsequent glycan reorganization take place on a faster

timescale than that of our labeling protocol, or that there are relatively few azide-labeled glycans in this segment of membrane.

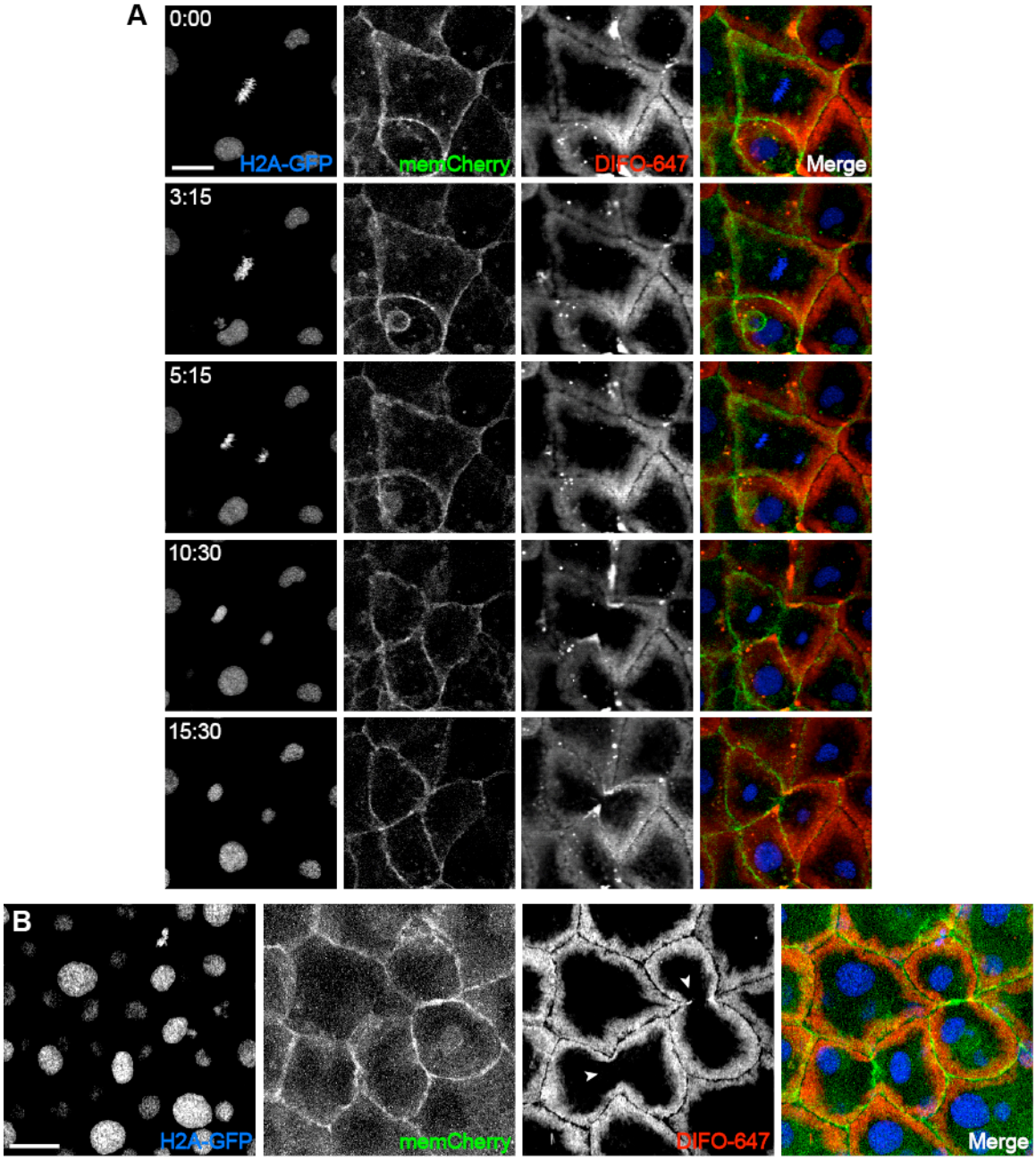

Figure 2.15. New membrane is formed between daughter cells but it is not labeled with DIFO-647. H2A-GFP transgenic zebrafish were microinjected into the blastomere cell at the one-cell stage with GalNAz and mRNA for memCherry. Embryos were allowed to develop to 10 hpf, at which point they were reacted with DIFO-647 and imaged. (A) Time-lapse imaging of a single cell. A single z-plane fluorescence image is shown at each time indicated (min:sec). (B) Two pairs of recently-divided cells. Arrowheads indicate the location of new membrane between daughter cells. Blue, H2A-GFP; green, memCherry; red, DIFO-647. Scale bars: 20 μm.

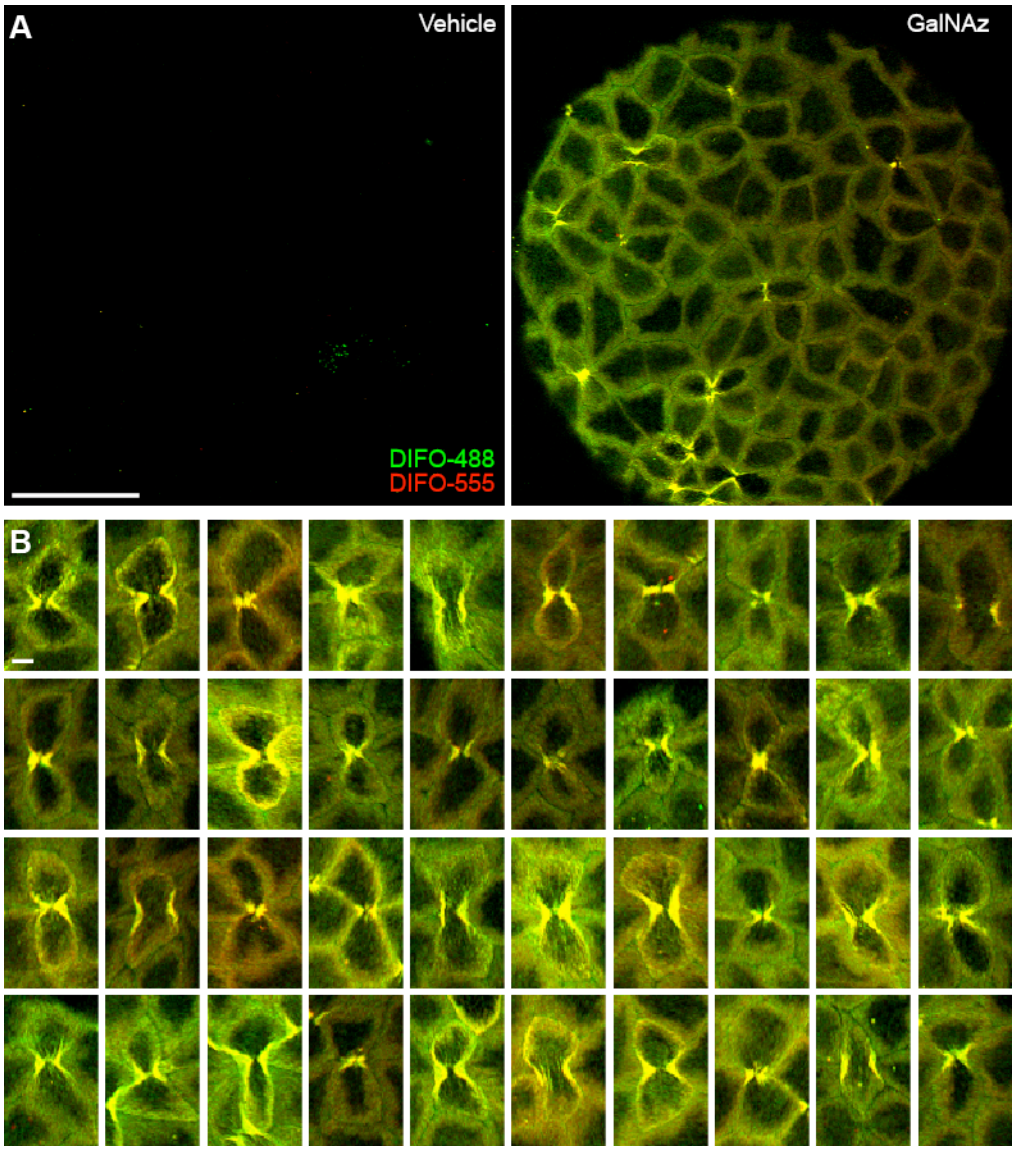

Figure 2.16. Multicolor imaging of GalNAz-labeled glycans at the cleavage furrow of dividing cells. Zebrafish embryos were microinjected with GalNAz or no sugar and allowed to develop to 10 hpf, at which point they were reacted with DIFO-555 for 1 h. Immediately following this reaction, the embryos were reacted with DIFO-488 for 15 min and imaged by confocal microscopy. Shown are maximum intensity z-projection fluorescence images. Green, DIFO-488; red, DIFO-555. Scale bars: 100 μm (A), 10 μm (B).

Conclusion

We have demonstrated that microinjection of simple and nucleotide azidosugars followed by labeling using copper-free click chemistry can enable visualization of glycan biosynthesis in the enveloping layer of zebrafish embryos as early as four hours after the onset of zygotic gene expression. Through these studies, we also found that cell-surface O-glycans are recruited to the cleavage furrow of dividing enveloping layer cells on second-to-minute timescales. An interesting direction for future study involves the identification of the protein scaffolds to which the glycans are anchored. These mucin-type glycoproteins may play a role in cell division that has not yet been characterized. More generally, this work represents the first study of glycan trafficking in living organisms during early embryogenesis and sets the stage for future studies of other sectors of the glycome, as well as other biomolecules such as proteins, lipids, and cofactors, that can be labeled by microinjection of functionalized biosynthetic precursors.

Experimental Methods

General materials and methods

All chemical reagents were of analytical grade, obtained from commercial suppliers, and used without further purification. Flow cytometry analysis was performed on a BD Biosciences FACSCalibur flow cytometer and analyses were performed using FloJo software. Cell viability was ascertained by gating the samples on the basis of forward and side scatter, and 5 x 10^4 live cells were analyzed for each sample. Wide-bore Pasteur pipets (borosilicate glass disposable serological pipets with wide tip) were purchased from Fisher Scientific. Dulbecco's phosphate-buffered saline (PBS) was obtained from HyClone Laboratories, fetal bovine serum (FBS) was obtained from Omega Scientific, and ethylene diamine tetraacetic acid (EDTA) was obtained from Gibco. Rhodamine-dextran (dextran, tetramethylrhodamine, 10,000 MW, lysine fixable) and aminooxy Alexa Fluor 488 were obtained from Invitrogen. Phenol red, *N*-phenylthiourea (PTU), pronase (protease, Type XIV, from *Streptomyces griseus*), tricaine (ethyl 3-aminobenzoate methanesulfonate), tris(2-carboxyethyl)phosphine (TECP) hydrochloride, and UDP-GalNAc were obtained from Sigma-Aldrich. GalNAz (*25*), UDP-GalNAz (*26*), DIFO-488 (*13*), DIFO-555 (*12*), and DIFO-647 (*13*) were prepared as described previously. memCherry mRNA (*21*) was generously provided by Emilie Delaune. Confocal microscopy was performed at the UC Berkeley Molecular Imaging Center.

Zebrafish stocks and husbandry

Wild-type AB-derived and H2A-GFP transgenic (*19*) zebrafish lines were kept at 28.5 °C on a 14-h light/10-h dark cycle. Embryos were obtained from natural spawnings and were maintained in embryo medium (150 mM NaCl, 0.5 mM KCl, 1.0 mM $CaCl_2$, 0.37 mM KH_2PO_4, 0.05 mM Na_2HPO_4, 2.0 mM $MgSO_4$, 0.71 mM $NaHCO_3$ in deionized H_2O, pH 7.4). Embryos and larvae were incubated at 28–29 °C and were developmentally staged according to Kimmel and coworkers (*27*).

Metabolic labeling of zebrafish by microinjection of embryos with azidosugars and detection by copper-free click chemistry

Zebrafish embryos at the one-cell, two-cell, or four-cell stage were microinjected into the yolk cell with 1–5 nL of a 5–125 mM solution of the appropriate sugar (UDP-GalNAz, UDP-GalNAc, GalNAz, or Ac_4GalNAz) and either rhodamine-dextran (5% w/v) or phenol red (0.1% w/v) in 0.2 M KCl. For experiments using memCherry, mRNA encoding memCherry was added to the 25 mM GalNAz solution (containing 0.1% w/v phenol red and 0.1 M KCl) at a concentration of 20 µg/mL; in this case, 1 nL was microinjected directly into the blastomere cell at the one-cell stage. Following microinjection, embryos were allowed to develop to 3 hpf, at which point they were manually cleaned. With the exception of the experiment shown in Figure 2.5, the embryos were then enzymatically dechorionated by incubation in a 1 mg/mL solution of pronase in embryo medium at ~28 °C for approximately 5 min, and rinsed five times.

Following dechorionation, the embryos were transferred, using a fire-polished wide-bore Pasteur pipet, into 1% agarose-coated Petri dishes containing embryo medium. All embryos younger than 12 hpf were stored in Petri dishes or 96-well plates coated with a 1% solution of agarose in embryo medium. When embryos were to be used for imaging beyond 24 hpf, 131 μM *N*-phenylthiourea (PTU) was included in all media starting at 24 hpf to inhibit melanin production. To detect cell-surface azide-labeled glycans, embryos were transferred to a flat-bottom 96-well plate containing DIFO-488, DIFO-555, or DIFO-647 (100 μL of a 100 μM solution in embryo medium) and allowed to react for 1 h at 28.5 ºC.

Labeling of GalNAz-containing glycans at 84 and 96 hpf

Zebrafish embryos at the one-cell or two-cell stage were microinjected into the yolk cell with 1 nL of a 25 mM solution of GalNAz or no sugar and phenol red (0.1% w/v) in 0.2 M KCl. The embryos were dechorionated using pronase and allowed to develop at 28.5 °C in embryo medium containing PTU. At 84 hpf, the embryos were transferred to a flat-bottomed 96-well plate containing DIFO-488 (100 μL of a 100 μM solution in embryo medium) and allowed to react for 1 h at 28.5 ºC. After the labeling reaction, the embryos were rinsed six times with embryo medium. The embryos were then reacted with 50 mM TCEP (pH 7.4) in embryo medium for 10 min at 28.5 °C. Following this reaction, the embryos were rinsed eight times with embryo medium and transferred to fresh PTU-containing embryo medium to develop for an additional 11 hours at 28.5 °C. At 96 hpf, the embryos were reacted with DIFO-555 (100 μL of a 100 μM solution in embryo medium) and allowed to react for 1 h at 28.5 ºC.

Detection of GalNAz-labeled glycans in dividing cells with two copper-free click chemistry reactions in rapid succession

Zebrafish embryos at the one-cell or two-cell stage were microinjected into the yolk cell with 1 nL of a 25 mM solution of GalNAz or no sugar and phenol red (0.1% w/v) in 0.2 M KCl. The embryos were dechorionated using pronase and allowed to develop at 28.5 °C in embryo medium. At 10 hpf, the embryos were transferred to a flat-bottomed 96-well plate containing DIFO-555 (100 μL of a 100 μM solution in embryo medium) and allowed to react for 1 h at 22 ºC. After the labeling reaction, the embryos were rinsed twice in embryo medium, then immediately transferred to a solution containing DIFO-488 (100 μL of a 100 μM solution in embryo medium) and allowed to react for 15 min at 22 ºC.

Preparation of labeled embryos for imaging

After the labeling reactions, embryos were rinsed by sequential transferring through six 15-cm Petri dishes filled with 25 mL of embryo medium. Embryos were then mounted between two cover slips, stabilized by vacuum grease in each corner, in a solution of 0.6% low melting point agarose in embryo medium. Embryos 24 hpf and older were anesthetized with 2.6 μM tricaine prior to mounting.

Image acquisition and analysis

Fluorescence images shown in Figure 2.15 were acquired on an Olympus FV1000 laser scanning confocal microscope equipped with 488 nm, 559 nm, and 635 nm laser lines and a 60x/1.20 UPlanSApo water immersion objective. All other fluorescence and brightfield images were acquired on a Zeiss LSM 510 META laser scanning confocal microscope equipped with 488 nm, 543 nm, and 633 nm laser lines. For Figures 2.3–2.11 and Figure 2.13, images were acquired using a 10x/0.30 Plan-Neofluar air objective with focus step sizes ranging from 5 to 7.5 µm. For Figure 2.16, images were acquired using a 20x/0.5 Achroplan water dipping objective with a 2.5 µm step size. For Figure 2.14, images were acquired using a 40x/0.80 Achroplan IR water dipping objective with a 0.5 µm step size. Images shown in Figure 2.12 and the inset of Figure 2.13 were acquired using a 63x/0.95 Achroplan IR water dipping objective with a 0.5 µm step size. All images were analyzed using Slidebook 4.2 (Intelligent Imaging Innovations).

Flow cytometry of GalNAz-labeled embryos

Zebrafish embryos were microinjected with 1 nL of a 25 mM solution of GalNAz or no sugar and phenol red (0.1% w/v) in 0.2 M KCl. At 3 hpf, the embryos were manually cleaned and dechorionated with pronase, then allowed to develop at 28.5 ºC. At 10 hpf, the embryos were reacted with DIFO-488 (100 µL of a 100 µM solution in embryo medium) for 1 h at 28.5 ºC. Following this reaction, the embryos were rinsed six times in embryo medium, then deyolked by passing through a 200 µL pipette tip in low-calcium Ringer's solution (116 mM NaCl, 2.6 mM KCl, 5 mM HEPES, pH 7.0). After a 5 min incubation in Ringer's, the embryos were transferred to a solution of 5 mM EDTA (pH 8.0) in PBS and incubated for 15 min at 28.5 ºC to dissociate the cells. The reaction was stopped by the addition of 5% FBS and 1 mM $CaCl_2$ in PBS. The cells were rinsed once with labeling buffer (PBS, pH 7.6, 1% FBS), then reacted with DIFO-647 (100 µL of a 100 µM solution in labeling buffer) for 30 min at 22 ºC. Following this reaction, the cells were rinsed three times with suspension buffer (PBS, pH 7.6, 1% FBS, 0.8 mM $CaCl_2$). After the final wash, the cells were resuspended in 800 µL of suspension buffer and passed through a 35 µm filter before analysis by flow cytometry.

References

1. Gilbert, S. F., Singer, S. R., Tyler, M. S., and Kozlowski, R. N. (2006) Developmental Biology, Sinauer Associates, Inc. Publishers, Sunderland, Mass.

2. Yaniv, K., Isogai, S., Castranova, D., Dye, L., Hitomi, J., and Weinstein, B. M. (2006) Live imaging of lymphatic development in the zebrafish, *Nat. Med. 12*, 711-716.

3. McMahon, A., Supatto, W., Fraser, S. E., and Stathopoulos, A. (2008) Dynamic analyses of *Drosophila* gastrulation provide insights into collective cell migration, *Science 322*, 1546-1550.

4. Keller, P. J., Schmidt, A. D., Wittbrodt, J., and Stelzer, E. H. (2008) Reconstruction of zebrafish early embryonic development by scanned light sheet microscopy, *Science 322*, 1065-1069.

5. Giepmans, B. N. G., Adams, S. R., Ellisman, M. H., and Tsien, R. Y. (2006) The fluorescent toolbox for assessing protein location and function, *Science 312*, 217-224.

6. Beis, D., and Stainier, D. Y. (2006) In vivo cell biology: following the zebrafish trend, *Trends Cell Biol. 16*, 105-112.

7. Laughlin, S. T., and Bertozzi, C. R. (2009) Imaging the glycome, *Proc. Natl. Acad. Sci. U.S.A. 106*, 12-17.

8. Varki, A., Cummings, R. D., Esko, J. D., Freeze, H. H., Stanley, P., Bertozzi, C. R., Hart, G. W., and Etzler, M. E. (2009) Essentials of Glycobiology, Cold Spring Harbor Laboratory Press, Cold Spring Harbor, N.Y.

9. Haltiwanger, R. S., and Lowe, J. B. (2004) Role of glycosylation in development, *Annu. Rev. Biochem. 73*, 491-537.

10. Prescher, J. A., and Bertozzi, C. R. (2006) Chemical technologies for probing glycans, *Cell 126*, 851-854.

11. Prescher, J. A., and Bertozzi, C. R. (2005) Chemistry in living systems, *Nat. Chem. Biol. 1*, 13-21.

12. Laughlin, S. T., Baskin, J. M., Amacher, S. L., and Bertozzi, C. R. (2008) In vivo imaging of membrane-associated glycans in developing zebrafish, *Science 320*, 664-667.

13. Baskin, J. M., Prescher, J. A., Laughlin, S. T., Agard, N. J., Chang, P. V., Miller, I. A., Lo, A., Codelli, J. A., and Bertozzi, C. R. (2007) Copper-free click chemistry for dynamic in vivo imaging, *Proc. Natl. Acad. Sci. U.S.A. 104*, 16793-16797.

14. Guerardel, Y., Chang, L. Y., Maes, E., Huang, C. J., and Khoo, K. H. (2006) Glycomic survey mapping of zebrafish identifies unique sialylation pattern, *Glycobiology 16*, 244-257.

15. Chang, L. Y., Harduin-Lepers, A., Kitajima, K., Sato, C., Huang, C. J., Khoo, K. H., and Guerardel, Y. (2009) Developmental regulation of oligosialylation in zebrafish, *Glycoconjugate J. 26*, 247-261.

16. Kane, D. A., and Kimmel, C. B. (1993) The zebrafish midblastula transition, *Development 119*, 447-456.

17. Hang, H. C., Yu, C., Kato, D. L., and Bertozzi, C. R. (2003) A metabolic labeling approach toward proteomic analysis of mucin-type O-linked glycosylation, *Proc. Natl. Acad. Sci. U.S.A. 100*, 14846-14851.

18. Kimmel, C. B., and Law, R. D. (1985) Cell lineage of zebrafish blastomeres. I. Cleavage pattern and cytoplasmic bridges between cells, *Dev. Biol. 108*, 78-85.

19. Pauls, S., Geldmacher-Voss, B., and Campos-Ortega, J. A. (2001) A zebrafish histone variant H2A.F/Z and a transgenic H2A.F/Z:GFP fusion protein for in vivo studies of embryonic development, *Dev. Genes Evol. 211*, 603-610.

20. Lowell, C. A. (2004) Src-family kinases: Rheostats of immune cell signaling, *Mol. Immunol. 41*, 631-643.

21. Megason, S. G. (2009) In toto imaging of embryogenesis with confocal time-lapse microscopy, *Methods Mol. Biol. 546*, 317-332.

22. Albertson, R., Riggs, B., and Sullivan, W. (2005) Membrane traffic: A driving force in cytokinesis, *Trends Cell Biol. 15*, 92-101.

23. Shuster, C. B., and Burgess, D. R. (2002) Targeted new membrane addition in the cleavage furrow is a late, separate event in cytokinesis, *Proc. Natl. Acad. Sci. U.S.A. 99*, 3633-3638.

24. Gromley, A., Yeaman, C., Rosa, J., Redick, S., Chen, C. T., Mirabelle, S., Guha, M., Sillibourne, J., and Doxsey, S. J. (2005) Centriolin anchoring of exocyst and SNARE complexes at the midbody is required for secretory-vesicle-mediated abscission, *Cell 123*, 75-87.

25. Baskin, J. M., Dehnert, K. W., Laughlin, S. T., Amacher, S. L., and Bertozzi, C. R. (2010) Visualizing enveloping layer glycans during zebrafish early embryogenesis, *Proc. Natl. Acad. Sci. U.S.A. 107*, 10360-10365.

26. Hang, H. C., Yu, C., Pratt, M. R., and Bertozzi, C. R. (2004) Probing glycosyltransferase activities with the Staudinger ligation, *J. Am. Chem. Soc. 126*, 6-7.

27. Kimmel, C. B., Ballard, W. W., Kimmel, S. R., Ullmann, B., and Schilling, T. F. (1995) Stages of embryonic development of the zebrafish, *Dev. Dyn. 203*, 253-310.

Chapter 3

Metabolic Labeling of Fucosylated Glycans

Chapter 3. Metabolic Labeling of Fucosylated Glycans[1]

Introduction

Fucosylation is essential for proper cell signaling and embryonic development. For example, the Notch receptor must be fucosylated for Notch signaling, which regulates stem cell fate decisions and organogenesis (*1-3*). Fucose also resides at the periphery of N- and O-glycans in structures such as Lewis x, an epitope also known as stage-specific embryonic antigen 1 (SSEA-1) that is found in mouse early embryogenesis (*4*, *5*). Lewis x is also present in the developing brain, where it is thought to be important for cell-cell interactions (*4*, *6*, *7*). In zebrafish, a mutant that is deficient in the *de novo* biosynthetic pathway for fucose exhibits neural migration defects (*8*). Mouse knockouts of fucose biosynthetic genes and fucosyltransferases have demonstrated that the sugar is necessary for diverse aspects of embryogenesis, organogenesis, and neurogenesis (*2*, *9-12*). However, determining the actual functions of fucosylation during these processes would benefit from an ability to analyze the fucose modification in a living organism.

This chapter describes a method for imaging fucosylated glycans *in vivo*. We chose the zebrafish as our model organism due to its well-defined developmental program, optically transparent embryos, and ease of microinjection with exogenous reagents (*13*). We applied the bioorthogonal chemical reporter strategy (*14*), which was used in Chapter 2 to image mucin-type O-glycans, for fucose labeling. In this strategy, azide-functionalized monosaccharides are incorporated into cell-surface glycans via the cells' own metabolic machinery. The azide is subsequently reacted with an imaging probe or pull-down reagent via copper-free click chemistry (*15*).

Results and Discussion

Strategy for metabolic labeling via the fucose salvage pathway and fucosyltransferase enzymes

To label fucosylated glycans, we utilized several analogs of fucose modified at the C6-position with an azide (FucAz, Figure 3.1). In mammalian cell culture, FucAz traverses endogenous metabolic pathways and is incorporated into cell-surface glycans (*16*, *17*). FucAz is utilized by the fucose salvage pathway, where it is first converted to FucAz-1-phosphate (FucAz-1-P) by fucose kinase (FUK) and then to GDP-FucAz by fucose-1-phosphate guanyltransferase (FPGT) (Figure 3.1). GDP-FucAz is transported into the Golgi apparatus, where it serves as a substrate for fucosyltransferases (FucTs) that install FucAz onto glycoproteins. At the cell surface, the azide-labeled glycans can be imaged via reaction with a difluorinated cyclooctyne reagent conjugated to Alexa Fluor 488 (DIFO-488) (*18*).

---

[1] Brendan Beahm, Thinh Huynh, Jeremy Baskin, and Scott Laughlin contributed to the work presented in this chapter.

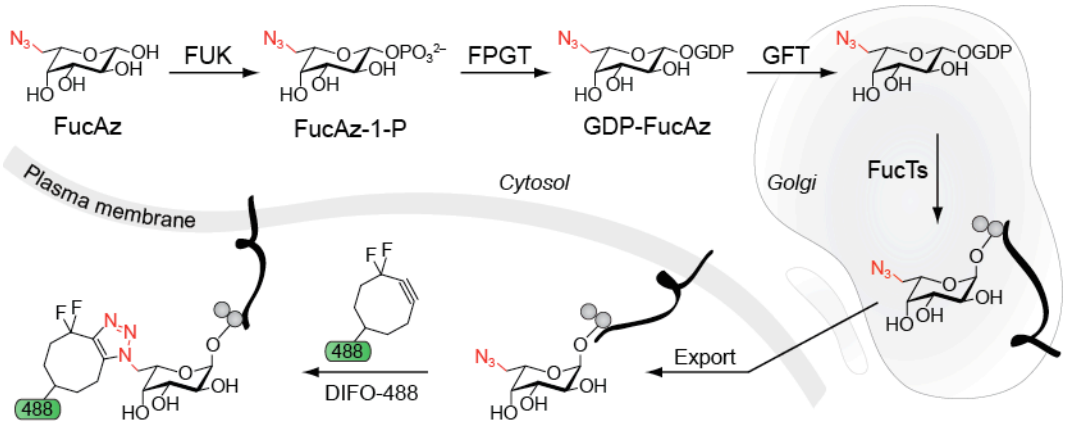

Figure 3.1. Pathway for metabolic labeling of fucosylated glycans using 6-azido fucose (FucAz). In the fucose salvage pathway, FucAz is converted to FucAz-1-phosphate (FucAz-1-P) and then to GDP-FucAz by the sequential actions of fucose kinase (FUK) and fucose-1-phosphate guanyltransferase (FPGT). GDP-FucAz is then transported into the Golgi lumen by the GDP-fucose transporter (GFT). Within the Golgi compartment, fucosyltransferases (FucTs) add FucAz to glycoproteins, which are then exported to the cell surface or secreted. To image FucAz incorporated into cell-surface glycans, the azide is reacted with an Alexa Fluor 488 conjugate of DIFO (DIFO-488).

For this strategy to be feasible in zebrafish, the salvage pathway and fucosyltransferase enzymes must be expressed in the embryo. The fucose salvage pathway, which is present in mammals but absent from *Drosophila* (*19*), has not been characterized in zebrafish, although salvage pathway candidate genes are registered in GenBank (accession numbers XP_001344272 and NP_001018590). The zebrafish mutant that is deficient in the *de novo* biosynthetic pathway for fucose retains the ability to fucosylate Notch, but its neural migration defect at 48 hours post-fertilization (hpf) is not rescued by injection of fucose (*8*). These observations suggest that fucose salvage occurs during early embryogenesis but perhaps at very low levels. Indeed, in mammalian cell lines, fucose salvage has been shown to account for only 10% of total fucosylation (*20*).

Expression of fucosylation pathway genes during zebrafish embryogenesis

We began our analysis by directly analyzing the expression of fucose salvage pathway enzymes. We used RT-PCR to detect mRNA transcripts at several stages of development (Figure 3.2). We found that both salvage pathway enzymes, FUK and FPGT, had detectable transcripts at the 16–32-cell stage, before zygotic transcription begins (*21*), indicating that these transcripts are provided maternally. Zygotic expression of FUK and FPGT was detectable after mid-segmentation stages. In contrast, transcripts for GDP-mannose 4,6-dehydratase (GMDS), a key enzyme in the *de novo* biosynthesis of GDP-fucose (*22*), were detected at all of the stages tested. Transcripts of the Golgi GDP-fucose transporter GFT were found at all stages as well.

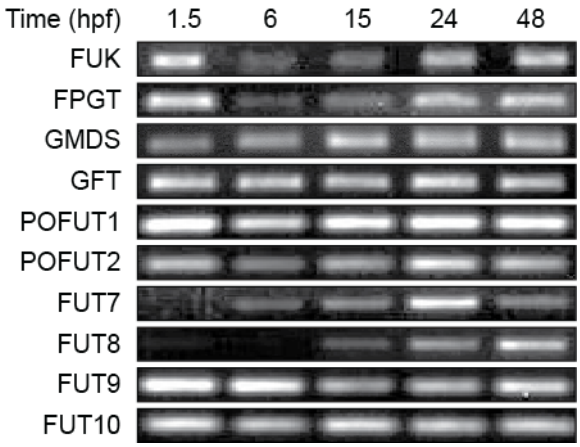

Figure 3.2. Expression of fucosylation pathway proteins during zebrafish embryogenesis. Transcripts were detected by RT-PCR analysis at various developmental stages (hpf, hours post-fertilization). FUK, fucose kinase; FPGT, fucose-1-phosphate guanyltransferase; GMDS, GDP-mannose 4,6-dehydratase; GFT, Golgi GDP-fucose transporter; POFUT1-2, protein O-fucosyltransferases; FUT7-10, various fucosyltransferases.

We also examined the expression of putative fucosyltransferase genes that are predicted from genome analysis (*8*). The corresponding enzymes are classified based on the type of fucosyl linkage that they are predicted to generate. The protein O-fucosyltransferases POFUT1 and POFUT2, which catalyze the addition of fucose to the hydroxyl groups of serine and threonine residues, were expressed at all of the stages tested. The former is required for Notch signaling (*2*), and the latter fucosylates thrombospondin type I repeats found in many extracellular matrix proteins from *Caenorhabditis elegans* to humans (*23*). Among the predicted α1,3-fucosyltransferases, which catalyze the addition of fucose to terminal glycan structures such as Lewis x, FUT9 was expressed at all of the stages tested, and FUT7 was expressed from 6 hpf onward. These results are consistent with existing *in situ* expression data for POFUT1 and FUT9 (*24*). Two additional α1,3-fucosyltransferases in zebrafish, FT1 and FT2, have been shown to synthesize Lewis x *in vitro* and are expressed only at 15–18 hpf and 72 hpf, respectively (*25*). Additionally, the predicted core N-glycan α1,3-fucosyltransferase FUT10 was expressed at all of the stages tested, and transcripts of the core N-glycan α1,6-fucosyltransferase FUT8 were detected from 15 hpf onward. The presence of these transcripts, along with those of the salvage pathway and *de novo* biosynthetic enzymes, suggests that fucosylated glycans are synthesized during early development and that the necessary machinery for metabolic labeling is present.

Metabolic labeling of fucosylated glycans with azide-derivatized precursors

Encouraged by these expression data, we attempted to label fucosylated glycans by treatment with FucAz. We bathed embryos in medium containing cell-permeable, peracetylated FucAz for two days and then reacted the embryos with DIFO-488 to

visualize FucAz that had been incorporated into cell-surface glycans. However, these embryos exhibited no azide-dependent cell-surface labeling (Figure 3.3).

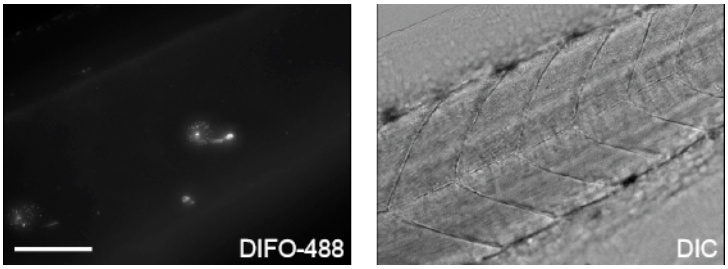

Figure 3.3. Bathing of zebrafish embryos in medium containing peracetylated FucAz did not provide cell-surface labeling of fucosylated glycans upon reaction with DIFO-488. Zebrafish embryos were dechorionated at 4 hpf and then bathed in embryo medium containing 5 mM peracetylated FucAz. At 48 hpf, the embryos were reacted with DIFO-488 and imaged. Left, maximum-intensity z-projection images of DIFO-488 fluorescence of the tail. Right, differential interference contrast (DIC) image. Scale bar: 100 μm.

This result suggested that one of the proteins in the biosynthetic pathway might not accept the unnatural azide-modified substrate. Because human FucTs can tolerate large modifications at the C6 position of fucose (*26*, *27*), we suspected that one of the salvage pathway enzymes or the Golgi GDP-fucose transporter formed a bottleneck. We therefore sought to systematically bypass enzymes in the pathway by metabolic labeling with the downstream intermediates FucAz-1-P and GDP-FucAz. Because these reagents are not cell-permeable, we microinjected them into the yolk of 1–8-cell zebrafish embryos. At this stage, small molecules injected into the yolk are taken up into the first cells of the organism and subsequently distributed to all of the daughter cells over the course of development (*28*, *29*).

As described in Chapter 2, we previously demonstrated that microinjection of zebrafish embryos with other azidosugars followed by reaction with DIFO-488 enables fluorescence imaging of cell-surface glycans in the enveloping layer (*29*). Using a similar method, embryos were microinjected with FucAz-1-P, GDP-FucAz, or vehicle alone and were allowed to develop for 10 h. The embryos were then bathed in a solution of DIFO-488 to react with azide-labeled glycans in the enveloping layer and imaged by confocal microscopy.

We observed robust cell-surface DIFO-488 fluorescence in the enveloping layer of embryos injected with GDP-FucAz and no detectable signal from embryos injected with vehicle alone (Figure 3.4, top). This result is consistent with a recent report of metabolic labeling using an alkynyl derivative of fucose (*30*). Embryos injected with FucAz-1-P displayed weak cell-surface fluorescence that was only detectable using higher laser power and detector gain (Figure 3.4, bottom). This result suggests that conversion of FucAz-1-P to GDP-FucAz is inefficient in zebrafish. This observation contrasts with the relatively efficient enzymatic conversion of azide-modified sialic acid precursors to sialosides in mammalian systems (*31*).

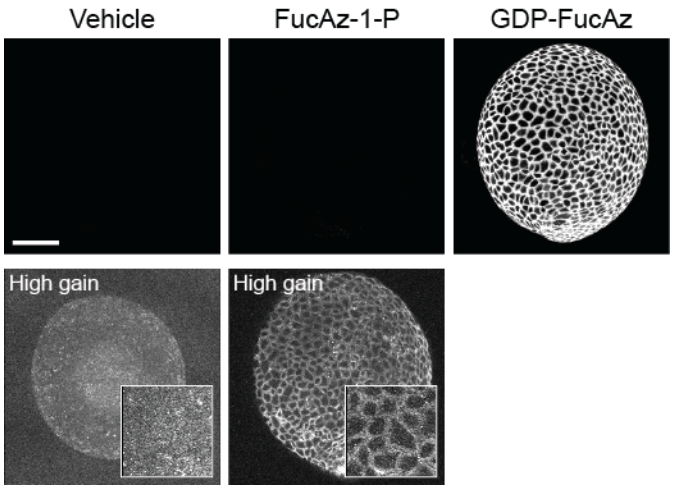

Figure 3.4. GDP-FucAz metabolically labels cell-surface glycans of the enveloping layer more efficiently than FucAz-1-P. Fluorescence images of embryos microinjected with GDP-FucAz or FucAz-1-P. Zebrafish embryos were microinjected with 75 pmol of GDP-FucAz, FucAz-1-P, or vehicle alone, allowed to develop to 10 hpf, and reacted with DIFO-488. Shown are z-projection images of DIFO-488 fluorescence in the enveloping layer (EVL). Top, laser and detector gain settings optimized for fluorescence of GDP-FucAz–treated embryos. Bottom, laser and detector gain settings optimized for fluorescence of FucAz-1-P–treated embryos. Scale bar: 200 μm.

For a more quantitative comparison of the efficiencies of FucAz-1-P and GDP-FucAz metabolism, we analyzed cells from metabolically labeled and then dissociated zebrafish embryos using flow cytometry. Embryos were microinjected with FucAz-1-P, GDP-FucAz, or vehicle alone, and were then allowed to develop to 15 hpf. The embryos were incubated with the *N*-hydroxysuccinimidyl ester of Alexa Fluor 488 (NHS-488), a charged dye that reacts with amines on the organism's surface, to specifically label cells of the enveloping layer. The embryos were then dissociated by treatment with ethylenediaminetetraacetic acid (EDTA), the cell suspension was labeled with DIFO-biotin followed by avidin-allophycocyanin (avidin-APC), and cellular fluorescence was quantified by flow cytometry.

Enveloping layer cells (identified by their high NHS-488 fluorescence) from GDP-FucAz–injected embryos displayed over 7-fold higher avidin-APC signal than cells from embryos injected with FucAz-1-P or vehicle alone (Figure 3.5, panel a, left). This result is consistent with the imaging analysis of the enveloping layer. Cells from the interior of the organism (identified by their low NHS-488 fluorescence) also exhibited avidin-APC signal that was higher in GDP-FucAz–injected embryos than in FucAz-1-P– or vehicle–injected embryos (Figure 3.5, panel a, right). This observation indicates that internal cells also incorporate FucAz into their glycans by 15 hpf, although apparently to a lesser extent than enveloping layer cells (Figure 3.5, panel b). However, a direct comparison of enveloping layer and internal cells by flow cytometry is difficult because the analysis involves a heterogeneous population with different cell types, sizes, and granularities.

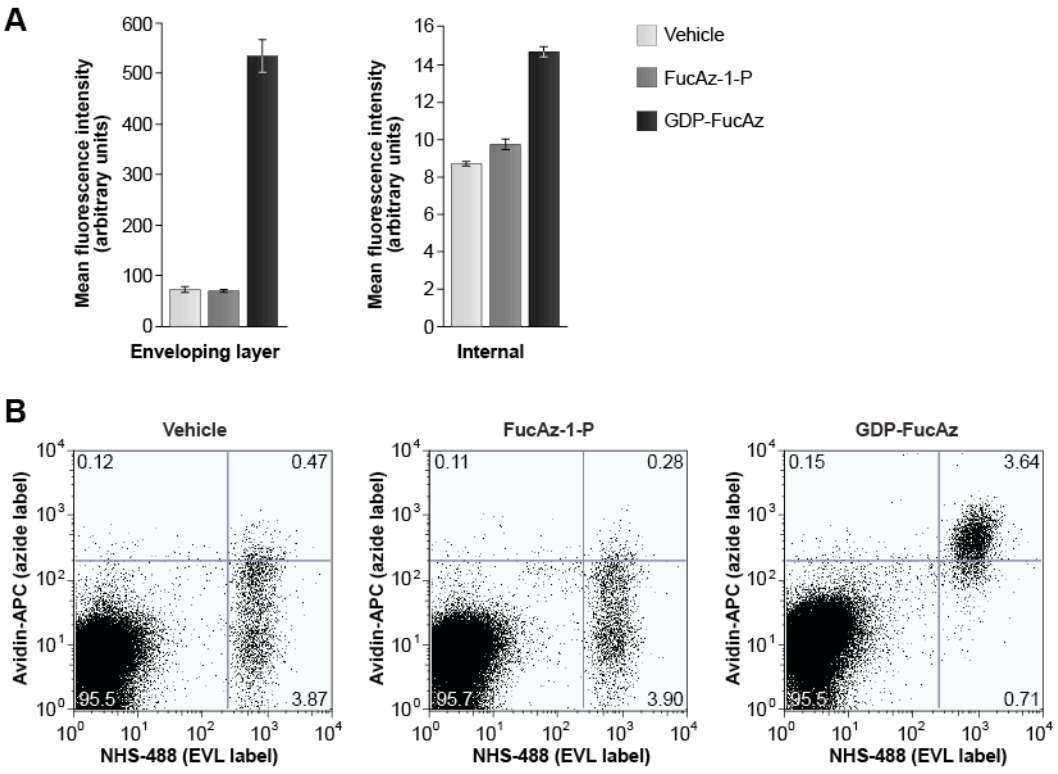

Figure 3.5. Flow cytometry analysis of EVL and internal cells after metabolic and chemical labeling. (A) Zebrafish embryos were microinjected with 75 pmol of the indicated sugar and allowed to develop to 15 hpf. Cells of the EVL were labeled with NHS-488. The embryos were dissociated and the resulting cell suspension was reacted with DIFO-biotin, incubated with avidin-APC, and analyzed by flow cytometry. Error bars represent standard error for three replicates. (B) FucAz labeling is most pronounced on EVL cells (detected with NHS-488). Shown are representative flow cytometry plots corresponding to data shown in A. Each plot includes at least 50,000 cells. Numbers in corners of quadrants represent the percent of total.

The ability of GDP-FucAz to label fucosylated glycans implies that this unnatural substrate enters the Golgi lumen and is utilized by fucosyltransferase enzymes. Although the mechanism of entry into the secretory pathway is unknown, it is expected to occur via active transport by the Golgi GDP-fucose transporter GFT (*32*). We sought to determine whether GDP-FucAz labeling was dependent on GFT expression. Using a translation-blocking morpholino oligonucleotide, we suppressed GFT expression and observed no decrease in DIFO-derived signal in embryos injected with the GFT morpholino compared to control embryos (Figure 3.6). This result suggests that there may be a second GDP-fucose transporter in zebrafish. Indeed, the zebrafish genome contains a homolog of Slc35c2, which has been proposed in recent studies to be a second GDP-fucose transporter in mammalian cells (*33*).

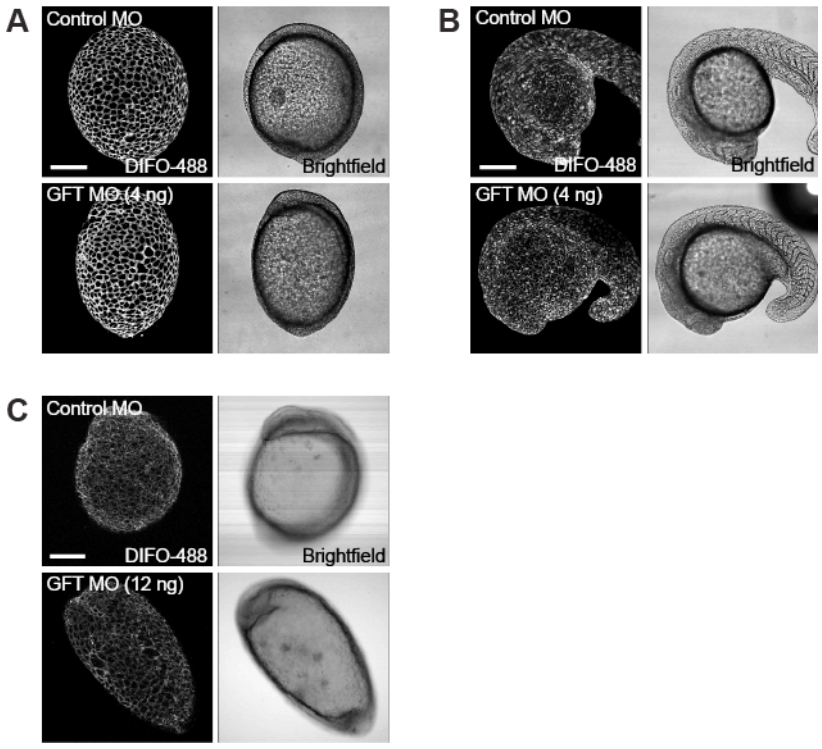

Figure 3.6. A translation-blocking morpholino (MO) against the Golgi GDP-fucose transporter GFT does not cause a decrease in labeling by GDP-FucAz and DIFO-488. Zebrafish embryos were microinjected with 25 pmol (A, B) or 5 pmol (C) of GDP-FucAz along with either 6 ng of a standard control morpholino (A, B, C, top panels), or 4 (A, B, bottom panels) or 12 (C, bottom panel) ng of a morpholino blocking translation of GFT. The embryos were allowed to develop and then were reacted at 11 hpf (A, C) or 24 hpf (B) with DIFO-488 and imaged. Shown are maximum-intensity z-projection images of DIFO-488 fluorescence and corresponding brightfield images. Scale bar: 200 μm.

The lack of labeling by FucAz-1-P, in contrast to the robust labeling with GDP-FucAz, suggests that the salvage pathway enzyme FPGT does not tolerate the 6-azido modification. Indeed, human FPGT is 160-fold less efficient when using an analog of fucose extended at the C6 position by a methyl group as a substrate (*34*). This observation may also explain the weak labeling by FucAz in cultured mammalian cells (*16*, *17*). Alternatively, although RT-PCR analysis showed that transcripts for the salvage pathway enzymes were present, this method is not quantitative, and it is possible that salvage pathway enzyme levels were not high enough to yield efficient labeling. Notably, FucAz is toxic to mammalian cells in culture (*16*); however, we did not observe any adverse effects on zebrafish embryos during incubation with 5 mM peracetylated FucAz in the medium or after microinjection of up to 125 pmol of FucAz-1-P or GDP-FucAz.

Imaging fucosylated glycans during the first five days of development using GDP-FucAz

We used GDP-FucAz as a metabolic substrate to determine the onset and extent of fucose labeling during early development. Embryos were microinjected with GDP-FucAz or vehicle alone, then reacted with DIFO-488 and imaged at several stages of

development. Cell-surface labeling of the enveloping layer was observed as early as 65% epiboly, or 7 hpf (Figure 3.7). The labeling intensity increased from mid-gastrulation to early segmentation periods (Figure 3.8). These dynamics are similar to those observed for expression of mucin-type O-glycans (*29*) and N-glycans (*35*), both of which can be modified by fucosylation. Fluorescence derived from FucAz-labeled glycans in the enveloping layer decreased from 24 hpf onward (Figure 3.8). This decrease in signal could be due to depletion or degradation of the GDP-FucAz substrate, or it could reflect decreasing levels of endogenous fucosylation. Indeed, labeling of fucosylated glycans in the enveloping layer by the fucose-binding *Aleuria aurantia* lectin (AAL) also decreased from 12 to 24 hpf, as determined by flow cytometry analysis (Figure 3.9). Nevertheless, signal from FucAz-labeled glycans remained strong enough to observe FucAz-dependent signal over the first five days of development.

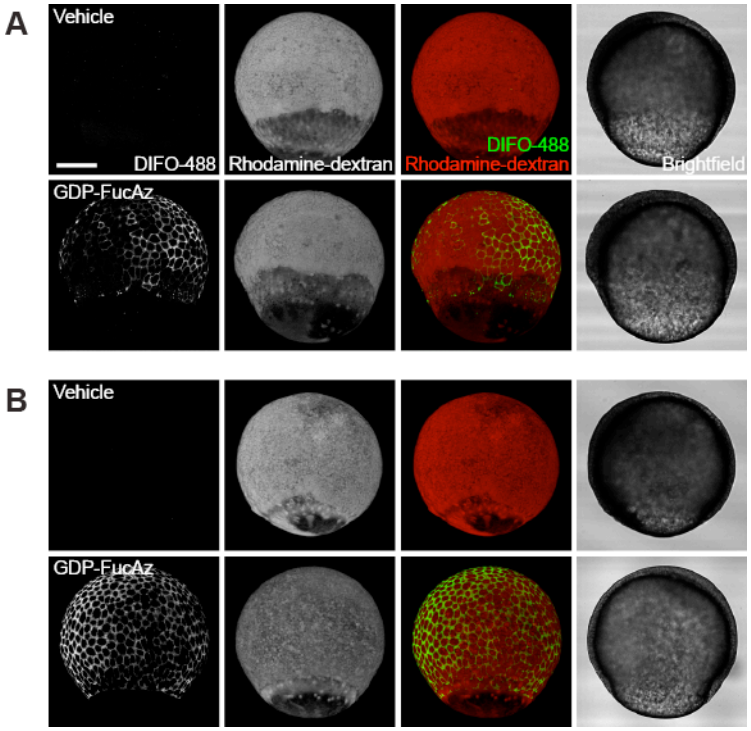

Figure 3.7. GDP-FucAz enables imaging of fucosylated glycans as early as 7 hpf. Zebrafish embryos were microinjected with 125 pmol of GDP-FucAz or vehicle alone, along with the tracer dye rhodamine-dextran. The embryos were allowed to develop and then were reacted with DIFO-488 and imaged at (A) 7 hpf or (B) 8.5 hpf. Shown are maximum-intensity z-projection images of DIFO-488 (green) and rhodamine-dextran (red) fluorescence and corresponding brightfield images. Scale bar: 200 μm.

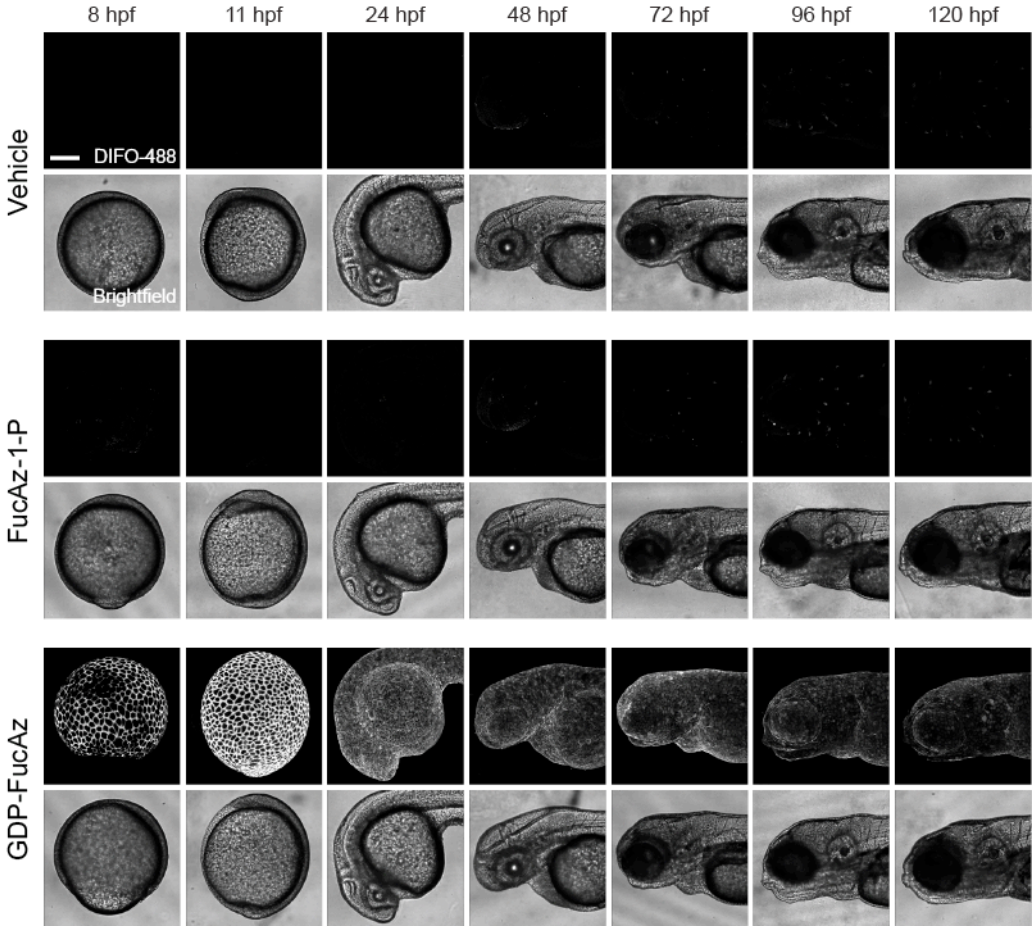

Figure 3.8. Microinjection of GDP-FucAz followed by copper-free click chemistry enables imaging of fucosylated glycans during the first five days of development. Zebrafish embryos were microinjected with vehicle alone (top), 75 pmol of FucAz-1-P (middle), or 75 pmol of GDP-FucAz (bottom) and allowed to develop, then treated with DIFO-488 and imaged at the time indicated. Shown are z-projection DIFO-488 fluorescence images of the EVL (rows 1, 3, 5) and corresponding brightfield images (rows 2, 4, 6). Scale bar: 200 μm.

During these studies we observed no toxicity or developmental defects due to FucAz incorporation into zebrafish glycans. This may suggest that the azide modification does not interfere with the normal functionality of fucosylated glycans, or that FucAz replaces a small enough fraction of natural fucose that its biological effects are indiscernible. The efficiency of the subsequent reaction of cell-surface azides with DIFO-488 is enhanced by the intrinsically high bimolecular rate constant of copper-free click chemistry (*18*) and the molar excess of DIFO utilized in these experiments. Thus, metabolic labeling with FucAz followed by copper-free click chemistry is an effective and non-toxic method for imaging fucosylated glycans *in vivo*.

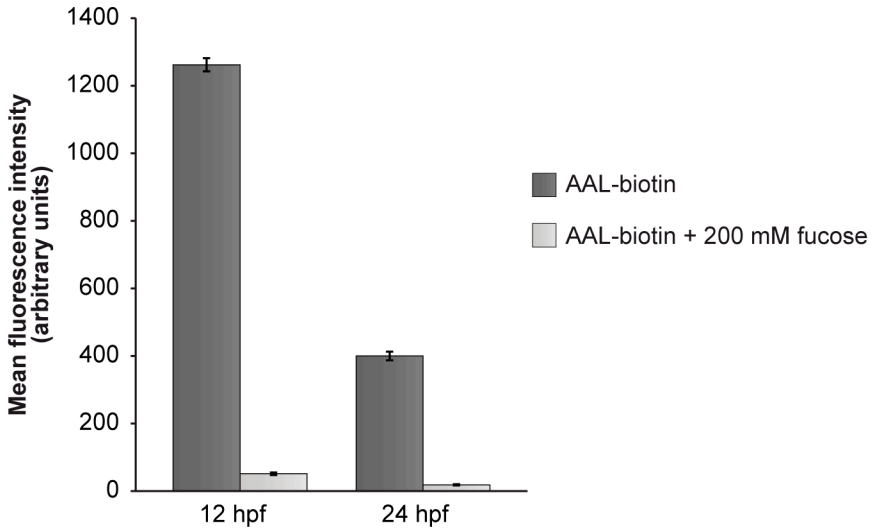

Figure 3.9. Flow cytometry analysis of enveloping layer (EVL) cells after embryo dissociation and labeling with fucose-binding *Aleuria aurantia* lectin (AAL). Zebrafish embryos at 12 or 24 hpf were reacted with NHS-647 to label cells of the EVL. Embryos were then dissociated, and the resulting cell suspension was treated with AAL-biotin in the presence or absence of 200 mM fucose as a competitor. The cells were incubated with avidin-FITC and analyzed by flow cytometry. Error bars represent standard error for three replicates.

Conclusion

In conclusion, we have successfully applied the chemical reporter strategy to enable visualization of fucosylation during zebrafish development. During these studies, we discovered that the fucose salvage pathway is expressed in zebrafish embryos but does not process azide-modified substrates efficiently. In contrast, fucosyltransferase enzymes readily utilize GDP-FucAz, thereby incorporating the azide into newly synthesized glycoconjugates. In addition to its use in imaging applications, the azide modification can be exploited for isolation and identification of fucosylated glycoproteins during development.

Experimental Methods

General materials and methods

All chemical reagents were of analytical grade, obtained from commercial suppliers, and used without further purification. DIFO-488 and DIFO-biotin (*18*), peracetylated FucAz (*16*), and FucAz-1-P and GDP-FucAz (*36*) were synthesized as previously described. Phenol red, *N*-phenylthiourea (PTU), pronase (protease, Type XIV, from *Streptomyces griseus*), tricaine (ethyl 3-aminobenzoate methanesulfonate), L-(–)-fucose, and avidin-fluorescein isothiocyanate (avidin-FITC) were obtained from Sigma-Aldrich. Rhodamine-dextran (dextran, tetramethylrhodamine, 10,000 MW), *N*-hydroxysuccinimidyl esters of Alexa Fluors 488 and 647 (NHS-488 and NHS-647), avidin-allophycocyanin (avidin-APC), TRIzol Reagent, Superscript III reverse transcriptase, and oligo(dT)20 primers were obtained from Invitrogen. Other primers were synthesized by Bioneer. Morpholino oligonucleotide reagents were designed and synthesized by Gene Tools. Biotinylated *Aleuria aurantia* lectin (AAL-biotin) was obtained from Associates of Cape Cod. Collagenase P was obtained from Roche Applied Science. Flow cytometry was performed on a BD Biosciences FACSCalibur flow cytometer, and analyses were performed using FlowJo software (Tree Star). All images except those shown in Figure 3.3 were acquired at the UC Berkeley Molecular Imaging Center on a Zeiss LSM 510 META laser scanning confocal microscope using a 10x/0.30 Plan-Neofluar air objective, 488 nm and 543 nm laser lines, and a focus step size of 5 μm. The images shown in Figure 3.3 were acquired on a Zeiss 200M epifluorescence microscope and deconvolved using a nearest neighbor deconvolution algorithm. All images were analyzed using Slidebook 5.0 (Intelligent Imaging Innovations).

Zebrafish stocks and husbandry

Adult wild-type AB zebrafish were kept at 28.5 °C on a 14-h light/10-h dark cycle. Embryos were obtained from natural spawning and were maintained in embryo medium (150 mM NaCl, 0.5 mM KCl, 1.0 mM $CaCl_2$, 0.37 mM KH_2PO_4, 0.05 mM Na_2HPO_4, 2.0 mM $MgSO_4$, 0.71 mM $NaHCO_3$ in deionized water, pH 7.4). Embryos were developmentally staged according to Kimmel and coworkers (*37*).

RT-PCR analysis

Total RNA was isolated from embryos at the indicated developmental stages using TRIzol Reagent and the Macherey-Nagel Total RNA Isolation kit. The first strand cDNA was synthesized using Superscript III reverse transcriptase and oligo(dT)20 as the first strand primer. The cDNA was amplified by PCR using the primers shown in Table 3.1, and the products were analyzed by agarose gel electrophoresis.

Table 3.1. Primer sequences for fucosylation pathway genes analyzed by RT-PCR.

Gene	Accession	Forward sequence	Reverse sequence	Product
FUK	XM_001344236	CCTACACACGGGACGAGATT	GTCCAGCGGTGGAGTAACAT	460 bp
FPGT	NM_001020754	CAGAACGCGGAAACGTCTAT	GGGAGGATCTGCAAACACAT	224 bp
GMDS	NM_001102475	ATGAACGGAGACAGCAAGAG	GCTGTCGGTCAAGTCTCCAT	229 bp
GFT	NM_001008590	AAGTTTGATTTGCGGGTGTC	CACCACCGGCAATACTTTCT	348 bp
POFUT1	NM_205718	TCTGAGGATCGGCTCTGATT	TGCAAGCTCACCACTTTCAC	285 bp
POFUT2	NM_001077630	AATACATCAGCTCCGCATCC	AAAACCCCAAAACCAACCTC	259 bp
FUT7	NM_001037390	AGGTGGGTTTGGCTTTCTTT	ACTCAGGGCCTTAACGGATT	519 bp
FUT8	NM_001003855	AGGTGGAGAATGGTGTGAGG	GGGTGAAGACTGTCCACGAT	544 bp
FUT9	NM_001007454	GCTTCATGCAACACCACACT	CCAAACCCACAGGAGTAGGA	276 bp
FUT10	NM_001012374	AAGAGGCTGGACAAGAACGA	CGCCAGACTTTAGGTGGAAG	224 bp

Metabolic labeling of zebrafish by microinjection of GDP-FucAz and FucAz-1-P

Zebrafish embryos at the 1–8-cell stage were microinjected into the yolk with 1–5 nL of 25 or 50 mM solutions of GDP-FucAz, FucAz-1-P, or no sugar (for doses of 75–125 pmol) in 0.2 M KCl, with rhodamine-dextran (5% w/v) or phenol red (0.05% w/v) as tracer dyes. Once the embryos developed to 4 hpf, they were enzymatically dechorionated by incubating for 10 min in a 1 mg/mL solution of pronase in embryo medium. All embryos younger than 12 hpf were maintained in 1% agarose-coated dishes. Embryos older than 24 hpf were incubated in embryo medium containing 131 μM PTU to inhibit melanin production.

Detection of cell-surface glycans by copper-free click chemistry and confocal microscopy

Embryos were reacted with 100 μM DIFO-488 in embryo medium for 1 h at 28.5 ºC. The embryos were rinsed by transfer through six successive 15-cm tissue culture dishes containing embryo medium. For imaging by confocal microscopy, the embryos were mounted between two cover slips in a solution of 0.6% low melting point agarose in embryo medium. Embryos 24 hpf and older were first anesthetized with 2.6 μM tricaine, and tricaine and 131 μM PTU were included in the agarose solution for mounting.

Flow cytometry of FucAz-labeled embryos

Zebrafish embryos were microinjected with 75 pmol of the indicated sugar and phenol red as described. At 15 hpf, the embryos were reacted with NHS-488 (50 μM in embryo medium with 1% DMSO) for 30 min at 28.5 ºC. After this reaction, the embryos were rinsed four times in embryo medium and were transferred to calcium-free Ringer's

solution (116 mM NaCl, 2.6 mM KCl, 5 mM HEPES in deionized water, pH 7.0) and deyolked by passage through a 200-µL pipette tip. The embryos were then incubated for 15 min at 28.5 ºC in a solution of 5 mM EDTA in phosphate-buffered saline (PBS), pH 7.6, to dissociate the cells. The reaction was stopped by the addition of 5% fetal bovine serum (FBS) and 1 mM $CaCl_2$ in PBS. The cells were rinsed once with labeling buffer (PBS, pH 7.6, 1% FBS). The cell suspension was reacted with DIFO-biotin (100 µM in labeling buffer) for 30 min at 28.5 ºC. Following this reaction, the cells were rinsed once with labeling buffer and then incubated with avidin-APC (50 µg/mL in labeling buffer) for 15 min on ice. The cells were then rinsed and reacted a second time for 30 min with avidin-APC. The cells were washed three times and resuspended in 300 µL of labeling buffer and passed through a 35-µm filter before analysis by flow cytometry.

Zebrafish cell labeling with AAL-biotin and analysis by flow cytometry

Embryos at 12 or 24 hpf were reacted with NHS-647 (50 µM in embryo medium with 1% DMSO) for 30 min at 28.5 ºC. After this reaction, the embryos were rinsed twice in embryo medium and then were transferred to calcium-free Ringer's solution and deyolked by passage through a 200-µL pipette tip. The embryos were incubated for 15 min at 28.5 ºC in a solution of 5 mM EDTA and 2 mg/mL collagenase P in PBS, pH 7.6, to dissociate the cells. The reaction was stopped by the addition of 5% FBS and 1 mM $CaCl_2$ in PBS. The cells were rinsed once with labeling buffer (PBS, pH 7.6, 1% FBS). The cell suspension was treated with a solution of AAL-biotin (20 µg/mL, alone or with a 20-min pre-incubation of lectin with 200 mM L-fucose as a competitor, in labeling buffer) for 45 min on ice. Following this reaction, the cells were rinsed twice with labeling buffer and incubated with avidin-FITC (50 µg/mL in labeling buffer) for 30 min on ice. The cells were washed twice and resuspended in 400 µL of labeling buffer and passed through a 35-µm filter before analysis by flow cytometry.

Treatment with morpholino oligonucleotides

Embryos at the 1–4-cell stage first were injected with 1 nL of 5 or 25 mM solutions of GDP-FucAz (in deionized water with 0.2 M KCl and 5% w/v rhodamine-dextran) and then were injected with 1–6 nL of solutions containing morpholino oligonucleotides (2 ng/nL) in Danieau solution (58 mM NaCl, 0.7 mM KCl, 0.4 mM $MgSO_4$, 0.6 mM $Ca(NO_3)_2$, 5.0 mM HEPES, pH 7.6) with 0.1% phenol red. In order to reduce off-target effects mediated by activation of p53, a morpholino against p53 was included in each solution at the same dose as the experimental morpholino (*38*).
Sequences:
Gene Tools standard control oligo, 5'-CCTCTTACCTCAGTTACAATTTATA-3'
Gene Tools zebrafish p53 oligo, 5'-GCGCCATTGCTTTGCAAGAATTG-3'
GFT translation-blocking morpholino, 5'-TGGAGTCTGTGAAGGCCATTTTTAA-3'

References

1. Haltiwanger, R. S., and Lowe, J. B. (2004) Role of glycosylation in development, *Annu. Rev. Biochem. 73*, 491-537.

2. Shi, S., and Stanley, P. (2003) Protein O-fucosyltransferase 1 is an essential component of Notch signaling pathways, *Proc. Natl. Acad. Sci. U.S.A. 100*, 5234-5239.

3. Artavanis-Tsakonas, S., Rand, M. D., and Lake, R. J. (1999) Notch signaling: cell fate control and signal integration in development, *Science 284*, 770-776.

4. Becker, D. J., and Lowe, J. B. (2003) Fucose: biosynthesis and biological function in mammals, *Glycobiology 13*, 41R-53R.

5. Solter, D., and Knowles, B. B. (1978) Monoclonal antibody defining a stage-specific mouse embryonic antigen (SSEA-1), *Proc. Natl. Acad. Sci. U.S.A. 75*, 5565-5569.

6. Ma, B., Simala-Grant, J. L., and Taylor, D. E. (2006) Fucosylation in prokaryotes and eukaryotes, *Glycobiology 16*, 158R-184R.

7. Muramatsu, T., and Muramatsu, H. (2004) Carbohydrate antigens expressed on stem cells and early embryonic cells, *Glycoconjugate J. 21*, 41-45.

8. Ohata, S., Kinoshita, S., Aoki, R., Tanaka, H., Wada, H., Tsuruoka-Kinoshita, S., Tsuboi, T., Watabe, S., and Okamoto, H. (2009) Neuroepithelial cells require fucosylated glycans to guide the migration of vagus motor neuron progenitors in the developing zebrafish hindbrain, *Development 136*, 1653-1663.

9. Kudo, T., Fujii, T., Ikegami, S., Inokuchi, K., Takayama, Y., Ikehara, Y., Nishihara, S., Togayachi, A., Takahashi, S., Tachibana, K., Yuasa, S., and Narimatsu, H. (2007) Mice lacking alpha 1,3-fucosyltransferase IX demonstrate disappearance of Lewis x structure in brain and increased anxiety-like behaviors, *Glycobiology 17*, 1-9.

10. Ishikawa, H. O., Higashi, S., Ayukawa, T., Sasamura, T., Kitagawa, M., Harigaya, K., Aoki, K., Ishida, N., Sanai, Y., and Matsuno, K. (2005) Notch deficiency implicated in the pathogenesis of congenital disorder of glycosylation IIc, *Proc. Natl. Acad. Sci. U.S.A. 102*, 18532-18537.

11. Wang, X., Gu, J., Miyoshi, E., Honke, K., and Taniguchi, N. (2006) Phenotype changes of Fut8 knockout mouse: core fucosylation is crucial for the function of growth factor receptor(s), *Methods Enzymol. 417*, 11-22.

12. Smith, P. L., Myers, J. T., Rogers, C. E., Zhou, L., Petryniak, B., Becker, D. J., Homeister, J. W., and Lowe, J. B. (2002) Conditional control of selectin ligand

expression and global fucosylation events in mice with a targeted mutation at the FX locus, *J. Cell Biol. 158*, 801-815.

13. Lieschke, G. J., and Currie, P. D. (2007) Animal models of human disease: zebrafish swim into view, *Nat. Rev. Genet. 8*, 353-367.

14. Laughlin, S. T., and Bertozzi, C. R. (2009) Imaging the glycome, *Proc. Natl. Acad. Sci. U.S.A. 106*, 12-17.

15. Jewett, J. C., and Bertozzi, C. R. (2010) Cu-free click cycloaddition reactions in chemical biology, *Chem. Soc. Rev. 39*, 1272-1279.

16. Rabuka, D., Hubbard, S. C., Laughlin, S. T., Argade, S. P., and Bertozzi, C. R. (2006) A chemical reporter strategy to probe glycoprotein fucosylation, *J. Am. Chem. Soc. 128*, 12078-12079.

17. Sawa, M., Hsu, T.-L., Itoh, T., Sugiyama, M., Hanson, S. R., Vogt, P. K., and Wong, C.-H. (2006) Glycoproteomic probes for fluorescent imaging of fucosylated glycans in vivo, *Proc. Natl. Acad. Sci. U.S.A. 103*, 12371-12376.

18. Baskin, J. M., Prescher, J. A., Laughlin, S. T., Agard, N. J., Chang, P. V., Miller, I. A., Lo, A., Codelli, J. A., and Bertozzi, C. R. (2007) Copper-free click chemistry for dynamic in vivo imaging, *Proc. Natl. Acad. Sci. U.S.A. 104*, 16793-16797.

19. Roos, C., Kolmer, M., Mattila, P., and Renkonen, R. (2002) Composition of *Drosophila* melanogaster proteome involved in fucosylated glycan metabolism, *J. Biol. Chem. 277*, 3168-3175.

20. Yurchenco, P. D., and Atkinson, P. H. (1977) Equilibration of fucosyl glycoprotein pools in HeLa cells, *Biochemistry 16*, 944-953.

21. Mathavan, S., Lee, S. G. P., Mak, A., Miller, L. D., Murthy, K. R. K., Govindarajan, K. R., Tong, Y., Wu, Y. L., Lam, S. H., Yang, H., Ruan, Y., Korzh, V., Gong, Z., Liu, E. T., and Lufkin, T. (2005) Transcriptome analysis of zebrafish embryogenesis using microarrays, *PLoS Genet. 1*, 260-276.

22. Sullivan, F. X., Kumar, R., Kriz, R., Stahl, M., Xu, G.-Y., Rouse, J., Chang, X.-jia, Boodhoo, A., Potvin, B., and Cumming, D. A. (1998) Molecular cloning of human GDP-mannose 4,6-dehydratase and reconstitution of GDP-fucose biosynthesis in vitro, *J. Biol. Chem. 273*, 8193-8202.

23. Luo, Y., Koles, K., Vorndam, W., Haltiwanger, R. S., and Panin, V. M. (2006) Protein O-fucosyltransferase 2 adds O-fucose to thrombospondin type 1 repeats, *J. Biol. Chem. 281*, 9393-9399.

24. Thisse, B., and Thisse, C. (2004) Fast release clones: A high throughput expression analysis, *ZFIN Direct Data Submission (http://zfin.org)*.

25. Kageyama, N., Natsuka, S., and Hase, S. (1999) Molecular cloning and characterization of two zebrafish alpha(1,3)fucosyltransferase genes developmentally regulated in embryogenesis, *J. Biochem. 125*, 838-845.

26. Srivastava, G., Kaur, K. J., Hindsgaul, O., and Palcic, M. M. (1992) Enzymatic transfer of a preassembled trisaccharide antigen to cell surfaces using a fucosyltransferase, *J. Biol. Chem. 267*, 22356-22361.

27. Vogel, C., Bergemann, C., Ott, A.-J., Lindhorst, T. K., Thiem, J., Dahlhoff, W. V., Hällgren, C., Palcic, M. M., and Hindsgaul, O. (1997) Synthesis of carbon-backbone-elongated GDP-L-fucose derivatives as substrates for fucosyltransferase-catalysed reactions, *Liebigs Ann. 1997*, 601-612.

28. Kimmel, C. B., and Law, R. D. (1985) Cell lineage of zebrafish blastomeres: I. Cleavage pattern and cytoplasmic bridges between cells, *Dev. Biol. 108*, 78-85.

29. Baskin, J. M., Dehnert, K. W., Laughlin, S. T., Amacher, S. L., and Bertozzi, C. R. (2010) Visualizing enveloping layer glycans during zebrafish early embryogenesis, *Proc. Natl. Acad. Sci. U.S.A. 107*, 10360-10365.

30. Soriano del Amo, D., Wang, W., Jiang, H., Besanceney, C., Yan, A. C., Levy, M., Liu, Y., Marlow, F. L., and Wu, P. (2010) Biocompatible copper(I) catalysts for in vivo imaging of glycans, *J. Am. Chem. Soc. 132*, 16893-16899.

31. Luchansky, S. J., Argade, S., Hayes, B. K., and Bertozzi, C. R. (2004) Metabolic functionalization of recombinant glycoproteins, *Biochemistry 43*, 12358-12366.

32. Puglielli, L., and Hirschberg, C. B. (1999) Reconstitution, identification, and purification of the rat liver golgi membrane GDP-fucose transporter, *J. Biol. Chem. 274*, 35596-35600.

33. Lu, L., Hou, X., Shi, S., Körner, C., and Stanley, P. (2010) Slc35c2 promotes Notch1 fucosylation and is required for optimal Notch signaling in mammalian cells, *J. Biol. Chem. 285*, 36245-36254.

34. Quirk, S., and Seley, K. L. (2005) Substrate discrimination by the human GTP fucose pyrophosphorylase, *Biochemistry 44*, 10854-10863.

35. Takemoto, T., Natsuka, S., Nakakita, S.-I., and Hase, S. (2005) Expression of complex-type N-glycans in developmental periods of zebrafish embryo, *Glycoconjugate J. 22*, 21-26.

36. Wang, W., Hu, T., Frantom, P. A., Zheng, T., Gerwe, B., del Amo, D. S., Garret, S., Seidel, R. D., and Wu, P. (2009) Chemoenzymatic synthesis of GDP-l-fucose and the Lewis X glycan derivatives, *Proc. Natl. Acad. Sci. U.S.A. 106*, 16096-16101.

37. Kimmel, C. B., Ballard, W. W., Kimmel, S. R., Ullmann, B., and Schilling, T. F. (1995) Stages of embryonic development of the zebrafish, *Dev. Dyn. 203*, 253-310.

38. Robu, M. E., Larson, J. D., Nasevicius, A., Beiraghi, S., Brenner, C., Farber, S. A., and Ekker, S. C. (2007) p53 activation by knockdown technologies, *PLoS Genet. 3*, e78.

Chapter 4

Imaging Sialic Acids in Zebrafish Embryos using a Metabolic Labeling Approach

Chapter 4. Imaging Sialic Acids in Zebrafish Embryos using a Metabolic Labeling Approach[1]

Introduction

All cells in vertebrates are adorned with sialic acids, a family of negatively-charged monosaccharides displayed on cell-surface glycoproteins and glycolipids. Because sialic acids often occupy terminal positions on these structures, they are well-situated to control biological interactions at the cell surface. For example, on N- and O-glycans, sialic acids present recognition sites for sialic acid-binding proteins and mask underlying antigenic epitopes such as terminal galactose (*1*, *2*). Linear polymers of sialic acid, which are called polysialic acid and found primarily on neural cell adhesion molecule (NCAM), provide a steric barrier to cell-cell adhesion (*3*, *4*) and regulate neuronal migration and differentiation during development (*5*, *6*). Finally, sialic acids in ganglisides, which are highly sialylated glycolipids especially abundant in the brain but also found on all other vertebrate cells, mediate cell-cell interactions and regulate the responsiveness of some signaling receptors, such as insulin and epidermal growth factor receptors (*7*). Disruption of de novo sialic acid biosynthesis in mice causes embryonic lethality, demonstrating that sialic acids are essential for mouse development (*8*).

Sialylated glycans can be labeled in cultured cells and live mice by supplying the sialic acid salvage pathway with azide-labeled analogs of *N*-acetylmannosamine (ManNAc), a precursor of sialic acids (*9*, *10*). In this strategy, cells are treated with cell-permeable, peracetylated *N*-azidoacetylmannosamine (Ac_4ManNAz), which is converted to azido sialic acid (SiaNAz) and incorporated into cell-surface glycans (Figure 4.1) (*11*, *12*). To visualize the azide, the cells are reacted with a difluorinated cyclooctyne (DIFO) reagent conjugated to an imaging probe (*13*).

We sought to extend this strategy toward imaging sialylated glycans in developing zebrafish. Zebrafish are a popular vertebrate model organism due in part to their well-characterized, external development (*14*) and transparent embryos, which are excellent for optical imaging (*15*). As described in Chapters 2 and 3, we have previously used a metabolic labeling strategy based on azide-derivatized monosaccharide precursors to image mucin-type O-glycans and fucosylated glycans during zebrafish development (*16*-*18*). This chapter presents a similar strategy to label and image sialylated glycans.

Results and Discussion

Metabolic labeling of sialic acids with Ac_4ManNAz

We first attempted to label sialic acids in zebrafish embryos over the first four days of development using Ac_4ManNAz. We incubated dechorionated embryos in medium containing Ac_4ManNAz from 4 to 96 hpf. Then at several stages of development, we reacted the embryos with DIFO-488 and then imaged them by confocal

[1] Jeremy Baskin and Scott Laughlin contributed to the work presented in this chapter.

microscopy. We observed robust signal in the enveloping layers of embryos from 24 to 96 hpf (Figure 4.2). Importantly, we observed little background signal in embryos incubated in medium that did not contain Ac_4ManNAz, indicating that the DIFO-488 signal that we observed was azide-specific. Additionally, the azidosugar and DIFO treatments did not result in any toxicity or developmental abnormalities in the treated embryos.

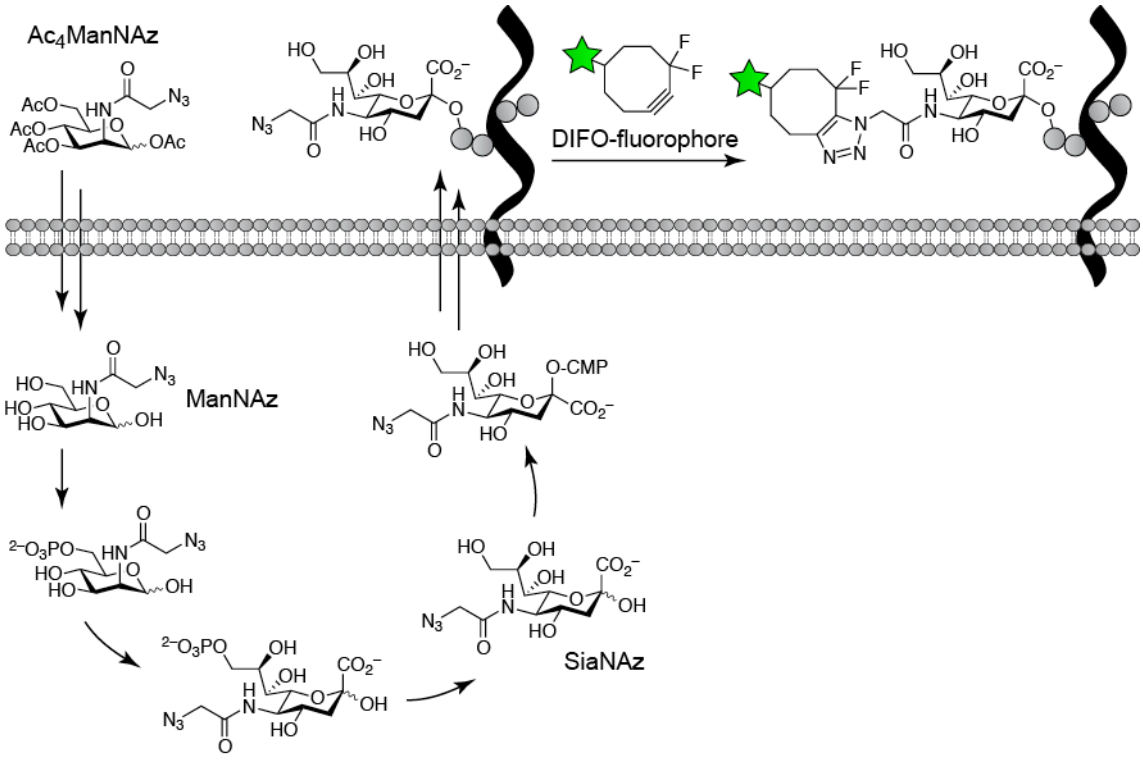

Figure 4.1. Strategy for metabolic labeling with *N*-azidoacetylmannosamine (ManNAz) and subsequent reaction with difluorinated cyclooctyne (DIFO) probes. Cell-permeable Ac_4ManNAz enters the cell and its acetate groups are cleaved by intracellular esterases. ManNAz then traverses the steps of the salvage pathway, through which it is converted to azido sialic acid (SiaNAz). SiaNAz is activated as a nucleotide sugar and then acts as a substrate for sialyltransferase enzymes that add it to glycoconjugates. At the cell surface, SiaNAz is visualized by reaction with DIFO-fluorophore conjugates.

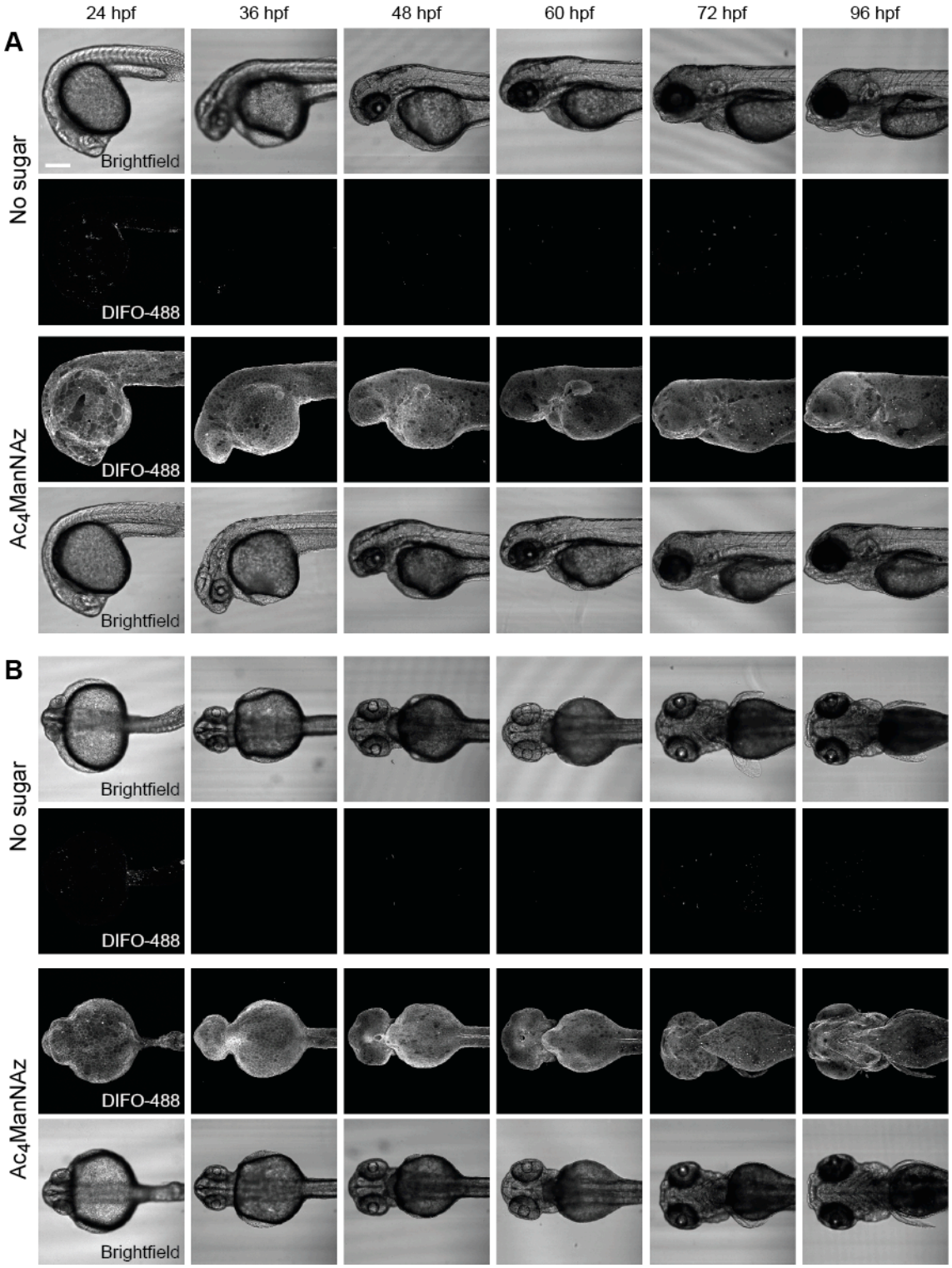

Figure 4.2. Treatment with Ac_4ManNAz followed by reaction with DIFO-488 provides labeling of sialic acids in the enveloping layer of zebrafish embryos. Embryos were incubated in a solution containing Ac_4ManNAz (or no sugar) beginning at 4 hpf and then were reacted with DIFO-488 at the indicated timepoints. Shown are z-projection images of DIFO-488 fluorescence and corresponding brightfield images of embryos, viewed laterally (A) and ventrally (B). Scale bar: 200 μm.

Two-color labeling for visualization of de novo sialic acid expression

Next, we sought to visualize the dynamic expression of cell-surface sialic acids over the course of development. We performed two DIFO labeling reactions in succession to probe for sialic acids biosynthesized at different stages of development (Figure 4.3). Zebrafish embryos were bathed in medium containing Ac_4ManNAz from 4 to 72 hpf, then reacted with DIFO-488 to visualize the sialic acids that had been synthesized during that period. After this reaction, any remaining cell-surface azides were quenched with tris-(2-carboxyethyl)phosphine (TCEP), a mild reducing agent. The embryos were returned to medium containing Ac_4ManNAz for an additional 3 h so that they could continue to incorporate SiaNAz into newly-synthesized glycans. These new SiaNAz-containing cell-surface glycans were reacted with DIFO-555. In this way, glycans synthesized between 73 and 76 hpf, labeled with DIFO-555, could be distinguished from those synthesized during the first three days of development.

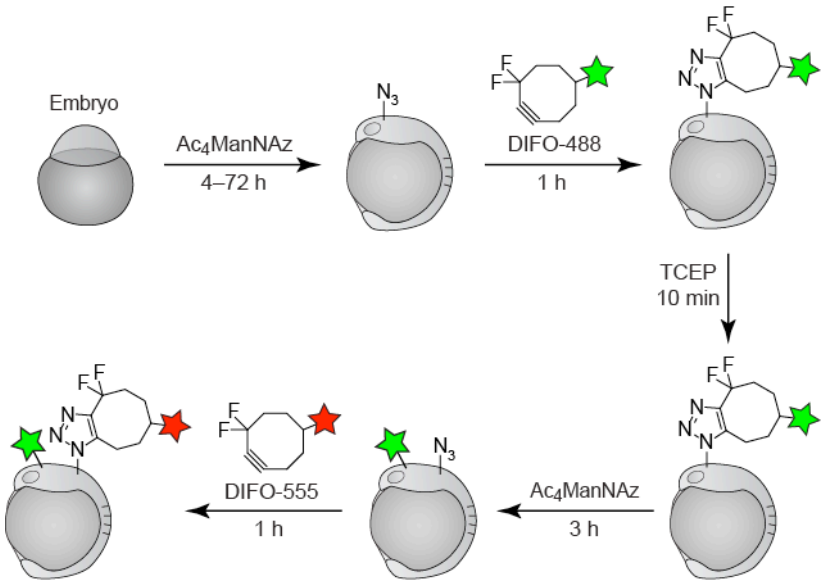

Figure 4.3. Strategy for two-color labeling of de novo sialic acid biosynthesis. Embryos were incubated with Ac_4ManNAz from 4 to 72 hpf and then were reacted with DIFO-488. Unreacted cell-surface azides were quenched by treatment with tris-(2-carboxyethyl)phosphine (TCEP) and the embryos were returned to medium containing Ac_4ManNAz for further metabolic labeling. Newly-synthesized SiaNAz-containing glycans were reacted DIFO-555.

This method revealed several areas of the embryo in which the pattern of new glycosylation differed from the old. Cells in the ventral jaw region of the embryo, for example, exhibited a corrugated pattern of labeling, with DIFO-488-labeled glycans concentrated in peaks that extended outward from the ventral surface, and DIFO-555-labeled glycans concentrated in troughs located more dorsally (Figure 4.4, panels A-C). In the olfactory organ, older glycans labeled by DIFO-488 were concentrated in the epithelium and at the opening of the olfactory pit, whereas newly synthesized, DIFO-555-

labeled glycans appeared primarily at the base of the olfactory pit (Figure 4.4, panels D-F).

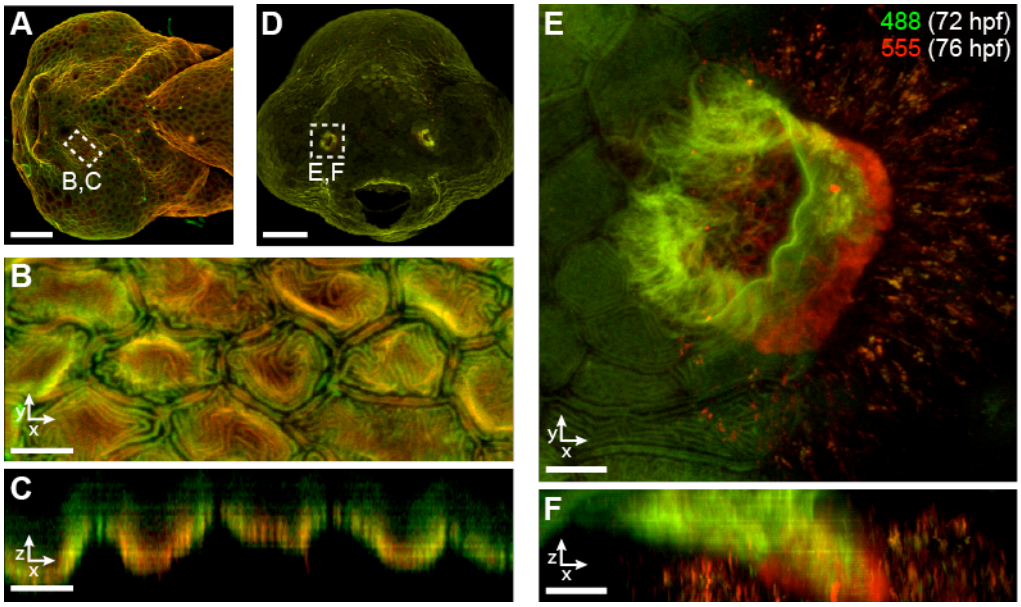

Figure 4.4. Two-color labeling of sialylated glycans at 72 and 76 hpf. Embryos were first reacted with DIFO-488 at 72 hpf, allowed to further incorporate SiaNAz for 3 h, and then reacted with DIFO-555 at 76 hpf. (A) Z-projection of DIFO-488 and DIFO-555 fluorescence from an embryo's ventral surface, with the area of interest for B and C indicated. (B) Z-projection fluorescence image of enveloping layer cells in the ventral jaw region. (C) A single x-z plane from the middle of the region indicated in A and B, from an image linearly interpolated by a factor of 3 along the z-axis. (D) Frontal view of an embryo with the area of interest for E and F indicated. (E) Z-projection fluorescence image of the olfactory organ and surrounding epithelium. (F) Y-projection of the same region shown in D, from an image linearly interpolated by a factor of 3 along the z-axis. Green, DIFO-488 (72 hpf); red, DIFO-555 (76 hpf). Scale bars: 100 μm (A, D); 10 μm (B, C, E, F).

We then extended the time between the first and second reactions, first labeling with DIFO-488 at 72 hpf and then with DIFO-555 at 79 hpf. Using this protocol, we observed a similar pattern of labeling in the olfactory organ (Figure 4.5, panel A). In most of the epithelium, we observed labeling by both DIFO-488 and DIFO-555, suggesting that sialylated glycans were expressed throughout the experiment, both before and after 72 hpf (Figure 4.5, panel B). However, portions of cells near the junctions with one another were labeled primarily with DIFO-555. Perhaps de novo glycan biosynthesis occurs at higher levels at these cell junctions, or perhaps those regions of the cells became solvent-exposed during the 6 h time lapse, and so were not accessible to the DIFO-488 reagent during the first reaction.

Finally, we performed labeling experiments with a 24-h Ac_4ManNAz incubation between the first and second DIFO reactions. For these experiments, embryos were labeled first with DIFO-555 at 72 hpf and then with DIFO-488 at 97 hpf. We observed particularly striking DIFO-488 labeling of the kinocilia of mechanosensory hair cells,

indicating that the glycosylation of these structures had occurred primarily between 72 and 97 hpf (Figure 4.6). Together, the results of these labeling experiments are similar to those observed for mucin-type O-glycans labeled with Ac_4GalNAz, which is not surprising considering that sialic acids are often found as terminal sugars on O-glycans.

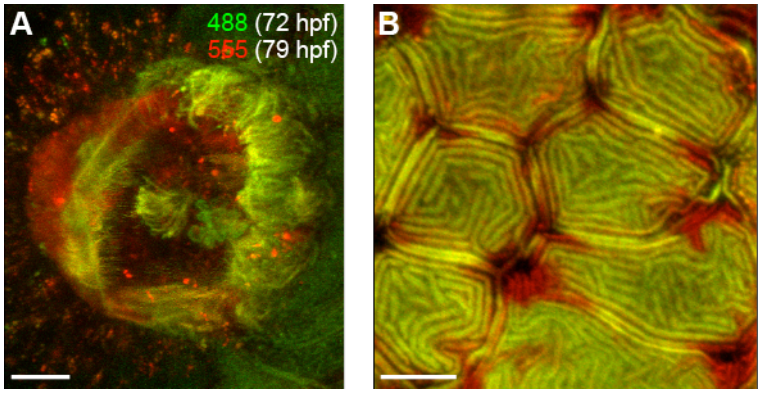

Figure 4.5. Two-color labeling of sialylated glycans in the olfactory organ and epithelium at 72 and 79 hpf. Embryos were first reacted with DIFO-488 at 72 hpf, then returned to Ac_4ManNAz-containing medium for 6 h and finally reacted with DIFO-555 at 79 hpf. (A) Z-projection of DIFO-488 and DIFO-555 fluorescence in the olfactory organ and surrounding epithelium. (B) Z-projection of DIFO-488 and DIFO-555 fluorescence of epithelial cells. Green, DIFO-488 (72 hpf); red, DIFO-555 (79 hpf). Scale bars: 10 μm.

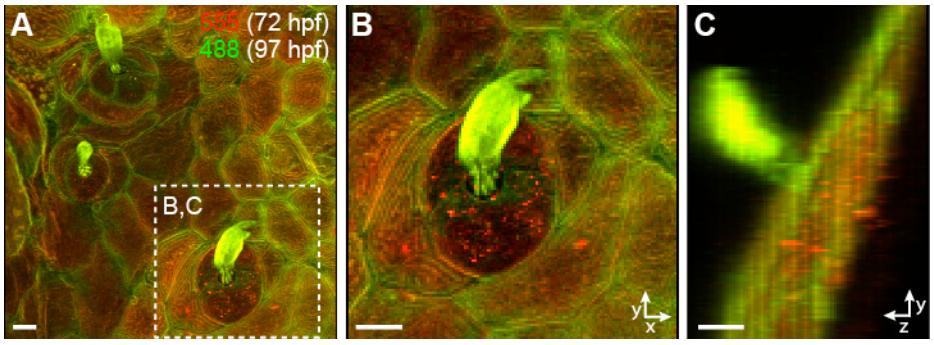

Figure 4.6. Two-color labeling of sialylated glycans on mechanosensory hair cells at 72 and 79 hpf. Embryos were first reacted with DIFO-555 at 72 hpf, then returned to Ac_4ManNAz-containing medium for 24 h and finally reacted with DIFO-488 at 97 hpf. (A) Z-projection fluorescence image of several kinocilia from mechanosensory hair cells. (B) A closer view of the hair cell indicated in A. (C) X-projection fluorescence image of the region shown in A, from an image linearly interpolated by a factor of 4 along the z-axis. Red, DIFO-555 (72 hpf); green, DIFO-488 (97 hpf). Scale bars: 10 μm.

Microinjection of the downstream intermediate SiaNAz provides labeling during early embryogenesis

To image sialic acids in zebrafish embryos before 24 hpf, we turned to microinjection of the downstream metabolic intermediate SiaNAz. As described in Chapters 2 and 3, microinjection of embryos at the 1–8-cell stage with the azidosugars GalNAz and GDP-FucAz provided labeling of mucin-type O-glycans and fucosylated glycans, respectively, as early as 7 hpf. We sought to extend this strategy toward imaging of sialic acids during early embryogenesis. We microinjected embryos with SiaNAz and allowed the embryos to develop, then reacted them with DIFO-488 at several timepoints. We observed cell-surface labeling of sialic acids at 9 hpf, during the gastrulation stage of development (Figure 4.7). However, the azide-derived signal was not far above the background signal observed in embryos injected with vehicle alone. This suggests that either incorporation of SiaNAz into sialylated glycans is inefficient, or that zebrafish have low levels of sialic acids during the first 12 hours of development.

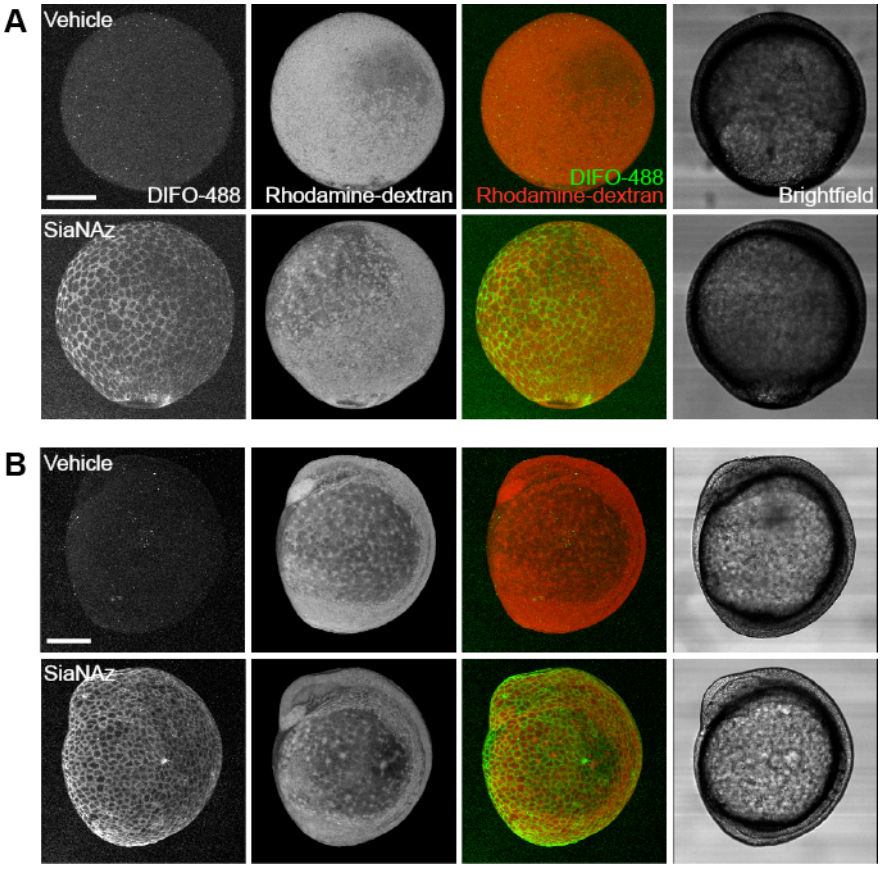

Figure 4.7. Microinjection of SiaNAz followed by detection with DIFO-488 enables visualization of sialic acids during gastrulation and early segmentation periods. Embryos were microinjected with SiaNAz or vehicle alone, along with rhodamine-dextran as a tracer. The embryos were reacted with DIFO-488 at either 8 hpf (A) or 10 hpf (B) and imaged. Shown are z-projection images of DIFO-488 and rhodamine-dextran fluorescence and corresponding brightfield images. Scale bars: 200 μm.

We allowed the SiaNAz-injected embryos to continue to develop over the next four days. On each day, we reacted several embryos with DIFO-488 and imaged them by confocal microscopy. We observed signal in the enveloping layer of embryos injected with SiaNAz and no signal in embryos injected with vehicle alone over the four-day experiment (Figure 4.8). Furthermore, as with Ac_4ManNAz treatment, we observed no developmental abnormalities in SiaNAz-injected embryos, indicating that SiaNAz incorporation and copper-free click chemistry are not toxic.

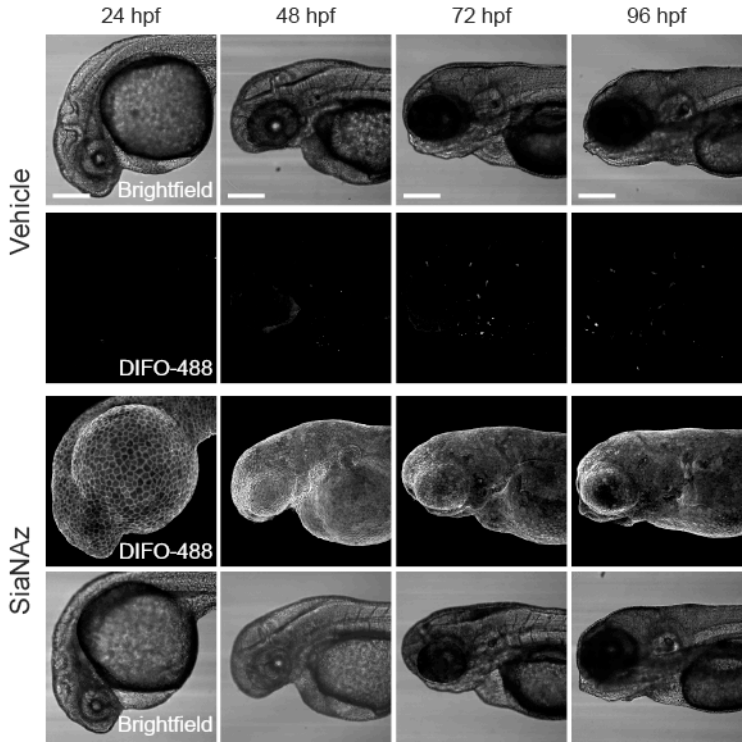

Figure 4.8. Microinjection of SiaNAz provides labeling of sialylated glycans during the first 96 h of development. Embryos were microinjected with SiaNAz or vehicle alone, allowed to develop to the developmental stages shown, and then reacted with DIFO-488. Shown are z-projection images of DIFO-488 fluorescence and corresponding brightfield images. Scale bars: 200 μm.

Conclusion

We have applied the metabolic labeling strategy to image sialic acids in embryonic and larval zebrafish. Microinjection of SiaNAz into embryos at the 1–8-cell stage afforded labeling during the gastrulation and early segmentation periods of development. As a complementary technique, incubation in medium containing Ac_4ManNAz provided robust labeling beginning at 24 hpf and continuing to 96 hpf. This metabolic labeling strategy enabled dynamic imaging of sialic acid biosynthesis using two DIFO reactions in rapid succession and revealed areas of particularly robust new

glycan expression in the olfactory organ and on the kinocilia of mechanosensory hair cells at different stages of development. These methods provide a platform for future sialic acid imaging and glycoproteomic applications.

Experimental Methods

General materials and methods

All chemical reagents were of analytical grade, obtained from commercial suppliers, and used without further purification. Pronase (protease, Type XIV, from *Streptomyces griseus*), *N*-phenylthiourea (PTU), tricaine (ethyl 3-aminobenzoate methanesulfonate), and tris-(2-carboxyethyl)phosphine (TCEP) hydrochloride were obtained from Sigma-Aldrich. Rhodamine-dextran (dextran, tetramethylrhodamine, 10,000 MW, lysine fixable) was obtained from Invitrogen. Ac_4ManNAz (*9*), SiaNAz (*19*), DIFO-488 (*13*), and DIFO-555 (*16*) were prepared as described previously. Confocal microscopy was performed at the UC Berkeley Molecular Imaging Center.

Zebrafish stocks and husbandry

Wildtype, AB-derived adult zebrafish were kept at 28 °C on a 14-h light/10-h dark cycle. Embryos were obtained from natural spawnings and raised at 28.5 °C in embryo medium (150 mM NaCl, 0.5 mM KCl, 1.0 mM $CaCl_2$, 0.37 mM KH_2PO_4, 0.05 mM Na_2HPO_4, 2.0 mM $MgSO_4$, 0.71 mM $NaHCO_3$ in deionized H_2O, pH 7.4). Embryos were staged developmentally according to Kimmel *et al.* (*14*).

Labeling of sialic acids with Ac_4ManNAz and DIFO-488

Zebrafish embryos were dechorionated with pronase (1 mg/mL in embryo medium) at 4 hpf. The embryos were incubated in embryo medium containing 5 mM Ac_4ManNAz over the course of development. PTU (131 μM) was included in the medium beginning at 12 hpf to inhibit melanin production. At each developmental timepoint (24, 36, 48, 72, and 96 hpf), embryos were removed from the Ac_4ManNAz-containing solution, rinsed, and incubated in embryo medium containing DIFO-488 (100 μM) for 1 h at 28.5 °C. They were rinsed by sequential transfers through six 25-cm tissue culture dishes. The embryos were anesthetized with tricaine (2.6 μM) and mounted between two cover slips in embryo medium containing 0.6% low melting point agarose, 2.6 μM tricaine, and 131 μM PTU.

Two-color labeling of sialic acids

At 72 hpf, embryos were removed from Ac_4ManNAz-containing medium and rinsed. For the images shown in Figures 1.4 and 1.5, the embryos were incubated in embryo medium containing DIFO-488 (100 μM) for 1 h at 28.5 °C. The embryos were rinsed and then incubated in embryo medium containing TCEP (50 mM, pH 7.4) for 10 min. The embryos were rinsed six more times and then returned to Ac_4ManNAz-containing medium. After an additional 3 h or 6 h incubation with Ac_4ManNAz (at 76 or 79 hpf, respectively), the embryos were reacted with DIFO-555 (100 μM) for 1 h at 28.5 °C. Alternatively, for the images shown in Figure 4.6, the embryos were reacted first with DIFO-555, then reacted with TCEP and returned to Ac_4ManNAz-containing medium for an additional 24 h before a second reaction with DIFO-488. After both reactions, the

embryos were rinsed by sequential transfers through six 25-cm tissue culture dishes, anesthetized with tricaine (2.6 μM), and mounted between two cover slips in embryo medium containing 0.6% low melting point agarose, 2.6 μM tricaine, and 131 μM PTU.

Microinjection of SiaNAz and visualization of sialylated glycans with DIFO-488

Embryos at the 1–8-cell stage were microinjected with 4 nL of either vehicle alone (5% rhodamine-dextran and 0.2 M KCl in deionized water) or vehicle with 25 mM SiaNAz. The embryos were dechorionated with pronase at 4 hpf as described and allowed to continue to develop at 28.5 °C in agarose-coated dishes containing embryo medium. At 8 hpf (Figure 4.7, panel A) or 10 hpf (Figure 4.7, panel B), the embryos were incubated in embryo medium containing DIFO-488 (100 μM) for 1 h at 28.5 °C. They were rinsed by sequential transfers through six 10-cm agarose-coated dishes. The embryos were mounted between two cover slips in 0.6% low melting point agarose in embryo medium and imaged.

To continue to image SiaNAz-containing glycans over the next four days, the embryos were allowed to continue to develop at 28.5 °C in embryo medium containing PTU. At each developmental stage shown (24, 48, 72, and 96 hpf), embryos were incubated in embryo medium containing DIFO-488 (100 μM) for 1 h at 28.5 °C. They were rinsed, anesthetized with tricaine (2.6 μM), and mounted between two cover slips in embryo medium containing 0.6% low melting point agarose, 2.6 μM tricaine, and 131 μM PTU.

Imaging of glycans by confocal microscopy

All fluorescence and brightfield images were acquired on a Zeiss LSM 510 META laser scanning confocal microscope equipped with 488, 543, and 633 nm laser lines and the following objectives: 10x/0.30 Plan-Neofluar air objective, 20x/0.5 Achroplan water dipping objective, 40x/0.80 Achroplan IR water dipping objective, and 63x/0.95 Achroplan IR water dipping objective. All images were analyzed using Slidebook 5.0 (Intelligent Imaging Innovations). Images shown as x- or y-projections were linearly interpolated along the z axis using Slidebook's interpolation function.

References

1. Varki, A. (2007) Glycan-based interactions involving vertebrate sialic-acid-recognizing proteins, *Nature 446*, 1023-1029.

2. Schauer, R. (2009) Sialic acids as regulators of molecular and cellular interactions, *Curr. Opin. Struct. Biol. 19*, 507-514.

3. Johnson, C. P., Fujimoto, I., Rutishauser, U., and Leckband, D. E. (2005) Direct evidence that neural cell adhesion molecule (NCAM) polysialylation increases intermembrane repulsion and abrogates adhesion, *J. Biol. Chem. 280*, 137-145.

4. Rutishauser, U. (2008) Polysialic acid in the plasticity of the developing and adult vertebrate nervous system, *Nat. Rev. Neurosci. 9*, 26-35.

5. Weinhold, B., Seidenfaden, R., Röckle, I., Mühlenhoff, M., Schertzinger, F., Conzelmann, S., Marth, J. D., Gerardy-Schahn, R., and Hildebrandt, H. (2005) Genetic ablation of polysialic acid causes severe neurodevelopmental defects rescued by deletion of the neural cell adhesion molecule, *J. Biol. Chem. 280*, 42971-42977.

6. Angata, K., Huckaby, V., Ranscht, B., Terskikh, A., Marth, J. D., and Fukuda, M. (2007) Polysialic acid-directed migration and differentiation of neural precursors are essential for mouse brain development, *Mol. Cell. Biol. 27*, 6659-6668.

7. Lopez, P. H., and Schnaar, R. L. (2009) Gangliosides in cell recognition and membrane protein regulation, *Curr. Opin. Struct. Biol. 19*, 549-557.

8. Schwarzkopf, M., Knobeloch, K.-P., Rohde, E., Hinderlich, S., Wiechens, N., Lucka, L., Horak, I., Reutter, W., and Horstkorte, R. (2002) Sialylation is essential for early development in mice, *Proc. Natl. Acad. Sci. U.S.A. 99*, 5267-5270.

9. Saxon, E., and Bertozzi, C. R. (2000) Cell surface engineering by a modified Staudinger reaction, *Science 287*, 2007-2010.

10. Prescher, J. A., Dube, D. H., and Bertozzi, C. R. (2004) Chemical remodelling of cell surfaces in living animals, *Nature 430*, 873-877.

11. Saxon, E., Luchansky, S. J., Hang, H. C., Yu, C., Lee, S. C., and Bertozzi, C. R. (2002) Investigating cellular metabolism of synthetic azidosugars with the Staudinger ligation, *J. Am. Chem. Soc. 124*, 14893-14902.

12. Luchansky, S. J., Argade, S., Hayes, B. K., and Bertozzi, C. R. (2004) Metabolic functionalization of recombinant glycoproteins, *Biochemistry 43*, 12358-12366.

13. Baskin, J. M., Prescher, J. A., Laughlin, S. T., Agard, N. J., Chang, P. V., Miller, I. A., Lo, A., Codelli, J. A., and Bertozzi, C. R. (2007) Copper-free click chemistry for dynamic in vivo imaging, *Proc. Natl. Acad. Sci. U.S.A. 104*, 16793-16797.

14. Kimmel, C. B., Ballard, W. W., Kimmel, S. R., Ullmann, B., and Schilling, T. F. (1995) Stages of embryonic development of the zebrafish, *Dev. Dyn. 203*, 253-310.

15. Ko, S.-K., Chen, X., Yoon, J., and Shin, I. (2011) Zebrafish as a good vertebrate model for molecular imaging using fluorescent probes, *Chem. Soc. Rev. 40*, 2120-2130.

16. Laughlin, S. T., Baskin, J. M., Amacher, S. L., and Bertozzi, C. R. (2008) In vivo imaging of membrane-associated glycans in developing zebrafish, *Science 320*, 664-667.

17. Baskin, J. M., Dehnert, K. W., Laughlin, S. T., Amacher, S. L., and Bertozzi, C. R. (2010) Visualizing enveloping layer glycans during zebrafish early embryogenesis, *Proc. Natl. Acad. Sci. U.S.A. 107*, 10360-10365.

18. Dehnert, K. W., Beahm, B. J., Huynh, T. T., Baskin, J. M., Laughlin, S. T., Wang, W., Wu, P., Amacher, S. L., and Bertozzi, C. R. (2011) Metabolic labeling of fucosylated glycans in developing zebrafish, *ACS Chem. Biol.* in press.

19. Yu, H., Yu, H., Karpel, R., and Chen, X. (2004) Chemoenzymatic synthesis of CMP-sialic acid derivatives by a one-pot two-enzyme system: comparison of substrate flexibility of three microbial CMP-sialic acid synthetases, *Bioorg. Med. Chem. 12*, 6427-6435.

Chapter 5

Simultaneous Imaging of Two Distinct Classes of Glycans in Vivo

Chapter 5. Simultaneous Imaging of Two Distinct Classes of Glycans in Vivo[1]

Introduction

Advances in molecular imaging techniques, including the development of dozens of different fluorescent proteins, have provided a powerful toolkit for imaging proteins in living cells and organisms (*1*, *2*). It is now routine, for example, to image three or more proteins of interest at once using fluorescent fusion proteins of different colors. We sought to extend this capability to the simultaneous visualization of different classes of glycans in vivo.

In Chapter 1, I described several bioorthogonal reactions that can be used to label glycans in living systems. Some of those reactions, such as the oxime/hydrazone ligation and the azide-alkyne cycloaddition, are also orthogonal to one another. Thus, if an azide could be incorporated into one class of glycans, and an aldehyde introduced into another class, the two could be distinguished by appropriate cyclooctyne and aminooxy reaction partners fused to different fluorophores (Figure 5.1). This type of strategy has been validated in cultured cells via metabolic labeling of mucin-type O-glycans and sialylated glycans using azide- and ketone-containing precursors, respectively (*3*), but analogous experiments have not be performed in vivo.

We applied a similar strategy for simultaneously imaging these two classes of glycans in live zebrafish embryos. We metabolically incorporated GalNAz into O-glycans and introduced an aldehyde into cell-surface sialic acids by treatment with sodium periodate. We then imaged the two classes of glycans by reaction with difluorinated cyclooctyne (DIFO) and aminooxy probes.

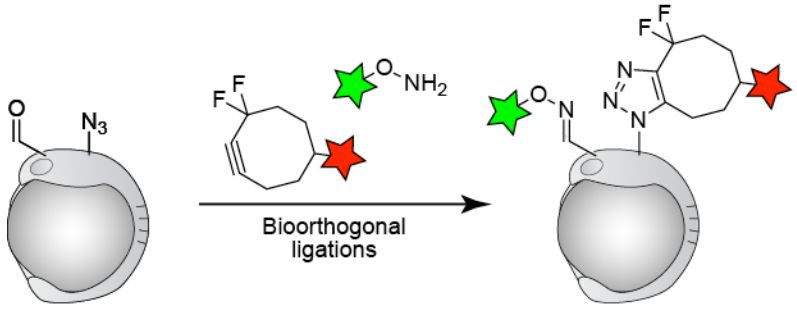

Figure 5.1. Strategy for simultaneous visualization of O-glycans and sialylated glycans using two independent bioorthogonal chemistries. Aldehydes exposed on sialic acids by oxidation with periodate are reacted with an aminooxy-functionalized fluorophore, and azidosugars incorporated into cell-surface glycans are reacted with a difluorinated cyclooctyne (DIFO) reagent conjugated to a different fluorophore.

[1] Jeremy Baskin contributed to the work presented in this chapter.

Results and Discussion

Imaging of sialylated glycans using an orthogonal, non-metabolic approach

Due to the relatively weak labeling that microinjection of SiaNAz provided during early embryogenesis (as described in Chapter 4), we sought a more sensitive technique for labeling sialylated glycans that would also provide a unique chemical reporter group. We turned to a non-metabolic method for modifying sialic acids. It has long been known that chemical treatment of cells or cell lysates with low concentrations of sodium periodate ($NaIO_4$) selectively oxidizes sialic acid residues (*4-8*), exposing an aldehyde that can be subsequently targeted by reductive amination or oxime/hydrazone-forming reactions (*9*). Recently, Paulson and coworkers utilized this approach to label sialylated glycans on the surfaces of live cells (*10*). We endeavored to extend this strategy to a whole-animal context by treating zebrafish embryos with $NaIO_4$ at various stages of embryogenesis and then reacting them with an aminooxy-derivatized Alexa Fluor 488 reagent (AO-488) (Figure 5.2).

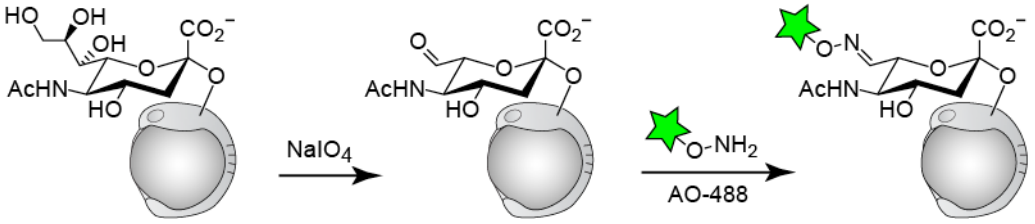

Figure 5.2. Strategy for imaging sialylated glycans using sodium periodate oxidation followed by detection with aminooxy-functionalized probes. Zebrafish embryos are treated with $NaIO_4$ to expose aldehydes on sialic acids, which are then visualized using aminooxy-fluorophore conjugates.

In periodate-reacted embryos, we observed modest labeling of cell surfaces beginning at 65% epiboly, or 7 hpf (Figure 5.3, panel A). However, at the microscope settings necessary to see signal in periodate-reacted embryos, we also observed background signal in embryos that were not treated with periodate. Furthermore, embryos treated with $NaIO_4$ and reacted with AO-488 prior to bud stage demonstrated substantial fluorophore labeling in the yolk cell. Therefore, in all subsequent experiments we employed embryos that had completed epiboly.

Beginning at 10 hpf, periodate-treated embryos exhibited robust cell-surface labeling, with no fluorescence signal in the yolk and no background signal in untreated embryos (Figure 5.3, panels B and C). These results are consistent with our experiences labeling sialic acids by metabolic incorporation of SiaNAz, described in Chapter 4. Using both techniques, we observed low fluorescence signal during gastrulation and more intense signal during somitogenesis, suggesting that substantial de novo production of sialic acid-containing glycans begins as gastrulation ends and somitogenesis begins.

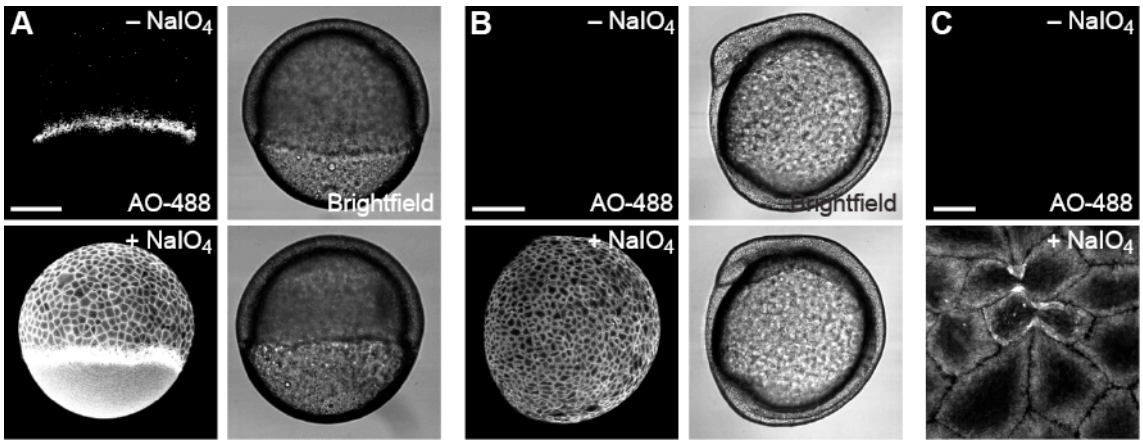

Figure 5.3. Visualization of sialylated glycans using sodium periodate oxidation followed by detection with aminooxy-488. Zebrafish embryos at 6 hpf (A) or 10 hpf (B, C) were bathed in embryo medium containing no reagent (top row) or $NaIO_4$ (bottom row), reacted with AO-488, and imaged by confocal microscopy. Shown are maximum intensity z-projection images of AO-488 fluorescence (A, B, left panels, and C) and corresponding brightfield images (A, B, right panels). Scale bars: 200 μm (A, B), 20 μm (C).

We confirmed that ManNAz-labeled glycans colocalize with those labeled by $NaIO_4$ and AO-488 (Figure 5.4), which is consistent with literature reports that this method is selective for sialic acids. This chemical approach did not result in any noticeable toxicity or developmental defects; embryos that were treated with $NaIO_4$ and aminooxy fluorophores and then were allowed to develop to 120 hpf were indistinguishable from untreated zebrafish larvae. Further, we reacted embryos with AO-488 and an aniline additive (*10*, *11*) to probe whether this nucleophilic catalyst might improve the labeling efficiency of periodate-oxidized glycans. In our system, the addition of aniline resulted in only a modest increase in cell-surface fluorescence (Figure 5.5), and due to the fragile nature of the embryo, we chose to omit this reagent from our labeling reactions.

Interestingly, during the course of these studies, we observed increased signal at what appeared to be the cleavage furrow of dividing cells (Figure 5.3, panel C). This result resembled the labeling of mucin-type O-glycans we had previously observed in embryos treated with GalNAz and DIFO-488, described in Chapter 2 (Figure 2.13). We were eager to determine whether we could distinguish subtle differences between O-glycan and sialylated glycan production. Because the two detection methods that we employed, oxime formation and copper-free click chemistry, are orthogonal to one another, we were able to address this question by performing both labeling reactions on the same population of embryos.

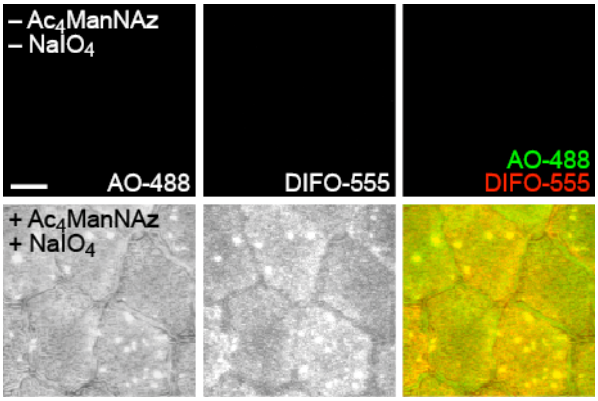

Figure 5.4. Dual labeling of sialic acids with $NaIO_4$ and ManNAz results in substantial colocalization of AO-488 and DIFO-555 signal. Zebrafish embryos were bathed in embryo medium containing Ac_4ManNAz or no sugar for three days, then treated with $NaIO_4$ or no reagent. Embryos were reacted in a mixture of DIFO-555 and AO-488 in PBS and imaged by confocal microscopy. Shown are maximum intensity z-projection fluorescence images. Green, AO-488; red, DIFO-555. Scale bar: 10 μm.

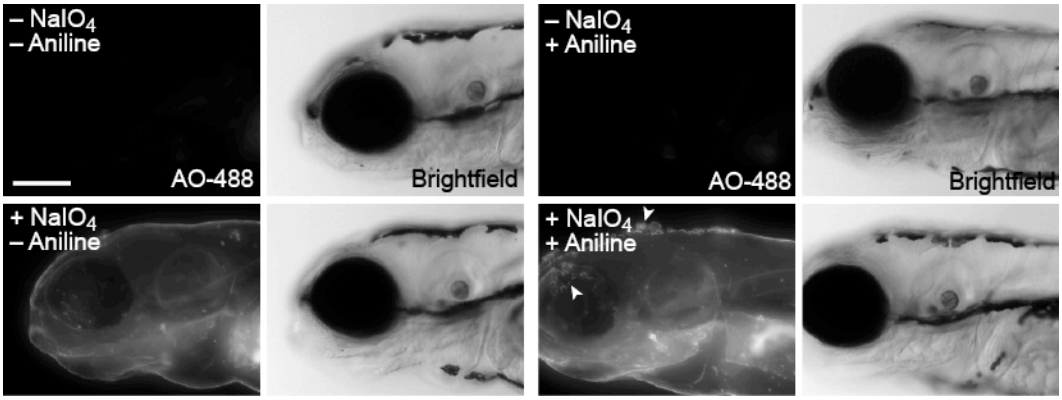

Figure 5.5. An aniline catalyst provides a modest increase in labeling of periodate-reacted glycans with aminooxy probes. Zebrafish embryos (120 hpf) were bathed in embryo medium containing no reagent (top row) or $NaIO_4$ (bottom row), then reacted with AO-488 in the presence (right) or absence (left) of 10 mM aniline. Shown are maximum intensity z-projection images of AO-488 fluorescence and corresponding brightfield images. Arrowheads indicate damage to the epidermis caused by aniline. Scale bar: 200 μm.

Simultaneous visualization of O-glycans and sialylated glycans using independent bioorthogonal chemistries

In order to ascertain the similarities and differences between O-glycan labeling, using GalNAz and DIFO-fluorophores, and sialic acid labeling, using $NaIO_4$ and aminooxy-fluorophores, we performed a dual labeling experiment within the same embryo. Embryos were microinjected with GalNAz or no sugar at the one-cell stage, allowed to develop to 10 or 24 hpf, and then incubated with $NaIO_4$ or no reagent. In all

cases, the embryos were subsequently reacted simultaneously with DIFO-555 to label azides and AO-488 to label aldehydes.

We observed substantial labeling with each fluorescent probe, and appropriate negative controls displayed minimal background fluorescence (Figure 5.6). The resulting images revealed considerable colocalization of the GalNAz-labeled and $NaIO_4$-reacted species (Figure 5.7). Similar results were observed in embryos that were labeled and imaged at 24 hpf (Figure 5.8). The significant colocalization of sialic acid- and O-glycan-derived signal was to be expected, because many sialic acids appear within mucin-type O-glycans, and many mucin glycoproteins also contain N-glycans, which often display terminal sialic acid residues. These experiments validate the ability of two independent bioorthogonal chemistries to be employed for simultaneous visualization of two classes of glycans within a single living organism.

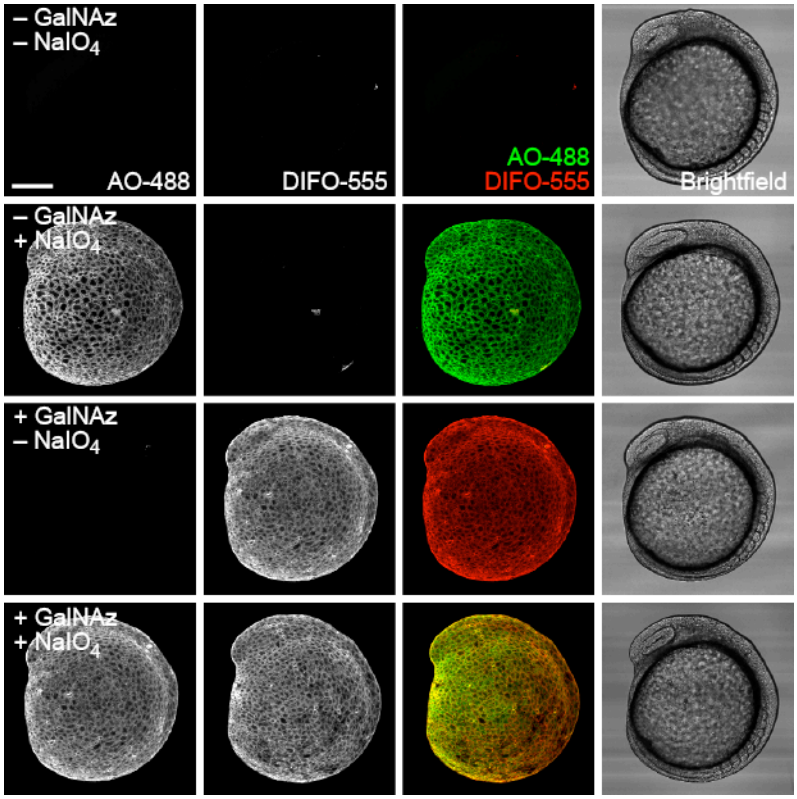

Figure 5.6. Simultaneous visualization of O-glycans and sialylated glycans using two independent bioorthogonal chemistries. Zebrafish embryos were microinjected with GalNAz or no sugar, allowed to develop to 10 hpf, and then bathed in embryo medium containing $NaIO_4$ or no reagent. Embryos were then reacted in a mixture of DIFO-555 and AO-488 in PBS for 1 h, rinsed, and imaged by confocal microscopy. Shown are maximum intensity z-projection fluorescence images. Green, AO-488; red, DIFO-555. Scale bar: 200 μm.

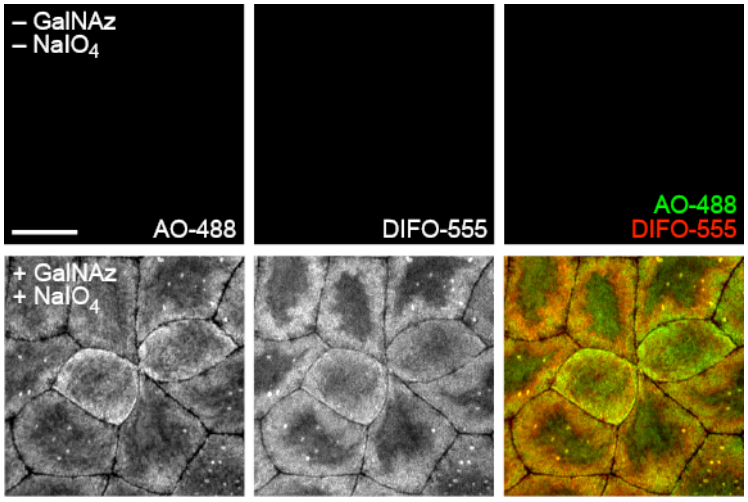

Figure 5.7. Simultaneous visualization of O-glycans and sialylated glycans in the enveloping layer during the early segmentation period. Zebrafish embryos were microinjected with GalNAz or no sugar, allowed to develop to 10 hpf, and then bathed in embryo medium containing $NaIO_4$ or no reagent. Embryos were then reacted in a mixture of DIFO-555 and AO-488 in PBS and imaged by confocal microscopy. Shown are maximum intensity z-projection fluorescence images. Green, AO-488; red, DIFO-555. Scale bar: 20 μm.

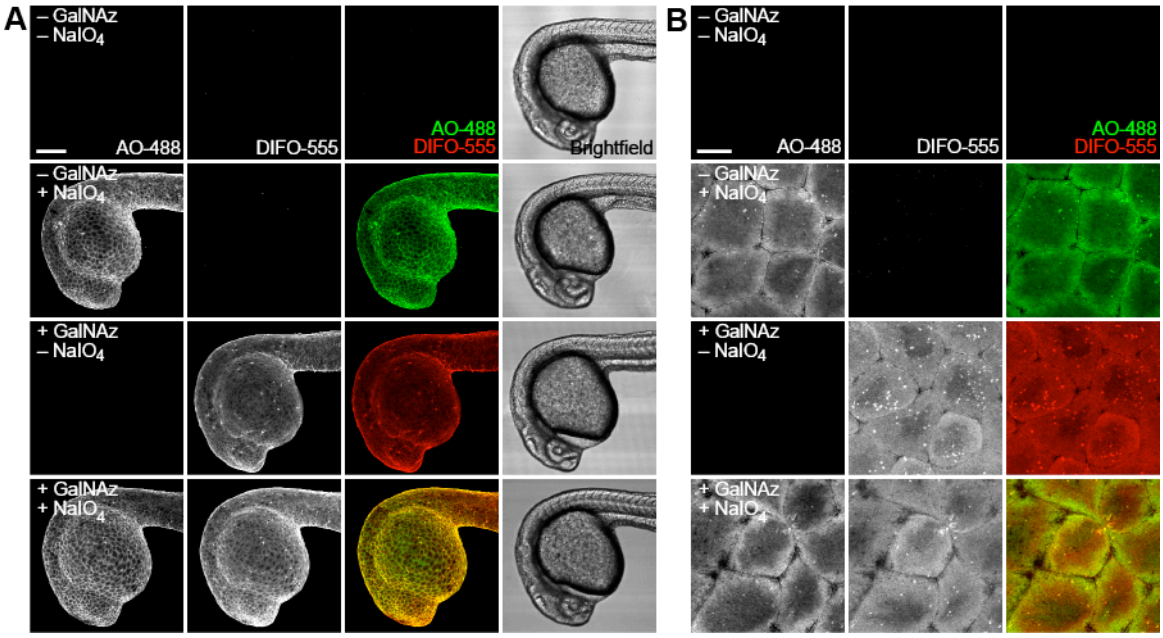

Figure 5.8. Simultaneous visualization of O-glycans and sialylated glycans at 24 hpf. Zebrafish embryos were microinjected with GalNAz or no sugar, allowed to develop to 24 hpf, and then bathed in embryo medium containing $NaIO_4$ or no reagent. Embryos were then reacted in a mixture of DIFO-555 and AO-488 in PBS and imaged by confocal microscopy. Shown are maximum intensity z-projection fluorescence images and corresponding brightfield images. Green, AO-488; red, DIFO-555. Scale bars: 200 μm (A), 20 μm (B).

Conclusion

We have shown that periodate oxidation is a sensitive, non-toxic method for labeling sialylated glycans in the enveloping layer of live zebrafish embryos. Furthermore, periodate treatment can be combined with azidosugar labeling followed by dual reaction with cyclooctyne and aminooxy probes to image two classes of glycans simultaneously with minimal cross-reactivity or background signal. The simultaneous visualization of O-glycans and sialylated glycans described in this chapter exposed subtle differences in the distributions of these two partially overlapping sectors of the glycome during embryogenesis. Development of new bioorthogonal ligation reactions for in vivo use could extend this strategy to additional classes of glycans and other biomolecules.

Experimental Methods

General materials and methods

All chemical reagents were of analytical grade, obtained from commercial suppliers, and used without further purification. Aminooxy Alexa Fluor 488 was obtained from Invitrogen. Phenol red, *N*-phenylthiourea (PTU), pronase (protease, Type XIV, from *Streptomyces griseus*), and tricaine (ethyl 3-aminobenzoate methanesulfonate) were obtained from Sigma-Aldrich. GalNAz (*12*), DIFO-555 (*13*), and Ac_4ManNAz (*14*) were prepared as described previously. Confocal microscopy was performed at the UC Berkeley Molecular Imaging Center.

Zebrafish stocks and husbandry

Wild-type AB-derived zebrafish lines were kept at 28.5 °C on a 14-h light/10-h dark cycle. Embryos were obtained from natural spawnings and were maintained in embryo medium (150 mM NaCl, 0.5 mM KCl, 1.0 mM $CaCl_2$, 0.37 mM KH_2PO_4, 0.05 mM Na_2HPO_4, 2.0 mM $MgSO_4$, 0.71 mM $NaHCO_3$ in deionized H_2O, pH 7.4). Embryos and larvae were incubated at 28–29 °C and were developmentally staged according to Kimmel and coworkers (*15*).

Chemical labeling of sialylated glycans using sodium periodate and aminooxy reagents

Zebrafish embryos were dechorionated at 3 hpf using pronase (1 mg/mL in embryo medium), then allowed to develop in embryo medium at 28.5 ºC. All embryos younger than 12 hpf were stored in Petri dishes or 96-well plates coated with a 1% solution of agarose in embryo medium. At various timepoints, the embryos were transferred to a dish containing a freshly-made solution of $NaIO_4$ (500 μM) or no reagent in embryo medium and incubated for 30 min at 28.5 ºC. The embryos were then transferred to a dish containing 10 mM glycerol for 2 min to quench any excess $NaIO_4$, followed by another transfer to a dish containing 1X phosphate-buffered saline (PBS), pH 6.7. Embryos were then transferred to a flat-bottom 96-well plate containing a solution of AO-488 (100 μL of a 100 μM solution in PBS, pH 6.7) and allowed to react for 1 h at 28.5 ºC. For the experiment shown in Figure 5.5, the embryos were first reacted with 1 mM $NaIO_4$ (or no reagent), and 10 mM aniline was included in the AO-488 incubation solution for the indicated embryos.

Dual labeling of sialic acids using Ac_4ManNAz and sodium periodate

Zebrafish embryos were allowed to develop to 3 hpf, at which point they were dechorionated using pronase (1 mg/mL) in embryo medium. The embryos were then incubated for three days at 28.5 ºC in embryo medium containing 5 mM Ac_4ManNAz and, beginning at 24 hpf, 131 μM PTU. At 72 hpf, the embryos were transferred to a freshly-made solution of $NaIO_4$ (500 μM) or no reagent in embryo medium and incubated for 30 min at 22 ºC. The embryos were then transferred to a dish containing 10 mM glycerol for 2 min to quench any excess $NaIO_4$, followed by another transfer to a dish

containing PBS, pH 6.7. The embryos were then transferred to a flat-bottom 96-well plate containing a solution of 100 μM AO-488 and 100 μM DIFO-555 (in 100 μL PBS, pH 6.7) and allowed to react for 1 h at 28.5 ºC.

Labeling of mucin-type O-glycans and sialylated glycans using GalNAz and sodium periodate followed by DIFO-555 and AO-488

Zebrafish embryos at the one-cell, two-cell, or four-cell stage were microinjected into the yolk cell with 1 nL of a 25 mM solution of GalNAz (or no sugar) and phenol red (0.1% w/v) in 0.2 M KCl. Following microinjection, the embryos were allowed to develop to 3 hpf, at which point they were dechorionated using pronase (1 mg/mL) in embryo medium. The embryos were allowed to further develop. At the timepoints shown, the embryos were reacted with sodium periodate (or no reagent) followed by glycerol as described above. The embryos were transferred to a flat-bottom 96-well plate containing a solution of AO-488 (100 μM) and DIFO-555 (100 μM) in 100 μL of PBS, pH 6.7, and allowed to react for 1 h at 28.5 ºC.

Preparation of labeled embryos for imaging

After the labeling reactions, the embryos were rinsed by transferring them through six 15-cm dishes filled with 25 mL of embryo medium. Embryos that were 24 hpf or older were anesthetized with 2.6 μM tricaine for imaging analysis. The embryos were then mounted between two cover slips, stabilized by vacuum grease in each corner, in a solution of 0.6% low melting point agarose in embryo medium.

Image acquisition and analysis

Fluorescence and brightfield images shown in Figure 5.5 were acquired on a Zeiss 200M epifluorescence microscope with a 10x air objective. All other fluorescence and brightfield images were acquired on a Zeiss LSM 510 META laser scanning confocal microscope equipped with 488 nm, 543 nm, and 633 nm laser lines. For Figures 5.3A–B, 5.6, and 5.8A, images were acquired using a 10x/0.30 Plan-Neofluar air objective with focus step sizes ranging from 5 to 7.5 μm. Images shown in Figures 5.3C, 5.4, 5.7, and 5.8B were acquired using a 63x/0.95 Achroplan IR water dipping objective with a 0.5 μm step size. All images were analyzed using Slidebook 4.2 (Intelligent Imaging Innovations).

References

1. Giepmans, B. N. G., Adams, S. R., Ellisman, M. H., and Tsien, R. Y. (2006) The fluorescent toolbox for assessing protein location and function, *Science 312*, 217-224.

2. Day, R. N., and Davidson, M. W. (2009) The fluorescent protein palette: tools for cellular imaging, *Chem. Soc. Rev. 38*, 2887-2921.

3. Chang, P. V., Prescher, J. A., Hangauer, M. J., and Bertozzi, C. R. (2007) Imaging cell surface glycans with bioorthogonal chemical reporters, *J. Am. Chem. Soc. 129*, 8400-8401.

4. Gahmberg, C. G., and Andersson, L. C. (1977) Selective radioactive labeling of cell surface sialoglycoproteins by periodate-tritiated borohydride, *J. Biol. Chem. 252*, 5888-5894.

5. De Bank, P. A., Kellam, B., Kendall, D. A., and Shakesheff, K. M. (2003) Surface engineering of living myoblasts via selective periodate oxidation, *Biotechnol. Bioeng. 81*, 800-808.

6. Van Lenten, L., and Ashwell, G. (1971) Studies on the chemical and enzymatic modification of glycoproteins. A general method for the tritiation of sialic acid-containing glycoproteins, *J. Biol. Chem. 246*, 1889-1894.

7. Spiro, R. G. (1964) Periodate oxidation of the glycoprotein fetuin, *J. Biol. Chem. 239*, 567-573.

8. Karkas, J. D., and Chargaff, E. (1964) Studies on stability of simple derivatives of sialic acid, *J. Biol. Chem. 239*, 949-957.

9. Hang, H. C., and Bertozzi, C. R. (2001) Chemoselective approaches to glycoprotein assembly, *Acc. Chem. Res. 34*, 727-736.

10. Zeng, Y., Ramya, T. N., Dirksen, A., Dawson, P. E., and Paulson, J. C. (2009) High-efficiency labeling of sialylated glycoproteins on living cells, *Nat Methods 6*, 207-209.

11. Dirksen, A., Hackeng, T. M., and Dawson, P. E. (2006) Nucleophilic catalysis of oxime ligation, *Angew. Chem. Int. Ed. 45*, 7581-7584.

12. Baskin, J. M., Dehnert, K. W., Laughlin, S. T., Amacher, S. L., and Bertozzi, C. R. (2010) Visualizing enveloping layer glycans during zebrafish early embryogenesis, *Proc. Natl. Acad. Sci. U.S.A. 107*, 10360-10365.

13. Laughlin, S. T., Baskin, J. M., Amacher, S. L., and Bertozzi, C. R. (2008) In vivo imaging of membrane-associated glycans in developing zebrafish, *Science 320*, 664-667.

14. Saxon, E., and Bertozzi, C. R. (2000) Cell surface engineering by a modified Staudinger reaction, *Science 287*, 2007-2010.

15. Kimmel, C. B., Ballard, W. W., Kimmel, S. R., Ullmann, B., and Schilling, T. F. (1995) Stages of embryonic development of the zebrafish, *Dev. Dyn. 203*, 253-310.